Measurements of Conductive Film

A thesis submitted for the degree of

Doctor of Philosophy

by

Anthony Samano

College of Engineering, Design and Physical Sciences

Brunel University London

Uxbridge, UB8 3PH

United Kingdom

January 2017

Supervision: Dr Yanmeng Xu and Professor David Harrison

Abstract

Printed electronics is a combination of electronics and printing technologies commonly used in the publication industry such as screen, inkjet, and roll to roll printing. The measurements of conductive film particularly the conductive paste is the main objective of this thesis. The conductive paste consists of conductive filler, adhesive and solvent. Each component affects the electrical, and mechanical properties of the finished conductive film product. The measurements of conductive film have three field of study. The first category is the lifetime performance measurement of conductive film using environmental testing. A screen printed carbon, silver and a developmental paste were categorised to environmental testing and third harmonic measurement. The second category is the measurement AC Impedance and DC resistance of conductive ink during cure. During the curing of the pastes, the AC impedance and DC resistance were monitored. A LabVIEW program was developed to control the AC impedance analyser, DC resistance ohmmeter, and convection oven. Samples were measured whilst curing at different curing temperatures and for a range of particle loadings. Particle loading is the percentage of conductive filler against the rest of the chemical in the conductive paste. The last category was defect detection using the combination of electromechanical testing, a Scanning Electron Microscope (SEM) and an Infrared (IR) imaging technique. Printed carbon and silver were mechanically aged by bending the printed structure up to 100 k times.

The results from the lifetime performance measurements on carbon, silver and the developmental paste showed the polymer resin behaviour in high humidity and high temperature environments. The increased oxidation rate due to the elevated temperatures affected the conductive particle of certain pastes. The third harmonic testing technique was able to detect failures on conductive film in the form of width reduction. The AC impedance measurement technique could indicate the final resistivity value. The AC impedance measurement was affected by the test frequency used while the ink is in liquid state. Correct test frequency setting will have less noise and less impedance value, vital in predicting the final cured resistance of the printed paste. The curing temperature affects the final cured resistance value while the particle loading affects the rate of curing of conductive film. The electrical measurement on mechanically aged samples showed that the carbon prints have its resistance readings below its initial value while the silver prints resistance increased. SEM images shows that the carbon print indicates no visual damage on the surface after 100 k bent cycle, while physical defects were observed in silver prints. The infrared measurements on carbon prints showed an increase in temperature while developments of

heat patches were observed on silver prints. Difference in emissivity values of materials used provided the contrast effect which plays an important role in detecting defect using infrared imaging technique because.

Third harmonic application to the printed electronics is new to this field. Normally, testing is done using environmental testing to determine the lifetime performance of the conductive film. This is effective however requires a lot of time and effort to produce a result.

AC Impedance is used widely and the application can be seen on cured printed electronics. The application and measurement of AC impedance during cure and DC resistance measurement has indicated initial resistivity values. The measurement has further the effect of using AC impedance on different curing temperature and particle loading. The phase measurement as well has brought insight of degree of curing.

The application of infra-red imaging technique to the mechanically aged device has produced a result that DC resistance and SEM imaging failed to detect. Normally DC resistance measurement was used as quality assessment tool but test shows on mechanically aged product failed to detect increase in resistance due to mechanical aging techqnique.

Acknowledgements

I would like to thank my Brunel University supervisors Dr. Yanmeng Xu and Professor David Harrison for giving me an opportunity to take the PhD studentship and their tremendous moral support. Also, very grateful for the National Physical Laboratory U.K. supervisors and they are Dr. Chris Hunt, Mr Martin Wickham, Dr. Adam Lewis and Dr. Owen Thomas. Special thanks to Dr. Peter Evans for proof reading my journal papers and Sam Gnaniah and Dipak Gohil for test equipment access and training.

Publication List

1. **Anthony Samano** , Yanmeng Xu , David Harrison , Chris Hunt , Martin Wickham , Owen Thomas "Third harmonic measurement in conductive film," Proceedings of 2014 3rd Asia-Pacific Conference on Antennas and Propagation, Harbin, 2014, pp. 889-891.

2. **Anthony Samano** , Yanmeng Xu , David Harrison , Chris Hunt , Martin Wickham , Owen Thomas , (2016) "Impedance and resistance of carbon ink during cure", Circuit World, Vol. 42 Iss: 3, pp.117 – 126

3. In the process of submission of journal paper to Circuitworld – **Anthony Samano** , Yanmeng Xu , David Harrison , Adam Lewis, Martin Wickham " Defect detection using Infrared thermal imaging technique on conductive film"

List of figures

List of tables

List of equations

Nomenclature

A list of symbols used together with a short description.

Symbol	Description
A	Area of the material
h	The heat flow coefficient
k	Thermal conductivity
l	length of slab in meter
Q	Quantity of heat
R	Resistance
RLEAD	Lead resistance
T	Temperature
t	Thickness of material
T1	Higher temperature
T2	Lower temperature
W	Radiant flux emitted per unit area
w	Width of material
X	Reactance
Z	Impedance
σ	Stephen-Boltzman constant
ρ	Resistivity
I	Current
V_m	Measured voltage

V_r	Device under test voltage

Abbreviation	**Description**
AC	Alternating current
AFM	Atomic Force Microscope
Ag	Silver
Al	Aluminium
ASTM	American Society for Testing and Materials
Au	Gold
CIELAB	Commision Internationale d'Eclairage
cm	Centimeter
CNT	Carbon NanoTubes
CT	Computer Tomography
CTE	Coefficient of Thermal Expansion
Cu	Copper
DC	Direct Current
DMA	Dynamic Mechanical Analyser
DSC	Differential Scanning Calorimetry
DUT	Device under test
EM	Electromagnetic
FD-OCT	Fourier Domain OCT
GEM	Gwent Electronics Materials
IC	Integrated Circuit
IR	Infrared

IV	Current – Voltage
LWIR	Long range wavelength Infrared
mm	Millimeter
MWCNT	Multiwalled carbon nanotube
MWIR	Midrange wavelength Infrared
NDT	Non-Destructive Testing
Ni	Nickel
nm	Nanometer
OCT	Optical Coherence Tomography
Pa	Pascal
PEN	Polyethylene-Naphthalate
PET	Poly(ethylene Terephthalate)
PI	Polyimide
SEM	Scanning Electron Microscope
SMT	Surface Mount Technology
SWCNT	Singlewalled Carbon Nanotube
TDR	Time Domain Reflectometry
TEM	Transmission Electron Microscope
Tg	Glass transition temperature
TGA	Thermo gravimetric analysis
THR	Third Harmonic Ratio

Table of contents

Author’s declaration

I, Anthony Samano, hereby certify that this dissertation is a product of my ideas and research. Other works and ideas that do not belong to me are given credits and were referenced accordingly. I declare that the dissertation is original and was not previously presented for any award of any other degree of any institution.

1. Chapter 1 – Introduction

Printed electronics uses graphic arts processing technique such as screen (Jewell, Hamblyn et al. 2013) , ink jet (Cummins, Desmulliez 2012) and press roller printing (Unander, Nilsson 2009)printing to create an electronic circuit. It provides less damage to the environment and is seen as an alternative to conventional type of subtractive processing technique. Wide range applications of conductive film are seen in electronic displays (Zacharatos, Makrygianni et al. 2016), Radio Frequency IDentification (RFID) antenna (Janeczek, Jakubowska et al. 2012), energy harvesting (Montanino, De Girolamo Del Mauro et al. 2015), and interconnect (Määttänen, Ihalainen et al. 2010).

This research is based primarily on measurement techniques for conductive paste to create interconnect using screen printing process. Conductive paste is composed of adhesive, solvent and conductive particle. Adhesive is used to hold particles together and to attach particles to the substrate. Solvent is essential to prevent particles from agglomeration and for smooth delivery of the conductive paste to the substrate. Once the paste is deposited to the substrate, then the solvent is no longer necessary. Curing the conductive paste will remove the solvent and this will produce a conductive structure through particle to particle contact. The conductive paste can only achieve the bulk resistivity of its highly conductive particle ingredients. There are different conductive particle used in conductive film and this is discussed in literature review section about materials together with commonly used substrates.

The research conducted aimed to develop novel measurement techniques that can be applied to conductive film. The application of measurement technique will increase the quality and reliability of the conductive film and at the same time bringing down the cost of manufacturing. The measurement techniques in conductive film will cover for the three categories which are the lifetime performance measurements, measurement during the conductive ink transition from liquid to solid structure and print defect detection.

The first objective of this thesis is to identify measurement techniques that will predict the lifetime performance of conductive film. Conductive film is low cost (Subramanian, Chang et al. 2008, Woerle, Rost 2011, Homola, Wu et al. 2014) and fast to manufacture (Wegener, Spiehl et al. 2016, Capasso, Del Rio Castillo et al. 2015), however the conductive film reliability is another major factor to consider. The development in conductive film is to increase its performance and decrease the manufacturing cost. The main contributing factor

to the cost of conductive ink is due to the amount of conductive particle. In addition, a large percentage of the conductive ink is made up of conductive filler. Effective lifetime performance testing is therefore needed to enable the conductive film producer to determine conductive film strength, and remove weak product to prevent early field failures.

There are two solutions to the lifetime performance assessment of conductive film that was used in this study. The first solution is to use environmental testing on silver and carbon prints. The result of this research will determine the strength of printed electronic against environmental stresses. The second solution for lifetime performance testing of conductive film comes in the form of third harmonic testing. Another method to assess the lifetime performance of conductive film is third harmonic measurement that is known to resistor manufacturing industry to remove weak products (Salomon, Troianello 1973, Spiralski 2003). The application of third harmonic testing to conductive film is novel and useful since it will determine lifetime performance of the device in least possible time. Investigation needs to be performed once the conductive film fails in third harmonic testing. Correction needs to be performed if there are problems that are caused by manpower, printing process, or materials.

The second objective of this thesis is to develop a novel measurement during conductive ink transition from liquid to solid structure. Most of the measurement techniques used in conductive film is often performed when it is cured. This measurement technique produces slow in determining result and increases manufacturing cost. AC impedance and DC resistance was measured one after the other during cure. The AC Impedance analyser and digital multi-meter was controlled using LabVIEW software. The novel measurement technique will provide early resistivity values and degree of cure, important to research and manufacturing industry.

The effect of particle loading and temperature curing are two of the parameters that will be investigated using this novel measurement technique. The particle loading and curing temperature is increased to achieve the bulk electrical properties. Increasing the amount of particle in the conductive ink causes more particles to conduct and carry current. Higher curing temperature will remove more solvent to the conductive ink increasing its conductivity. Different particle loading and curing temperature will affect the speed of curing and final impedance values.

The third measurement category is a non-contact measurement technique to detect defect and stresses in conductive film. It is also suitable for high speed printing of conductive paste. The normal method of measurement uses DC resistance and Scanning Electron Microscope

(SEM) to detect defect in conductive film. The development in conductive ink involves the use of nanomaterial to improve its electrical and mechanical characteristics (Kamyshny, Magdassi 2014). However, this has caused problem because the common measurement in conductive film was unable to detect defect and stress. A new method of detecting defect in conductive film is vital to maintain its quality and operation integrity.

Electromechanical equipment was built to induce aging and stress to the conductive film. The aged samples were subjected to Scanning Electron Microscope (SEM) imaging and Infrared (IR) imaging. Different voltage level was applied to the conductive film while temperature is being monitored by the thermal camera. The result of Infra-red measurement technique was found to be effective in conductive film due to the difference in emissivity values used in conductive film. These will mean less disruption to the high speed printing process of conductive film. The manufacturing cost will decrease but not compromising the quality and development of conductive film.

The structure of the thesis is as follows;

Chapter 2 is the literature review of conductive ink materials, deposition process and measurements in conductive film. Included in materials are type of conductive particles and substrate used. The process includes the roll to roll and ink jet printing system. The measurement includes the electrical, mechanical, and imaging techniques.

Chapter 3 is methodology used to achieve the main three measurement objectives. The printing, curing, and dimensional analysis is included in this chapter.

Chapter 4 is the result and discussion of the three main category areas. The first category is the lifetime performance assessment of conductive film followed by AC impedance and DC resistance measurement during cure. The third category is the measurement technique to defect detection using Infrared camera.

Chapter 5 is the conclusion of the three category areas. The assessment using environmental testing, third harmonic, AC impedance, and IR imaging technique are proven to be useful in measuring conductive film.

Contribution to knowledge

Third harmonic measurement is a novel technique in the field of conductive film. Third harmonic testing is a well-known measurement technique in the field of resistor manufacturing. The result of third harmonic measurement in conductive film shows that it can detect certain type of defect that will cause early field failures. The application of third harmonic testing to conductive film manufacturer could improve manufacturing process that will lead to increased quality.

A novel measurement technique was developed to can capture the transition of printed electronics from liquid to solid structure. AC Impedance and DC resistance measurement were taken right after the other using automatic testing equipment was controlled using LabVIEW program. This measurement technique can measure early sign of resistivity that is vital to prevent manufacturing wastage, as well as degree of cure measurement. To date, there is no measurement equipment that detects early indication of resistivity and measurement of degree of cure based on AC Impedance measurement. The result of the study will benefit both the conductive ink producer and conductive film manufacturer.

The application of Infrared thermal imaging to detect defect in conductive film is a novel measurement technique. The IR measurement result was correlated to DC resistance measurement and scanning electron microscope. The result of the measurement shows that mechanical stress present can be detected by Infrared thermal camera. Whereas DC resistance measurement failed to detect defect on certain type of paste, while Scanning Electron Microscopy is limited to surface quality even at higher magnification. The use of Infrared Thermal camera will mean high speed and high test coverage of conductive film that is very appealing for the manufacturer. Furthermore, IR measurement technique can be used while the conductive film is in operation, making it safe and less disruptive type of assessment.

2 Chapter 2 - Literature Review

2.1 Materials

Conductive film materials can be categorised into two main parts, first is the conductive ink and the substrate. The conductive ink is composed of adhesive, chemical vehicle and conductive particle. The chemical vehicle or solvent promotes the delivery of the conductive particle to desired location, and prevents particles from agglomeration while the ink is in the storage container. The conductive particle main characteristics are its electrical and chemical stability. In addition, the cost of the conductive particles plays an important role for large scale application. The electrical properties are commonly measured in terms of conductivity or its reciprocal resistivity.

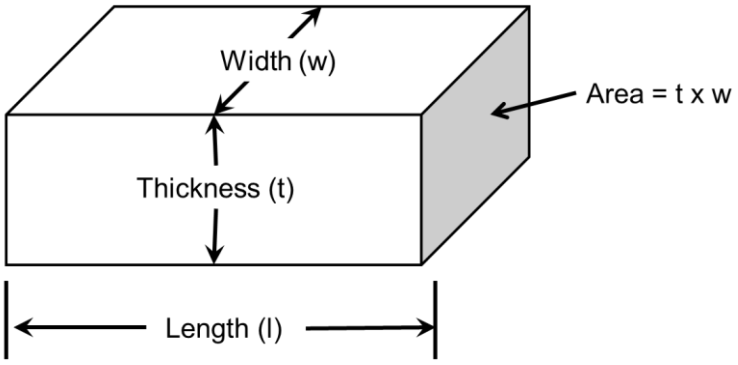

Figure 1 Dimensions for resistivity calculations

$$\rho = R \frac{t \times w}{l} \quad (1)$$

The formula for resistivity is given by equation 1, where ρ is the electrical resistivity of the material expressed in Ω.m regardless of its shape. R is the measured electrical resistance in Ω. The dimensions are t for thickness, w for width and l for length and are expressed in meter (m) are shown in Figure 1. The chemical stability of conductive particles is based on whether they have undergone oxidation that will increase or prevent electrical conduction, as well as, corrosion protection that will decrease their performance. Meanwhile, conductive film thermal performance depends on the substrate and the adhesive used in conductive film. There are different types of substrates that can withstand higher temperature. Higher curing

temperature is better for conductive film as it will cause an increase in the electrical conductivity provided that the curing temperature is below the glass transition of substrate and conductive paste adhesive.

2.1.1 Conductive Filler

The most important component of a conductive paste is the conductive filler. There are several conductive fillers that are widely used such as silver, copper and aluminium. The choice of conductive filler is mainly based on its conductivity, cost, and reaction to atmosphere. Each conductive particle has its own advantages and its advantages.

2.1.1.1 Silver - Ag

Silver has been the focus of studies in conductive film because of its high bulk electrical conductivity of $6.3 \times 10^7\ \Omega^{-1}.m^{-1}$ (Kamyshny, Magdassi 2014, Franey, Graedel et al. 1984, Gilleo 1995, Li, Moon et al. 2004, Perelaer, Klokkenburg et al. 2009, Felba 2011, Roberson, Wicker et al. 2012, Falat, Platek et al. 2012, Ten Cate, Gaspar et al. 2014). Another advantage of using silver over other metals, is that its oxide remains conductive. Non conducting oxides are a drawback among highly conductive metals particularly copper and aluminium (Kamyshny, Magdassi 2014, Gilleo 1995). There are several factors that affect the final electrical properties of printed silver conductor. One of which is the sintering technique used. There is a link between the creation of nanoparticles and the deposition of ink used. The sintering techniques that have been demonstrated for sintering of silver ink are electrical, IR lamp, and Argon Plasma (Kamyshny, Magdassi 2014). Silver nanowires can be used as transparent conductor in solar panels. Indium tin oxide was the primary material in the field of transparent conductor; however the price and vacuum deposition technique is its drawback, along with its tendency to crack when bent. The result of experiments shows that the composite of silver nanowire manage to perform both in its electrical and light transmittance requirements. The required sheet resistivity of transparent conductor is 100 Ω/sq and 80 % transmittance. The self-synthesis silver nanowire ink has sheet resistivity of 40 Ω/sq and maintains its required transmittance. (Yang, He et al. 2013). The limiting factor that inhibits silver from wide scale application is that it is affected by electro migration especially under high bias condition (Li, Wong 2006).

2.1.1.2 Copper - Cu

Copper is seen as best candidate to replace silver as metal filler in conductive film due to its conductivity and cost (Salam, Lai et al. 2011). The conductivity of copper is $5.96 \times 10^7\ \Omega^{-1}\cdot m^{-1}$ (Kamyshny, Magdassi 2014). The main drawback of this material is the requirement to be processed in an inert or vacuum environment. Copper readily oxidises in

air and its oxide surrounds the particle that forms a barrier that prevents particle to particle conduction. (Salam, Lai et al. 2011, Perelaer, Smith et al. 2010) In order to combat the oxidation of copper, Perelaer developed a low-viscosity conductive ink containing well-dispersed copper nanoparticles through a polyol process. There are several metals that can be used to coat the copper particle core to prevent it from oxidation. Materials such as silver and Graphene were used to encapsulate the copper. This method proved to be effective as no oxide were observed in the printed pattern and it was seen to be stable for several months. (Perelaer, Smith et al. 2010). The extra processing of copper will add to the processing cost of the conductive film. In addition, the solder ability of printed copper is poor as compared to etched copper due to high roughness of printed copper (Salam, Lai et al. 2011).

The oxidation of copper did not deter researchers from finding ways to process it through fast sintering methods such as intense pulsed light sintering (Khondoker, Mun et al. 2013). Microwave sintering is suitable for copper paste. The penetration depth of 2.45 GHz microwaves for metal powders is 1.6 mm (Perelaer, Smith et al. 2010). Microwave curing causes the increased in copper powder particles temperature that removes the copper oxide. This makes particle to particle contact possible (Qi, Vaidhyanathan et al. 2013). The electrical properties of copper, as for most material in conductive film depend on the curing and sintering temperature and duration (Espalin, Muse et al. 2014). The bulk resistivity of copper is 1.75×10^{-8} Ω m, copper that is cured at 150 °C resulted in a 2×10^{-6} Ω m resistivity that is 2 orders of magnitude larger than its bulk form. Increasing the sintering temperature to 400 °C and time to 60 minutes resulted in a 1.75×10^{-8} Ω m resistivity (Salam, Lai et al. 2011).

2.1.1.3 Gold – Au

Gold is also widely used as a conductive filler due to its highly conductive and inert nature. Gold has the conductivity of 4.42×10^{7} $\Omega^{-1} \cdot m^{-1}$ (Kamyshny, Magdassi 2014) and falls third in terms of conductivity rank. However, it is a noble metal and costs may be prohibitive for large volume applications (Li, Wong 2006b). The melting temperature of gold is 1063 °C, and with the help of the thermodynamic effect on 2 nm gold nanoparticle, the sintering temperature was decreased to 150 °C (Kamyshny, Magdassi 2014). The effect of using nano sized particle not only affect materials mechanical properties (Herrmann, Müller et al. 2007) but also its chemical, optical and electrical properties. This is because nano scale materials have a large surface to volume ratio, large surface energy and spatial confinement (Ko, Pan et al. 2007). Gold is inert in terms of oxidation, and its contact resistance is stable even when aged at 85 °C/ 85 RH (Li, Moon et al. 2004, Perelaer, J., and Schubert, U. S.

2010). This makes gold suitable for coating to make a reliable interfacial connection. Gold is used as coating on fine pitch electronics to prevent corrosion (Smith, Shin et al. 2006). The previous process to deposit gold is through electroplating, nowadays inkjet printing is available for electronics finish. The process can also be done under N_2 sintering and with nanoparticle to make the surface finish denser (Jang, Cho et al. 2011). Gold is also used as a protective coating on silver to prevent electro migration. (Smith, Shin et al. 2006). Another use of gold ink is in sensors that provide cheap, reusable, and point-of-care diagnostic devices (Ihalainen, Majumdar et al. 2013) and as a gold electrode coated with carbon for electro analytical use (García-González, Fernández-Abedul et al. 2015).

2.1.1.4 Aluminium – Al

Aluminium is another conductive material than can be used as filler material in conductive film because of its conductivity of $3.78 \times 10^7\ \Omega^{-1}\cdot m^{-1}$. Aluminium oxidise rapidly at a rate faster than copper, and therefore formulation is very hard to attain and the process of formulation becomes complex. Oxidation of aluminium can be avoided by using hydrocarbons solvents, low precursor concentration and processing in an inert atmosphere. Al undergoes rapid oxidation in air (~100 picoseconds) with formation of a dense thin amorphous non-conductive Al_2O_3 layer (2-6 nm) that results in loss of electrical conductivity and makes aluminium difficult to use for conductive ink formulations.

Only very recently, Al inks, which can be used at atmospheric pressure as printable formulations and not as part of a modified CVD process, have been claimed. Curtis et al. [212] printed amine coordination complexes of alane, H_3AlNR_3, and trialkyl aluminum compounds (R_3Al) on a silicon substrate of a solar cell heated to temperature greater than about 140 ºC, under inert N_2 atmosphere. Rockenberger et al. [213] refers to a broad range of aluminum compounds, stabilized with donor ligands and capable of decomposition at temperature around 100 ºC. The process is anticipating the expected use of printing and curing under inert conditions. The aluminum contact layer was printed on silicon substrate heated to 150 °C - 200 °C in inert atmosphere, Argon(Ar) or Nitrogen (N_2), with the use of organometallic Al compound (amine complex or alane) (Bonea, Brodeala et al. 2012). The aluminium paste was used as back emitter conductor in solar panels at 50 um thickness, that requires two passing, screen print (R. Woehl, J. Krause et al. 2011) Silicone glasses were added to a aluminium paste to make up a back contact of solar panel. The experiment reported an increase of 1.34 % in conversion efficiency from 16.01 % to 17.35 %. (Chiu, Cheng et al. 2014)

Study has been made in order to ink jet this material in micro sized particle. Nanometre sized Aluminium particle causes a ring effect of the material. This is because surface tension

forces the particle outwards, and stays out of the circle to create circle line when the ink dries. The result of using Electrohydrodynamic pulsed-inkjet EHD inkjet printer that can accommodate inks with larger size Al particle, with ink particle loading of 1- 10 % by weight (Kang, Lee et al. 2011). There has not been much interest on using aluminium paste, maybe because of oxidation and hazard of the material when handled in powder format. The material readily oxides in air, the oxide creation form a protection for further oxidation.

2.1.1.5 Carbon

In 1958, carbon paste was introduced by Ralph Adams of Arkansas University to function as electrode. The paste was a mixture of graphite powder and adhesive (Švancara, Vytras et al. 2009). Carbon has high thermal and electrical conductivity that has made other carbon containing materials such as graphite, carbon black and carbon nanotube (CNT) used as conductive fillers (Lebedev, Gefle et al. 2015). The conductivity of carbon is $1.25 \times 10^3\ \Omega^{-1} \cdot m^{-1}$. Graphite platelets and carbon black have been mixed together to form carbon ink. Carbon black, because of its submicron particle size, fills void between platelets to create dense films. The final electrical, mechanical and processing ability of the ink depends on the carbon black and graphite ratio (Jewell, Hamblyn et al. 2013). Screen printed fine lines can be achieved using low particle loading. Sheet resistance of between 8 and 130 Ω/sq can be achieved using screen printing method (Jewell, Hamblyn et al. 2013).

Mercury (Hg) was banned by The European Union as a sensing material for heavy metals and carbon is seen as a replacement. Carbon sensors can detect Lead, Cadmium and Copper in water (Honeychurch, Al-Berezanchi et al. 2011). The carbon paste used was electrode, sensor, and detector (Švancara, Vytras et al. 2009). Carbon is used as filler material in conductive film to create printed electrodes and resistors (Pudas, Halonen et al. 2005),(Subramanian, Chang et al. 2008),(Unander, Nilsson 2009). The application of carbon has been limited to certain applications because it has a high sheet resistivity value of 55 Ω/sq compared to silver with 0.1 Ω/sq applied using conductive pens (Kawahara, Hodges et al. 2014). Although carbon has a high resistivity value, it is cheap, light and chemically stable which means it does not corrode and is not easily affected by humidity (Unander, Nilsson 2009). Therefore, this material remains attractive for conductive film application. One of the improvements is the electrical properties of this material. Double filler method, mixing high conductivity filler material such as silver to low conductivity material such as carbon, has been incorporated to increase its electrical resistivity (Lebedev, Gefle et al. 2015). Carbon is also mixed with conductive polymer in order to produce anti-static coating (Omastova, Chodak et al. 1999). The flexographically printed sensor with carbon-based ink (RH4) did not deteriote at 20 % to 90 % relative humidity test (Unander, Nilsson 2009).

2.1.1.6 Carbon nanotube (CNT)

Carbon nanotubes are sheets of graphene rolled into cylinders, and are a recent form of carbon that was identified in 1991 by Sumio Iijima of NEC, Japan. Single wall carbon nanotubes (SWCNTs) and multiwalled CNTs (MWCNTs) are the type of nanotubes are shown in Figure 2 (Jing Li, J. K. Lumpp 2006). SWCNTs are composed of a single shell of graphene and typically have diameters ranging from 0.4 to 4 nm (Cummins, Desmulliez 2012). MWCNTs are composed of multiple, concentric shells of graphene and can have diameters ranging from several to tens of nanometres. SWCNTs can be rolled up in multiple ways, which can lead to some having semiconducting properties and others having metallic properties (Cummins, Desmulliez 2012). SWCNTs are usually produced by chemical vapour deposition using metal catalysts, but other growth techniques are available in the form of arc discharge, and laser ablation (Cummins, Desmulliez 2012, Jones, Lu et al. 2010) The metallic properties of MWCNTs are due to its roll direction (Cummins, Desmulliez 2012). Although, the inner tube of MWCNT has less contribution to its current carrying capability (Kamyshny, Magdassi 2014).

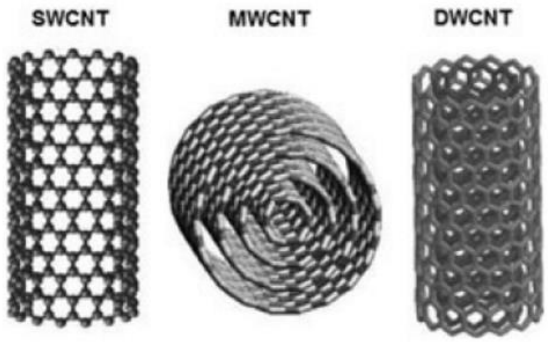

Figure 2 Illustration of a multiwalled carbon nanotube

The diameter could be from 1-50 nm and up to few mm in length and capped with fullerene dome consisting of five or six member rings (Njuguna 2013). Properties of CNT can be modified by attaching molecules to functionalize the nano-tube.

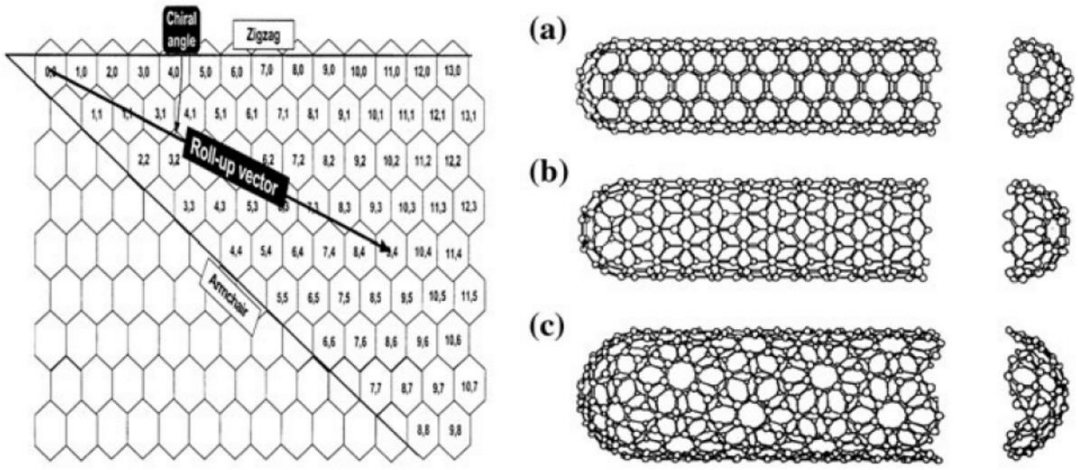

Figure 3 Illustration of carbon nanotube with different degree of twist

The chiral structures that forms the CNT (Njuguna 2013) functionalize the nano-tube to adjust its properties are shown in Figure 3. CNTs are chiral structures with a degree of twist such that the graphite rings join into cylinders (Jing Li, J. K. Lumpp 2006). The zigzag tubes are narrow gap semiconductors. The electrical properties can be varied and determined by the chirality, diameter of the tube, detailed curvature and local environment.(Katzir, Yochelis et al. 2014) CNT has electrical conductivity of $1.04 \times 10^{4}\ \Omega^{-1}\ m^{-1}$. Its thermal conductivity is 6600 $W \bullet m^{-1} \bullet K^{-1}$ and Young's modulus lays around 1 TPa. The tensile strength of CNT ranges from 30 GPa to 1 TPa. The density of MWCNT depends on its chirality and is is 2.6 g/cm^3 while SWCNT ranges from 1.33 to 1.40 $g \bullet cm^{-3}$ (Jing Li, J. K. Lumpp 2006). The environmental performance of CNT filed paste was tested on thermal cycling (-40 ° C/ 125 °C) for 1000 h, elevated temperature +65 °C for 30 minutes and low temperature storage -12 °C 10 cycles, and the performance of CNT revealed that it can withstand harsh conditions. The SEM analysis did not reveal any significant changes in their microstructure (Janeczek, Jakubowska et al. 2012).

2.1.1.7 Nickel - Ni

Highly conductive metals may have one or more of the following characteristics such as expensive, chemical reactivity, electro migration, corrosion and oxidation that limits their use in high volume applications as a conductive film conductive filler (Lin, Zhong 2008). Nickel is one of these highly conductive materials used as conductive filler in conductive film that has its own negative traits. Though a cheaper alternative to silver and gold in terms of interconnect, tests show that accelerated aging results in surface corrosion and oxidation (Li, Wong 2006b). This eventually led to instability of its electrical conductivity performance.

The accelerated testing was based on high-temperature and high humidity conditions (Li, Wong 2006b).

Nickel being inexpensive still attracts researchers to pursue its use in the conductive film world. It is compatible to conductive film processes such as inkjet printing and screen printing. Nickel ink that can be used in inkjet printing is a mixture of Ni salt, complex agent in a low molar mass and a reducing solvent. There has been work on sintering of nickel paste to form conductive lines using flash light irradiation. A mixture of nanoparticle sizes between 5 nm to 500 nm shows sintering. Nickel sintered using flash irradiation techniques produced a 76.34 μΩ cm resistivity, the electrical resistivity to be used as multilayer ceramic capacitors electrodes and super capacitors (Park, Kim 2014).

In order to be used in fine pitch interconnection at lower cost, polymeric particles are coated with mixture of Nickel and Gold (NiAu) (Li, Wong 2006b). Nickel alloy was used as a sacrificial layer to reduce the effect of galvanic corrosion on active metal. Galvanic corrosion occurs when a metal undergoes accelerated corrosion due to the presence of a corrosive electrolyte and an electrical contact with a non-metallic or a more noble material. . Nickel is used to coat silver to prevent electro migration (Li,Y. 2006) or by replacing the silver entirely with nickel conductive filler (Pudas,M. 2005).

2.1.2 Substrates for conductive film

The choice of substrate is important to conductive film as it can influence the thermal performance of the conductive film (Janeczek,K. 2012). The curing temperature and sintering temperature depends on the substrate glass transition temperature for polymer materials such as Poly(ethylene terephthalate) (PET), Polyethylene-naphthalate (PEN)
, and Polyimide (PI). Meanwhile paper and textiles main parameter of interest is the roughness and smoothness. The roughness and porosity will affect the electrical properties of the cured conductive film. The surface area increases as the roughness increases, and this causes the resistivity to increase. Paste tends to be absorb if the material is porous. With the same amount of ink, the porous substrate will result in higher resistivity than with the less porous substrate. Discussed in this chapter are the common substrates in conductive film that are compatible to conductive film. There is no limitation in selection of substrate material for conductive film, however proper consideration must be taken in order improve the final cured electrical properties. The curing temperature is based mostly on the substrate, and increasing the curing temperature will increase the conductivity of the conductive ink.

2.1.2.1 Poly(ethylene terephthalate) (PET)

Poly(ethylene terephthalate) (PET) is very popular substrate in conductive film because it is low cost, can be transparent, light weight, flexible, and robust (Homola,T. 2014, Woerle,J. 2011). This substrate is also compatible with large area roll to roll processing. However, PET has a low surface energy that results in a low surface wettability, poor adhesion to coatings and low printing properties. PET therefore requires surface treatment prior to any printing process (Homola,T. 2014). Several plasma treatments including ambient air plasma are available to increase the surface energy of PET films that is also applicable to roll-to-roll substrates (Homola,T. 2014).

2.1.2.2 Polyethylene-naphthalate (PEN)

Another widely used substrate in conductive film, besides PET is the polyethylene-naphthalate (PEN) because of optical transparency, smooth surface and excellent barrier properties (Zacharatos,F. 2016). In addition, it has high stiffness, mechanical strength, chemical resistance, low thermal shrinkage (0.4% in 75 °C•hr^{-1}) (Tsay,C.-Y. 2013; 341 Zacharatos,F. 2016; 150 Janeczek,K. 2012), and thermal barrier compared to other polymers such as polyethylene terephthalate (PET) (Montanino,M. 2015). But above all, it is the glass transition of 120 °C that is slightly better than PET that is only around 112 °C. PEN can even reachmechanical stability between 180 ° to 200 °C when it is categoryed to extra heat treatment (Yakimets, Barink et al. 2010). Using PEN as a substrate increases the hall mobility and electrical resistivity of Zinc Oxide (ZnO) coatings. ZnO has semiconducting ability and applications in chemical sensors, optical detectors, photovoltaic and transistors were realised (Tsay,C.-Y. 2013).

PEN substrate is compatible with solvent cleaning with acetone and isopropyl to remove surface residue. Wettability can be improved by using UV-Ozone treatment for 5 minutes UV Ozone decreases the water contact angle to about 34 ° after surface treatment. This promoted good wetting and adhesion (Montanino,M. 2015). The substrate was used in production of RFID antennas (Janeczek,K. 2012), polymer solar cells (Montanino,M. 2015), transistors, semiconductor films through spin coating (Tsay,C.-Y. 2013), flexible displays and sensors , and wearable medical applications (Zacharatos,F. 2016).

2.1.2.3 Polyimide (PI)

Polyimide is famous for high temperature properties, low dielectric constants, inertness to solvents, and long-term stability. Patented by Dupont in the 1950s, this was followed by commercial polyimide film introduced by Dupont in the late 1960s (Ghosh, M.K. 1996). This material has glass transition (Tg) of 400 °C and is compatible not only to conductive film but also with microelectronics processing (Zacharatos,F. 2016). Because of its high glass

transition, conductive ink can be cured at higher temperature. In order to improve or optimize the process, laser direct writing of conductive silver ink was administered. And the result was quite astonishing. Laser direct writing managed to achieve 4 times the bulk resistivity of the silver (Cai,Z. 2011). Substrate preparation for polyimide can be done using acetone and methanol bath in an ultrasonic cleaner for 10 minutes. The surface can also be activated to increase the adhesion of printing using Argon plasma for further 10 minutes (Xu,Jun 2011). Other processes to increase wettability on polymer substrates include corona discharges, ultraviolet irradiation, and electron bombardment (Goo,Yong-Sung 2010)

2.1.2.4 Paper

Paper is another popular substrate because of its abundance, cost and it is light in terms of weight. The most important characteristics of using paper as a substrate are because of its end of life processing. Paper can be recycled by deinking, more so metals can be recovered either by incineration or separation technique. These improve the life cycle assessment of its overall economic performance (Dogome,Kazutomo 2013;250 Määttänen,Anni 2010).

Special coatings are necessary to lessen the paper roughness and surface energy. The formulation of these special coatings is not general and is special to individual substrates based on their intended application (Denneulin,Aurore 2008) . The surface roughness, absorption and porosity are the main factors that affect the electrical conductivity of coatings on paper. The print thickness value needs to be larger than the size of the pores in the paper to form a conductive path (Määttänen,Anni 2010). Paper surface layers with small pore sizes and high porosities produced highly conductive, narrow silver tracks because of quick ink absorption, as observed in photo-quality ink-jet paper. Furthermore, the surface roughness induces a high resistance to peel-off force at the expense of conductivity, and this improvement in the peel-off resistance is considered to be achieved because of the anchor effect of silver nanoparticle inks which fall into dents present on the rough paper surfaces (Dogome,Kazutomo 2013). When the absorption and surface roughness is low, it is appropriate to match the surface energy of the substrate to that of the ink to improve the print resolution and conductivity (Öhlund,Thomas 2012) .

The level of conductivity and print resolution using paper as a substrate can be altered by pre-treating the paper. The level of conductivity of coatings on pre-treated paper can even match that of a polymer film that is traditionally used in electronic industry. The treatments are a suspension primer to improve smoothness, surface energy and absorption to that of polyethylene terephthalate (PET). Paper soaked in fluorinated polymer solution, a dissolved polymer solution, can affect surface energies of the paper. This causes the paper to be

hydrophobic and provide silver tracks with improved electrical conductivity and better print resolution. UV curing varnish, meanwhile, affects conductivity by smoothening substrate roughness (Denneulin,Aurore 2011).

2.1.3 Materials summary

The conductive filler used in conductive film is based on its bulk electrical properties. Conductive metals have been a material of choice as filler materials for conductive film because of its conductivity. Silver (Kamyshny, Magdassi 2014, Franey, Graedel et al. 1984, Gilleo 1995, Li, Moon et al. 2004, Perelaer, Klokkenburg et al. 2009, Felba 2011, Roberson, Wicker et al. 2012, Falat, Platek et al. 2012, Ten Cate, Gaspar et al. 2014), copper (Salam, Lai et al. 2011), gold, aluminium (Kamyshny, Magdassi 2014) and nickel (Lin, Zhong 2008) are the metals that are commonly used in conductive film. Metal conductive filler might be an obvious choice to achieve high conductive printed structure; however each has its own disadvantage too. Silver is susceptible to electromigration preventing it be used widely (Li, Wong 2006). Gold does not oxidise making it suitable for coating and interfacial connection (Li, Moon et al. 2004, Perelaer, J., and Schubert, U. S. 2010). The high cost of the gold is limiting factor for it be used in wide scale application (Li, Wong 2006b). Copper, aluminium and nickel are much cheaper alternative but it oxidises rapidly in air which forms an insulating barrier on its surface (Kamyshny, Magdassi 2014). Additional process is needed along with inert atmospheric condition for copper and nickel to be printed (Salam, Lai et al. 2011, Perelaer, Smith et al. 2010). Carbon is another conductive material for conductive paste which was introduced in 1958. Carbon can be in a form of graphite, carbon black and carbon nanotube (Lebedev, Gefle et al. 2015). Carbon black is a mixture of graphite platelets and submicron particle size, fill the void and between platelets . Identified in 1991, carbon nanotubes (CNT) are rolled graphite in to single or multiwall cylinders (Lebedev, Gefle et al. 2015). CNT can withstand harsh condition and behaves either metallic or semiconductor depending on chirality (Cummins, Desmulliez 2012).

The materials for substrate of the conductive film are either made out of plastic, paper or textile. The plastic are polyethylene terephthalate (PET), PEN and Polyimide. The plastic substrate differs mainly on the glass transition (Tg) and cost. Somehow, the cost of the plastic substrate is proportional to its glass transition. PET is the cheapest among the group and also has the lowest glass transition of 112 °C (Yakimets, Barink et al. 2010). PEN is known for optical transparency, smooth surface and excellent barrier properties. It has Tg of 120 °C (Yakimets, Barink et al. 2010). Ozone treatment was used to improve the wettability of this substrate (Montanino, De Girolamo Del Mauro et al. 2015). Polyimide was patented by dupont in 1950 has a high Tg of 400 °C (Zacharatos, Makrygianni et al. 2016, Ghosh,

Mittal 1996). Other properties of polymide are low dielectric constants inertness to solvents and long-term stability. Paper is cheap because it is abundant in nature. It is lightweight and recyclable making it attractive for conductive film (Määttänen, Ihalainen et al. 2010, Dogome, Enomae et al. 2013). Paper has the requirement for pre-treatment to improve surface roughness, similar to coatings made on photo quality paper (Dogome, Enomae et al. 2013).

2.2 Printing Processes

The aim of conductive film printing process literature review is to determine a suitable printing process that will produce a consistent conductive film. Printing process such as screen printing, press roller, and inkjet was studied. The printing process is simple as compared to the vacuum processing and subtractive processing technique. The complexity of printing of conductive film is caused by formulation of the paste to be used by different printing process. The conductive ink used by inkjet printing is not compatible with screen printing process because each process requires certain type of ink viscosity.

The printing of conductive film requires transferring of conductive paste from the ink reservoir to substrate to create an electronic device and interconnect. There are several factors to consider in each every print process. They are particle loading, and viscosity. Screen printing was the only process that was used extensively in this thesis. Screen printing of conductive film is an established printing process. In addition, the changing print design is relatively easier as compared to press roller printing.

Pressed roller printing means that a roller that contains an image will be transferred to the substrate by impression. Web speed is the term use to quantify the substrate travel speed in roll to roll printing. This type of printing technique is fast and preferred by the industrial scale manufacturing. However, for small scale and research purposes, to change print design will be costly and time consuming. The screen printing technique comes in second to pressed roller printing in terms of printing speed and ease of pattern change. The third technique is inkjet printing, which is flexible in terms of changing the design pattern. This is also cost effective for ink consumption as it only consumes the ink it needs. However this is very slow since it is printing line by line.

2.2.1 Screen Printing

Screen printing is an ancient technique which the Chinese and Egyptians utilised. The main application is in graphic art to make product more attractive. The company called Dupont de Nemours manufactured the first silver screen-printing paste in 1939. This is when the application of screen printing in electronics begun. The initial applications of screen printed devices were mica capacitors, carbon film resistors, conductive patterns on alumina substrates, and insulating films (Ménil,F. 2005). There was a rapid growth of screen printing activities to create electronic devices in the 1950s. Printed circuits were made on alumina substrates to create stacked wafer modules. 10-15 years ago, screen printing activities were concentrated on electronic circuits. Commercial pastes that can withstand higher temperature, normally above 150 °C, were developed. The thick film hybrid circuit has had a constant growth primarily because of the invention of the transistor and subsequently the integrated circuit (IC). The growth of screen printed electronic devices, however, declined at the beginning of nineties because of the increase in integrated circuits functionality and increase in density of surface mount technology (SMT). Nowadays, the application of screen printing in electronics is less obvious. It can be seen now in heating resistors, and gas sensors for the automotive industry (Ménil,F. 2005). The screen printing process can be transformed into a large scale and roll to roll process by using rotary screen printing. The screen is attached to a circular frame while the squeegee is inside to spread the ink. The substrate is fed between the rotary screen and the supporting roller (Krebs,F.C. 2009).

Screen printing has numerous process parameters that can affect the final cured properties. The parameters that are important to take note of are mesh count, mesh diameter, print speed and emulsion thickness. The print speed is programmed to the automatic screen printer. The screen parameters are important figures that are set by screen producer.

In order to print in high resolution the value of mesh count needs to be associated with a small wire diameter (Debeda-Hickel,H. 2005). The print speed has an effect on the resistance value of the cured conductive film. Increasing the print speed from 50 $mm \cdot s^{-1}$ to 200 $mm \cdot s^{-1}$ increases the resistance by 8% (Salam,B. 2011). The uniformity and print tolerance are also affected by changing the print speed. There is a 21 % improvement in print uniformity just by changing the speed from 50 $mm \cdot s^{-1}$ to 150 $m \cdot s^{-1}$. The print tolerance obtained was 10 % when the print speed was 200 $m \cdot s^{-1}$, although increasing the print speed will not improve the tolerance even further

The emulsion thickness affects the final cured thickness of the paste. Increasing the emulsion thickness will cause the thickness of the cured paste to increase (Debeda-

Hickel,H. 2005;Hobby,A. 1990). Printing with a thin emulsion screen will also produce high resolution structures. (Hobby,A. 1990).

The process of screen printing involves a mask with a structure that contains the design to be transferred to the substrate. The screens are made out of polymer material, stainless steel or silicon. Popular polymers used as screen fibres are nylon and polyester. Each of which have advantage and disadvantages. Mesh made out of polyester is often called polymesh screen (Hyun, Secor et al. 2015, Kim, Kim et al. 2010). The factors to consider in choosing the right material in screen printing electronics are its tensile strength, stiffness, moisture absorption, cost and print resolution. In order to produce high tensile strength and stiffness, screen filament requires being high tenacity. Meanwhile, low shock resistance is due to low resilience fibres. In terms of moisture absorption, mesh made out polyester and stainless steel performs very well. Moreover, polyester elasticity is greater than nylon and therefore has higher reproducible rate. Nylon is another popular polymer material used as screen mesh. It can produce 50 k to 100 k impressions, thanks to its high elongation rate, while the stainless steel can only perform 5 k impression. However, Nylon absorbs moisture and this greatly affect its application as screen fibre in printing electronics. The polyester screen represents the best compromise between lack of resilience of the stainless steel and high elongation of the nylon. The cheapest among the screens is the polyester screen. Although stainless steel produces high resolution structures, it is costly and only available in higher gauge meshes. The frame where the screen is attached is either made out of wood, aluminium alloy or plastic (Dubey,G.C. 1974).

Screen printing technology in printed electronic produces both the wiring interconnect, and interface and electronic devices. Screen printed devices include chemical (Ménil,F. 2005), and physical sensors, heating resistors, varistors, and capacitors (Debeda-Hickel,H. 2005). Silk-screen process was formed to make circuit patterns in the fabric (Kim,Y. 2010), fuel cell printing, (Rotureau,D. 2005;388 Ménil,F. 2005) and thermoelectric generator (Cao,Z. 2013). Screen printing of transparent conductors such as PEDOT:PSS, silver or silver-aluminium are commercially available screen printable ink formulations in solar cells (Krebs,F.C. 2009).

2.2.2 Press roller printing of electronics

One of the many attractions of conductive film is that it can be processed using roll to roll printing. The roll to roll printing technology can achieve 30 $m \cdot min^{-1}$ to 100 $m \cdot min^{-1}$, depending on the process, which is an obvious advantage for large area and high throughput printing (Cantatore 2012).

2.2.2.1 Flexography

Flexography is an improvement of letter press or rubber stamp that uses a flexible elastomeric plate. This type of printing is widely used on non-porous substrate for food packaging, but is also compatible with plastic, metallic films and paper substrates.

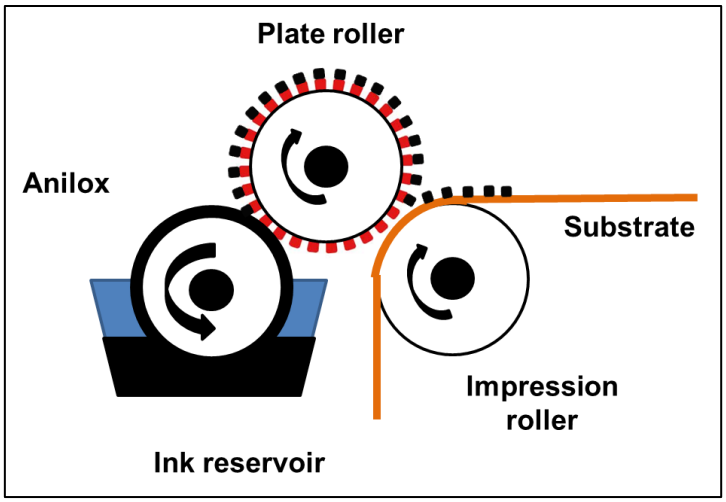

Figure 4 The diagram of flexography printer

The diagram of a basic flexography printer is shown in Figure 4. The main parts of flexography include ink reservoir, anilox roller, plate roller and the impression roller. The ink reservoir contains the ink to be deposited on the substrate. The anilox roller contains microcavities to fix volume ink transfer from ink reservoir to the plate roller. The plate roller contains the features on a raised surface, and transfers the ink from the anilox roller to the substrate. The impression roller presses the substrate to the plate roller that will transfer the ink to the substrate.

Photolithography techniques and laser engraving are the technology used to create the flexible elastomeric plate that is wrapped around the plate roller. Structure that has fine features is the result of ink development and elastomeric plate for pattern transfer. The following are the impact forces involved in flexography printing. Anilox force (F_a) is the force applied when the anilox roller is brought in contact to the print plate to transfer ink in the anilox cavity to the raised surface of flexo plate. Print Force (F_p) is required when flexo plate is to transfer the ink on the patterned surface onto substrate.

The effect of low print pressure is less spreading of ink and increase in variation of print structure. Increasing anilox force will cause the line width to increase by at least 25 % at low print force and 6% at high print force. Line width could be increased if more anilox force and

print force is applied. Anilox roller will pick more ink if pressure is increased. The elastomeric plate attached on the surface of the flexography plate deforms if the contact force is increased causing the ink to spread. A hollow effect in the centre of the lines could happen when excessive contact force is applied. This is mainly caused by the deformation of the plate. The majority of the ink squeezed to the edges of the patterned features on the plate (Keng,L.B. 2011).

2.2.2.2 Gravure printing

Gravure printing system consists of engraved gravure cylinder, doctor blade, impression roller and ink pan. The gravure cells that are engraved on the surface of the gravure cylinder transfers the ink from the pan to the substrate. The rotation of the gravure cylinder in the ink pan causes the gravure cells to be filled with ink.

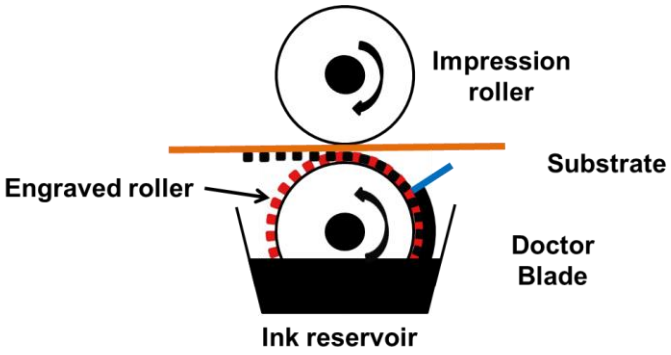

Figure 5 Basic structure of gravure printing technique

Shown in Figure 5 are the basic components of the gravure printing technique. The doctor blade removes excess ink from the gravure cylinder. The impression roller presses the substrate to the gravure cylinder that causes the ink from the gravure cells to be transferred to the substrate (Narakathu, Reddy et al. 2011).

2.2.3 Inkjet printing

Ink jet printing is line by line printing of structures using a drop of ink. This process is therefore has slower print speed of 20 $m \cdot min^{-1}$ (Cui, Zhou et al.)compared to roll to roll printing, however this is a process of choice for small scale printing. Inkjet printing is susceptible to nozzle clogging. The development of ink that is compatible to inkjet printing that is not particle based has been achieved (Dang, Dung Dang et al. 2013). Large particle is the main cause of nozzle clogging in inkjet printing. Ink jet printing can be categorised by two main types. First is the continuous ink jet and the second is drop on demand. Inkjet printing

is the process of choice in small scale printing because print structure can be changed in an instant.

2.2.3.1 Continuous Ink Jet (CIJ)

A continuous stream of droplets that is uniformly sized and spaced is forced out of the inkjet nozzle. The ink is pumped out of the ink reservoir into ink jet nozzle. Droplets are being form by the transducer that is driven by the signal from the controller. Each droplet is charged by an electrode that is connected to the charge driver.

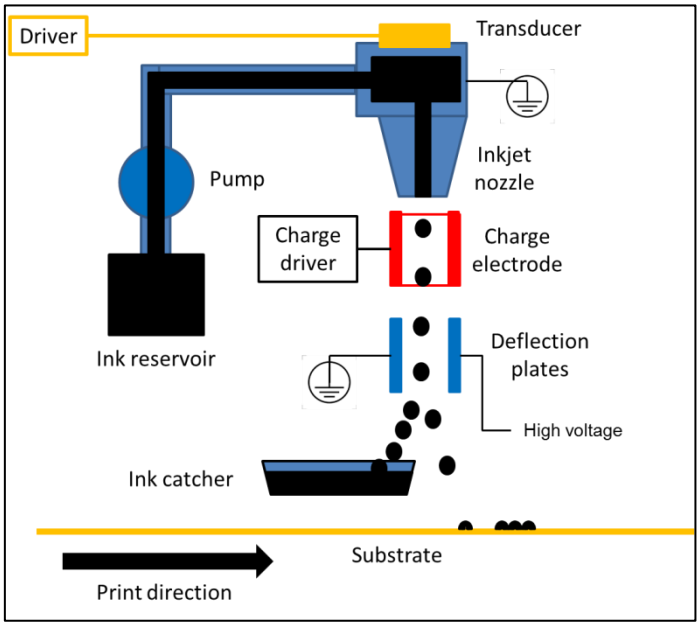

Figure 6 Schematic of continuous type ink-jet system

The continuous type ink-jet system is shown in Figure 6. The charged droplets can be steered to the desired location and those that are not charged will hit the gutter and be used for recycling. IBM produced the first commercial CIJ printer in 1976. This type of inkjet is complex and the recycled ink degrades when it is exposed to the ambient condition (55 Cummins,G. 2012).

2.2.3.2 Drop on Demand (DOD) Inkjet

Inkjet printing starts with the creation of a design layer, a rectangular matrix that is a black and white bitmap design file. Drop on demand inkjet is an alternative process to continuous inkjet. This type of inkjet is much simpler than its CIJ counterpart because it removes the requirement for droplet charging, deflection and ink recirculation. Radio Corporation first used this type of inkjet in 1940 in the form of a fax machine but unfortunately did not achieve commercial production.

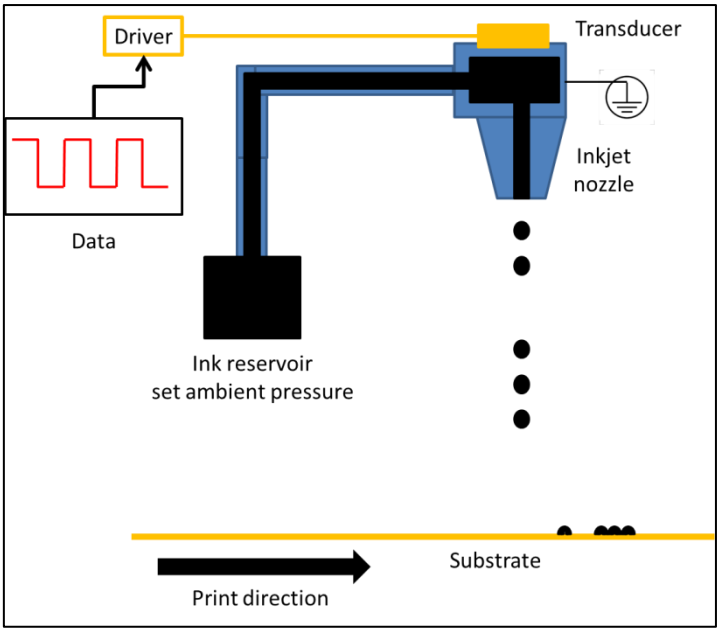

Figure 7 Schematic of a drop-on-demand ink-jet system

The schematic of drop-on-demand ink-jet system is shown in Figure 7 (55 Cummins,G. 2012). Different types of drop on demand ink jet are categorised by the orientation and process of producing droplets. The different drop on demand ink jets are squeeze, bend mode, push mode, thermal, electrostatic and Inktillegent ®. In the squeeze mode approach transient pressure waves are formed during the application of voltage to a piezoelectric disc. The mechanical deflection of the piezoelectric disc will cause droplets to be ejected out of the print nozzle. The thermal print head uses a heating element to form an air bubble. The bubble changes the volume of the ink chamber thereby forcing ink out of the nozzle. Electrostatic ink jet printing uses the charge on the ink to form droplets. Inktillegent uses an atomiser to create tiny droplets that are carried to the nozzle by a stream of air. Inktillegent is similar to aerosol technology. Drop on demand print head - Squeeze mode - Electrostatic

The electrostatic printer is suitable for highly viscous thick film ink. The ink reservoir has a conductive nozzle that is weakly pressurized. The pressure together with gravitational pull forms a convex meniscus at the tip of the nozzle. The size and shape of the meniscus contributes to the print quality. The nozzle is connected to high voltage potential while the substrate is connected to the ground. This connection will create a high electrostatic field to form a droplet. The ink flow depends on the potential of applied voltage.

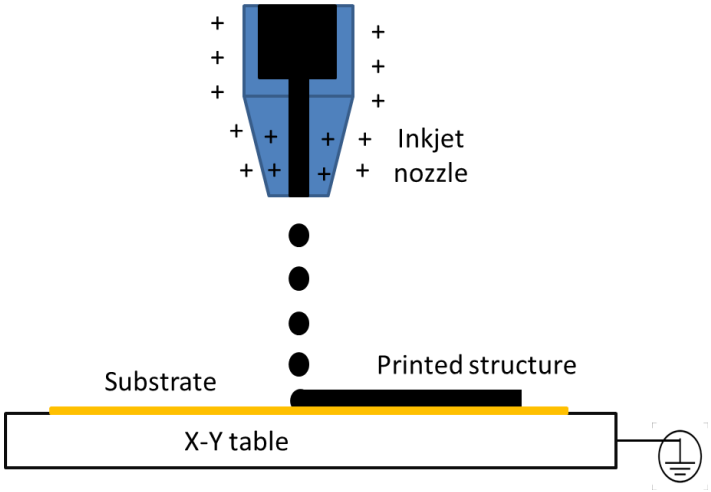

Figure 8 Schematic of electrostatic thick-film printing

The schematic of electrostatic thick-film printing is shown in Figure 8. The ink ejection is determined by two forces such as electric force and surface force. Electric force is produced by the application of high voltage, further increase of the potential will lead to overcoming the surface force resulting in ink ejection. High electrostatic stress located at the bottom tip of the droplet pulls down the tip of the droplet even further to form an ink cone. The highest stress point is located at the tip of the ink cone. The droplets travel from the high electrical potential to the low electrical potential on the substrate along the electric field lines. The highest concentration of the ink ejection is along the shortest field line, thus leading to the thicker spray from the tip of the cone.

A certain voltage called critical voltage is when the induced electric force equals the surface force of the ink at the tip of the ink cone. The critical voltage is dependent on the shape of the nozzle, the ink solvent and humidity of air, which affects the electrical resistivity of air. If the electric force is larger than the surface force of the ink, ink ejection occurs. A high electrical voltage is applied to the nozzle and the substrate is grounded. The applied voltage is increased until it overcomes the surface tension of the ink, where the ejection of droplets is produced. Further increase in voltage will increase the rate of ejection and will cause corona discharge will occur. Semi-spherical droplets at the tip of the nozzle form due to the pressure inside the reservoir and due to gravitational force. High electrostatic stress forms at the bottom tip of the droplet because it is a sharper point and positioned close to the grounded substrate. The high electrostatic stress pulls down the ink to form droplets.

Electrostatic printing is affected by cone formation at the nozzle, the voltage, the pressure, and the distance between the nozzle and the substrate. The ink meniscus at the

tip of the nozzle is dependent on ink viscosity, applied voltage, nozzle diameter, and the pressure inside the ink channel.

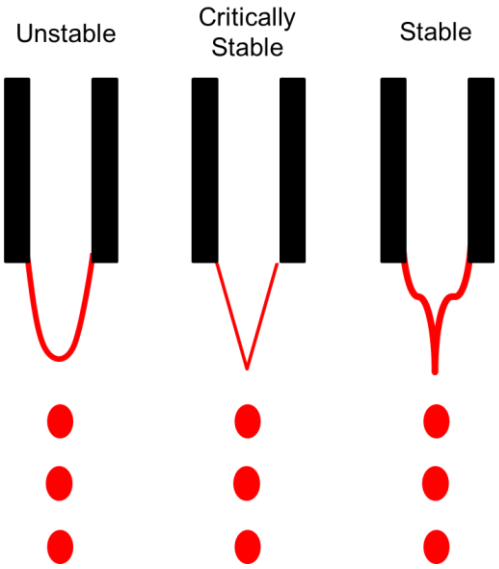

Figure 9 The shape of droplets in the electrostatic print nozzle

Convex shaped meniscus has a high probability to stop ink flow and a high chance of ink drift occurring. In the critically stable case represented by a triangle shaped meniscus the chance of stoppage depends on external factors. The concave shaped meniscus is provides stable printing and unlikely to stop ink flow unless great force is applied.

The instability of the print is dependent on the size and thickness of the convex meniscus as shown in Figure 9. The pressure inside the ink chamber has an effect on the meniscus formation and print quality. Right amount of pressure will cause convex meniscus, while high pressure will result in ink to drift and low little pressure will prevent formation of any meniscus. It was found out that the pressure and voltage potential are indirectly dependent parameter. There is a certain pressure at different voltages that produces clear defined print. Electric field is formed when voltage is applied between the nozzle and the substrate. These cause the ejection of ink droplets to the substrate.

Tests have been performed on the amount of voltage to be applied between the nozzle and the substrate. Application of high voltage will cause corona discharge, and low voltage will prevent the formation of droplets, the voltage was set between 3 k to 4 kV to produce best result. Electric field is also affected by the distance between the nozzle and the substrate, and external influences that reflect in print quality and repeatability.

Aerodynamic drag resistance is proportion to the distance between the nozzle and the substrate. The velocity and direction of the droplet is affected by aerodynamic drag. The following are the drawbacks of using this type of printer. Water based ink that is low resistivity is difficult to implement while it is easier to print high resistivity solvent based ink. The dielectric property of the substrate should low for best result. Metallic substrate causes corona discharge. Plastic substrate cause severe haze (Teng, Mostafa et al. 1990).

2.2.3.3 Drop on demand print head - Inktelligent

The aerosol is produced by the “Atomiser” from the suspension. The carrier gas permits the movement of the aerosol to the printhead. Ultrasonic source or high velocity air stream can produce aerosol that has a diameter of 1 µm to 5 µm. The sheath gas in the print head focuses the aerosol beam and prevents the nozzle from clogging.

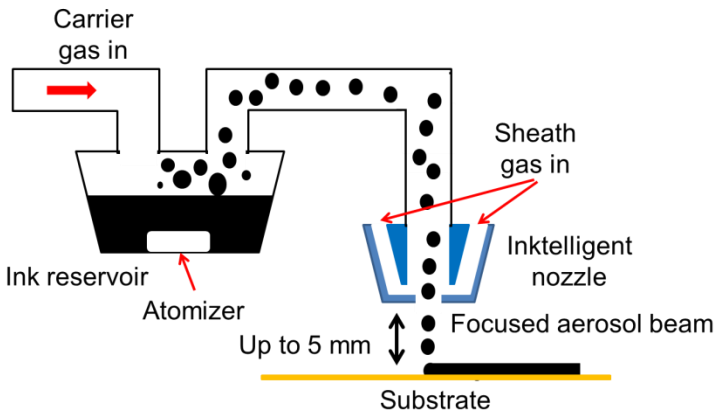

Figure 10 The aerosol jet technology developed by Optomec, Inc.

The schematic of the Inktelligent system is shown in Figure 10. The printed suspension needs to be at viscosity range of 0.7 to 1000 mPa and particle size of 1 µm. The aerosol jet printing is effective if the suspension has viscosity of 0.7 to 1000 mPa and the particle size is 1 µm or less in diameter. The minimum line width of around 10 µm can be used to print on both planar and non-planar surface. This printing technique can print an entire device structure, from substrate, conductive structure, and protective layer of polymer to protect the metal structure from the elements (435 Maiwald,M. 2010).

2.2.4 Process summary

The ancient printing technique of screen printing still continues to be develop into high speed and roll to roll printing (Krebs 2009). This perhaps is the reason why the first silver conductive paste developed by DuPont in 1939 is based on this process (Ménil, Debéda et al. 2005). The important parameters in screen printing are the mesh count, mesh diameter,

print speed and emulsion thickness. Mesh count and mesh diameter is associated with print resolution (Debeda-Hickel, Lucat et al. 2005). Print speed affects the final resistivity of the print and print quality. Print emulsion affects the print thickness. The material for screen is based on number of impression and the quality it brings to the final product. Screens are made out of either polymer material or metal. Polymer material can make more impression and cheaper than metal, however metal can provide high resolution print (Dubey 1974).

The roll to roll printing is the process of choice for large scale, and high speed manufacturing. The speed on which the substrate travels through the printer is called web speed. Roll to roll printers differs mainly on the plate roller which contains the print design. Flexography is like a rolled rubber stamp while the on the gravure has engraved roller. On the flexographic roller, ink sits on top of the rubber feature wrapped around the plate roller (Keng, Lai et al. 2011). The gravure printer carries the ink through the gravure cells (Narakathu, Reddy et al. 2011).

Inkjet printer is very cost effective because there is no requirement for template changes and mask design. The circuit designer will be able to print the design straight substrate of choice, making it very cost effective process. This is a process of choice for small scale and research purposes. The drawback of using inkjet printing is that the nozzle tends to clog easily. This is due to the viscosity of the liquid and the particle size. The two main category of ink jet printer is the drop on demand and continuous printing. Drop on demand is an improvement of continuous inkjet printer because the ink is not exposed to the environment which prevents it from degrading. The inkjet types are based on the position of the orientation of the piezoelectric device. Other variations of inkjet printer are based on electrostatics and aerosol deposition (Cummins, Desmulliez 2012).

The printing process used in conductive film varies from manufacturing scale to laboratory scale. Press roller printing produces conductive film in manufacturing scale. However, the changing print design will be time consuming. The inkjet printing offers a flexible print design because it does not the requirement of print mask. This printing process is perfect in laboratory scale; however changing variables such as ink composition will be a problem. Inkjet printing has tendency to have a problem with nozzle clogging if the ink is not prepared properly. Screen printing has been the process of choice since the beginning of conductive film development, hence the first conductive film made out of silver was screen printed.

The novel measurement technique requires a finish product that contains less variation. Eliminating inconsistency that affects inconsistencies measurement result is a great concern for this study. Screen printing technique was the process of choice to produce the conductive film in this thesis because it was found to be an established printing process. The

conductive pastes are available with different conductive filler; furthermore automatic printing equipment can produce a consistent conductive film with less variation. This will satisfy the purpose of producing a conductive film that will supply a quality product. The application of measurement technique is, however, not limited to screen printing alone. Therefore, the knowledge about different printing process is an important aspect of the literature review.

2.3 Measurement in Conductive film

2.3.1 Electrical

The electrical characterisation most performed in conductive film is to measure its resistivity. However most of the measurements to date were performed on cured conductive film. The literature search on electrical measurement includes reliability testing, defect detection, coefficient of thermal expansion of substrate, and resistance measurement. Also included are the non-contact measurements which are compatible to roll to roll printing of conductive film.

2.3.1.1 Third Harmonic (TH) testing

Third harmonic measurement is an in-line screening tool that can eliminate failure at early stage of passive components. The method is fast, low cost and convenient. A pure sine wave contains a fundamental frequency or first harmonic. The amplitude of the series of harmonics is much less as compared to the fundamental frequency. Distortion is expressed as the ratio of the sum of all higher harmonics over fundamental frequency. Measurement of the distortion of the third harmonic is enough to represent the higher harmonics.

TH measurement is performed by forcing an AC Voltage on first harmonic and measuring the third harmonic component of the signal. The resulting measurement will be able to detect in homogeneities in thin-film layers, holes or other defects on surfaces, insufficient or incomplete trim cuts and contact resistance. Third Harmonic technique was first implemented in the early 1960s. The purpose of the measurement is to remove weak parts in the circuit that will cause failure and thereby increase the reliability of the product. It has been found out in the 1980s that the method has superior ability in detecting defects on cylindrical SMD called metal electrode face bonded (MELF). The optimized 100% linearity screening was made possible because of the release of equipment called CLT1 with rapid testing capability on that period. Advanced non-linearity testing equipment has the capability to make measurements on single components or as 100% in-line screening e.g. Danbridge CLT10.

One paper by Kwon (448 Kwon,D. 2009) discussed the limitations of linearity measurement with respect to reliability of the component tested. High voltage and pulse load applications accumulate in different places and are not distributed regularly across application. The paper introduces another type of testing which uses pulses to characterise the material. The paper called the technique Super-Screening pulse test which has four parameters which are 1.) Voltage gradient of pulse rise and pulse, 2.)Pulse width , 3.) Pulse Height and 4.) delta R/R rejection limit. Combination of Third Harmonic and super pulse test resulted in an excellent defect detection in component. The component that has passed the test has near perfect quality because it meets all the specification limits and can be used even in harsh condition. The result was verified by the data taken in harsh automotive application.

The automotive industry applied continuous pulse loading above the component specification. The initial field report had a high failure rate between 1 parts per million (ppm) to 10 ppm. After the pulse screening application, there has been no report of failure in the field .The failure rate went into sub-ppb level even at extreme harsh overload application (448 Kwon,D. 2009). More information is needed about super pulse screening because according to this paper that the measurement can be detected using this technique.

The pulse screening was applied to resistor manufacturing industry, meanwhile third harmonic measurement has been a mature technology that has potential to be applied in conductive film manufacturing technique.

2.3.1.2 Eddy currents

Eddy currents can be used to measure conductive material over non-ferrous material such as paint or aluminium. A frequency higher than 10 MHz is used to make the surface of the instrument near to conduction level. The assignment of AC signal frequency is based on the amount of inductance it will create. The AC signal is applied to the coil creating an alternating magnetic field (Jerance, Bednar et al. 2013).

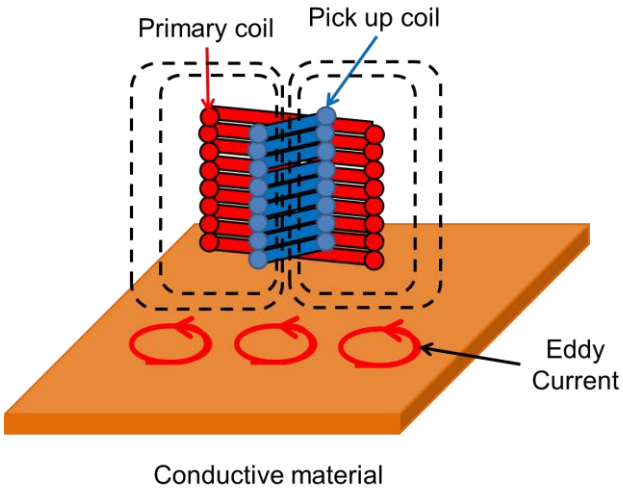

Figure 11 Eddy current measurement

The magnetic field creates eddy currents on the surface of the sample as shown in Figure 11 The amount of eddy current depends on the distance between coil and sample, type of material and sample thickness. The eddy current creates an opposing magnetic field which is detected by either the same coil (360 Jerance,N. 2013) or by another sensing coil (468 - Uchino,K.) . The eddy current will cause the reduction in inductance. The distance between the target and the coil is about half of the diameter of the coil. The advantage of using eddy current is that it is non-contact measurement and therefore causes no wear and tear, it is insensitive to dirt and humidity, high temperature range, and has no requirement for magnetic materials (360 Jerance,N. 2013).

Eddy current sensing technique is a non-destructive testing (NDT) method of testing that can be used in defect detection of metallic, non-metallic, magnetic and non-magnetic pipes used in petrochemical plants and power-generation sites (351 Fenniri,H. 1994; 360 Jerance,N. 2013; 362 Chen,X. 2007; 363 Robinson,D. 2000). Furthermore, the eddy current measurement can be applied to both ferromagnetic and non-ferromagnetic materials. Ferromagnetic materials contain iron, nickel, cobalt and their alloys. The relative permeability of this materials ranges from one hundred to two hundreds (García-Martín, Gómez-Gil et al. 2011). Meanwhile, pulse eddy current can measure metal parameters such as thickness, conductivity, corrosion and sub-surface crack measurements (361 He,Y. 2010). Flexible eddy current sensor arrays can be used in irregular shapes surface, or gap between curved surfaces (360 Jerance,N. 2013; 362 Chen,X. 2007). Other uses of eddy current can be seen in a variety of applications as proximity sensors (362 Chen,X. 2007).

2.3.1.3 Capacitance

A highly sensitive capacitance-change (CC) technique was used to measure the coefficient of thermal expansion (CTE) (Tong, Saenger et al. 1993). A Kapton Polymide with CTE value of 81 +/- 4 ppm•°C^{-1} was used and tested over the range of 50 °C to 150 °C. The measurement was correlated with Fabry-Perot laser interferometer and thermomechanical analysis. The equipment was developed to measure z-directional CTE of 5-mil-thick Kapton H film supplied by Dupont Company. The highly sensitive two-terminal capacitance change measurement technique uses two fused quartz plates. The plates contain square electrodes that are connected to the capacitance meter. The electrodes space is equalled to the thickness of the polymer film that is being measured. The thickness of the polymer creates an air gap between the electrodes. If there are any changes in the thickness of the film it will be reflected in the capacitance measurement. The sandwiched electrodes with the polymer film in the middle are placed on the hotplate. The sample is subjected to thermal cycling, that

creates change in the thickness of the film in z-direction. The measured capacitance provides the calculation for z-directional CTE and thickness of the film.

The measurement of CTE discussed in the paper was Fabry-Perot laser interferometry. The sample with an opening on the centre was sandwiched by beam splitter and a reflective substrate. The air gap created by the hole in the sample was beamed through by a low-power HeNe laser. While the material is undergoing thickness variation due to thermal cycling, the top and bottom surfaces interfering reflections is causing phase change. The change in phase causes oscillation on reflected intensity. Therefore, the film thickness can be calculated through reflected intensity. A single layer is enough for the laser interferometer measurement due to its sensitivity. The TMA needs 5 layer of film in order to measure CTE. The sensitivity of capacitor change measurement is 3×10^{-12} m. CC can be used to detect metal stress using cantilever beam, metal strains during tensile testing, and on polymers with thickness exceeding 1 cm, and thin film poly(vinylidene fluoride) films.

2.3.1.4 Resistance measurement

In terms of electrical measurement, the resistance and resistivity are the most important parameters. Often times, the measured resistance will be converted to resistivity and then it will be compared to the bulk resistivity of the conductive material (Salam, Lai et al. 2011).
If the material is made out of double filler, meaning that two kinds of conductive material were used (Lebedev, Gefle et al. 2015); the resistivity will then be compared to the material with lowest resistivity value.

2.3.1.5 DC Resistance measurement

There are two main types of DC resistance measurements. They are two and four wires measurement. Four wires measurement is better DC resistance measurement because it eliminates the lead resistance.

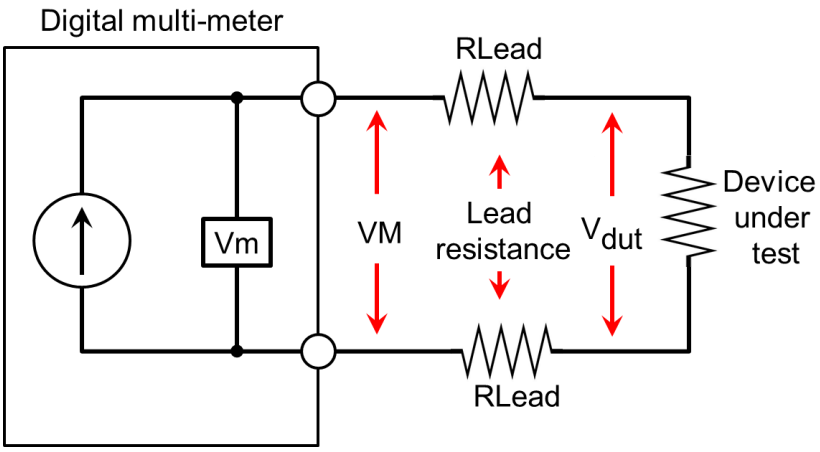

Figure 12 Two wires DC resistance measurement (Ballou 2015)

The two wires DC resistance measurement is shown in Figure 12. The measured resistance can be calculated by the formula,

$$R=\frac{V_m}{I}=R_{DUT}+(2\times RLead) \qquad (2)$$

Where R is the resistance in ohms (Ω), V_m is the measured voltage and I is the current. The equation 2 shows that the measured resistance includes the resistance lead. Two wires DC resistance measurements have a problem with the measurement of low resistance devices because of addition of lead resistance. At low resistance, more current will pass through RLead which will cause the voltage drop across it to increase. The voltage reading will be significantly affected by the voltage drop across the RLead that the voltage drops across the device under test (DUT) voltage (V_{dut}).

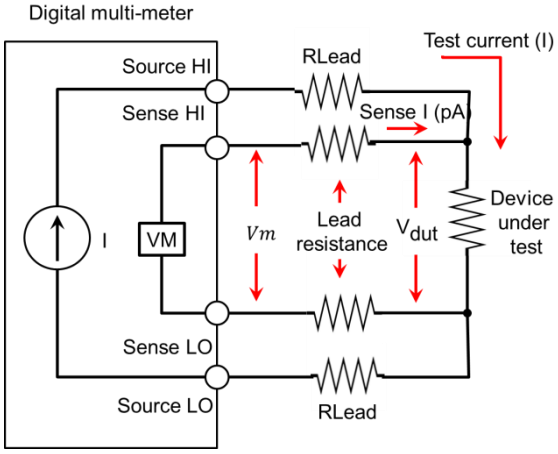

Figure 13 Four wire DC resistance measurement (Ballou 2015)

$$R = \frac{V_m}{I} = \frac{V_{dut}}{I} \quad (3)$$

Where R is the resistance in ohms (Ω), V_m is the measured voltage and I is the current in ampere (A) and V_{dut} is the voltage across the DUT. The four wire DC Resistance measurement setup is shown in Figure 13. The equation 3 shows the how to determine the value of resistance under test. On four wire measurement technique, the current is force on device under test on a separate pair of wire known as force terminal. Voltage is measured on the other pair of wire known as sense terminal. The voltmeter V_m measures the voltage across the device under test V_{dut} . The current passing the voltmeter is in pA range compared to the current that pass through the device under test. The voltage drop on voltmeter test lead is negligible and therefore the error is small regardless of the resistance of device under test (Ballou 2015).

2.3.1.6 Wheatstone Bridge DC Resistance Measurement

The accurate resistance measurement of the test setup is due to the measurement of voltage rather than resistance. The test configuration consists of four resistors. Two of which, R1 and R2, are fixed and have equal value. The DUT is placed in the position of Rx while R3 is a potentiometer which is adjusted until the galvanometer G indicates zero.

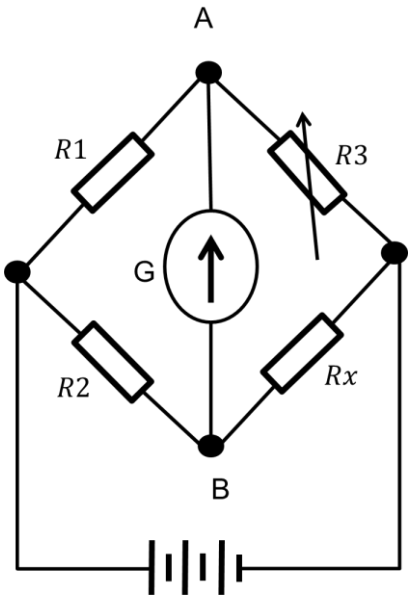

Figure 14 Wheatston bridge diagram (Bird 2003)

The Wheatstone bridge test configuration is shown in Figure 14. These will mean that no current is flowing to the meter, and will make the bridge balanced. The voltage between point A and point B is also equal when the bridge is balanced

$$Rx=\frac{R2R3}{R1}\Omega \quad (4)$$

The Wheatstone bridge formula is given by equation 4. Where Rx is the unknown resistance, R1 and R2 are two fixed resistors and $R3$ is the potentiometer all expressed in ohms (Ω)(Bird 2003).

2.3.1.7 Corona charger

Corona charger provides a surface charge to the surface of the material. The travelling motion of the surface charge was measured by surface potential detectors. The surface resistivity of the material is dependent on the travelling speed of the surface charge. This concept creates a non-contact measurement technique (Sugimoto,T. 2012).

The detector, a cylindrical body, is made out of corona-charger, induction probe A, B and surface potential probe C. Probe A, B and C are measuring probes that are attached to the body of the cylinder. Corona charge was created using needle electrode on the middle connected to high positive DC voltage power supply and a ring electrode with diameter of 4mm is connected to the ground. The distance of probe A, B and C from the charger is 20, 44, and 72 mm respectively. The distance between the sample and the cylinder is 1mm. An oscilloscope is directly connected to Probe A and B which are electrically isolated. The surface potential probe C is available commercially (Sugimoto,T. 2012).

The samples were supplied by corona ions which are high in potential energy. A potential difference was generated because of the creation of high surface charge near the corona generator with respect to surrounding areas. The surface charge will flow towards lower surface charge potential. The sample that was used in the paper was conducting polymer on different sheet resistivity. The measurement technique was consistent with the contact type measurement tester (Sugimoto, Abe et al. 2012).

2.3.1.8 Colorimetry

Colorimetry is non-contact measurement which has been used to determine the degree of cure in conductive film. It was used to characterise conductive film on flexible polyethylene terephthalate substrate in order to represent sheet resistance. The significant shift in a* and b* color represent the change of conductivity of the material during sintering process. The value of a* and b* shows the greenness or redness and yellowness of the colour as shown in Figure 15. The explanation for this phenomenon is stated in the Lorenz-Mie theory of electromagnetic scattering. This measurement technique can be applied on roll to roll conductive film manufacturing that uses nanoparticle conductive ink (Cherrington, Claypole et al. 2012).

Colorimetry is a well establish method in the graphics printing industry as a quality control tool. The colorimetry measurement result correlates to the sheet resistivity of printed nanoparticle silver ink. This measurement technique was developed by the printing industry to detect colour changes. Colorimetry technique is applied in emulsion of colour products, the effect of weathering in coated strip steel, waste discoloration, and dental discoloration assessment.

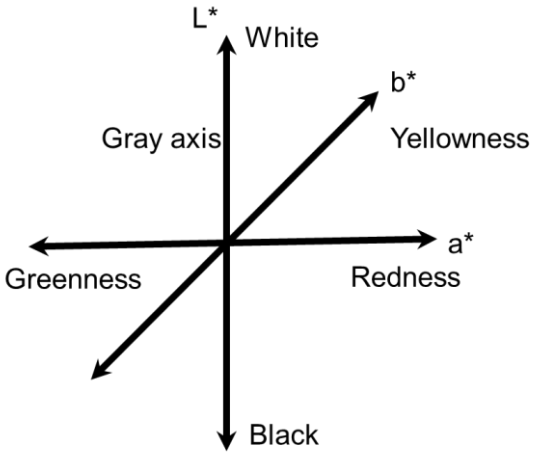

Figure 15 The CIELAB axes

The reflectance spectra are translated into a series of colour coordinate values that signifies a 3D colour space to be able to quantify any shift in colour. The CIEL*a*b* (CIELAB) as defined by International Commision on Illumination (Commision Internationale d'Eclairage) is the most complete colour space visible to human eye. CIELAB was a device independent model to be used as a reference.

The three coordinates of CIELAB are a*, b* and L*. The a* coordinate denotes the position between red and green as shown in Figure 15. Green is indicated by negative value while red is positive value. The b* coordinate is the coordinates between yellow and blue, on which blue is negative value and yellow is the positive value. L* represents the lightness of color the yields L*=0 as black and L*=100 signifies white color.

The relationship between the three colour space coordinates (a*,b* and L*) and sheet resistance is that high resistance produces very negative a* and positive b* value. Low sheet resistance measurement will generate almost zero a* value and a reduced b* value. Meanwhile, L* has no correlation to sheet resistance. The experiment shows that low resistance sheet produces green colour which signifies best sintered silver. Damaged or

cracked track has positive a* value which mean an increased resistance. The data in the experiment shows that the yellow colour is the result of the resistance decreasing and the sintering of the ink.

The change of colour during sintering is due to the agglomeration of silver nanoparticles to create a continuous film. The formation of continuous film produces a green/yellow colour that can be explained by Lorenz-Mie theory of electromagnetic (EM) scattering. Gold and Silver nanoparticles exhibit similar absorption of electromagnetic range of 500nm and 600nm which corresponds to green and yellow during sintering. Sintering will remove the green color and reduce the yellow color,, during this time EM scattering stops because the particle forms a continuous film.

This method measures indirectly the electrical performance of Conductive film by using Colorimetry and CIELAB Industry standard. The sintering of silver ink result a change in a* and b* coordinates (Cherrington, Claypole et al. 2012).

2.3.1.9 IV Measurement

The current – voltage (IV) measurement setup enable the sweeping of applied voltage across the sample while the current is being monitored. Improvement in conductivity was discovered on specially treated silver conductive adhesive.

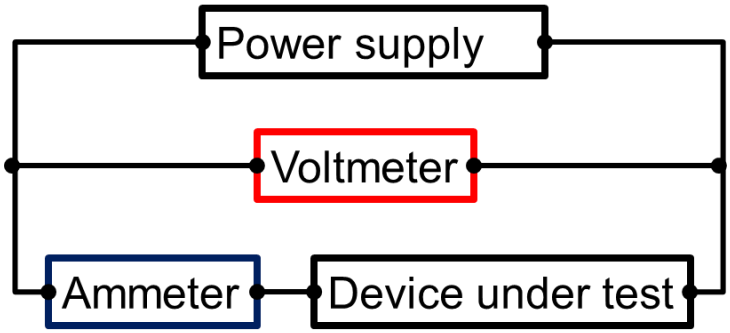

Figure 16 IV sweep measurement setup

The (IV) sweep measurement setup is shown in Figure 16. IV sweep can be performed by sweeping voltage and measurement current or sweeping current and measuring voltage. The resistance decreased while the maintaining its current rating (Li, Wong 2006a). IV measurement was performed on the sample that was environmentally aged on conductive adhesives (Kim,J.-W. 2008).

2.3.1.10 Time Domain Reflectometry (TDR)

Time Domain Reflectometry (TDR) is measurement of impedance mismatches and discontinuities by detection of discreet peaks and their location. In order to make TDR measurement, impulse or step signal is sent through the transmission lines in which it creates a reflected signal caused by impedance mismatches. TDR measurement is expressed in reflection coefficient which is the ratio of reflected signal over transmitted signal on the same port (449 Kang,J.S. 2010). The number and shape of the reflected signals characterise the impedance mismatch in the transmission line.

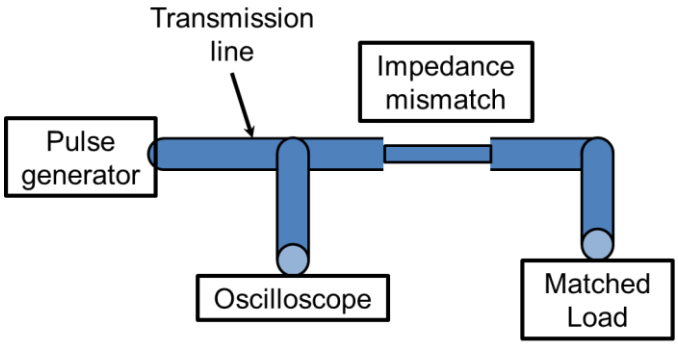

Figure 17 TDR basic components

The basic components of a TDR system are shown in Figure 17. A pulse generator creates an excitation to the transmission line. The signal will be split to an oscilloscope and the other will travel up to the matched load. The oscilloscope will display the pulse created by the pulse generator and a second pulse is the signal reflected by the wire (Lacoste 2009).

Another way of performing TDR is using a network analyser that sweeps a certain frequency range to get the reflection coefficient. The result in frequency domain is inversed Fourier transformed to produce a result in the time domain (Kang,J.S. 2010). Time Domain Reflectometry (TDR) profile and frequency characterisation h used in conductive film that uses textile as a substrate. The frequency characteristics of transmission line were measured using vector network analyser (VNA) up to 3 GHz (Kim,Y. 2010). TDR reflection coefficient was determined using 500 MHz to 6.7 GHz frequency band because current commercial product operates in this region (Kang,J.S. 2010).

2.3.2 Mechanical and temperature testing

The mechanical test in this section includes different test platforms to measure stiffness or Young's modulus, glass transition (Tg), flexibility, bending capability and temperature of conductive film.

2.3.2.1 Vibration testing

Vibration analysis adopting wave approach has been used to obtain dynamic properties of inkjet-printed thin films on flexible polyimide (PI). The sample was fabricated by depositing Ag- nanoparticle suspension on plasma-treated PI substrate and sintered at different temperature. The sample was cut into 30 mm length and 0.6 mm width by pico-second laser pulse cutting and was used as the cantilever in the vibration test. The type of sample cutting and preparation used were precise cutting tool and the cleaning involved and the activation of surface would produce a better result. The sample was vibrated at one end on the tip and positioned in horizontal orientation. The effect of the gravity and self-loading will therefore be avoided. The bend stiffness and loss factor will be obtained by measuring the frequency through exciting the base of the sample. The calculation of Young's modulus and loss factor will be possible through these characteristics. Vibration testing was used to investigate the effect of sintering and film thickness on the dynamic properties. Nano-indentation was used as reference to correlate vibration measurement result. It was found out that the sintering temperature has greater effect than film thickness on Young's modulus and loss factor (Park,J. 2009).

2.3.2.2 Bend testing

This simple bend test setup contains two parallel positioning plates that can reach small radii of curvature. One plate is stationary and one is moving. The test provide two types of test. First it causes stress on the outside curvature of the bent, while strain on the inner part of the curvature. The radii of the curvature are the half of the distance between the plates.

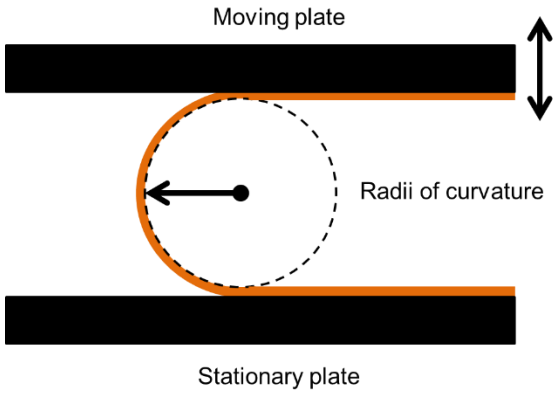

Figure 18 Bend test setup

One mechanical bend test setup is shown in Figure 18. The mechanical reliability and flexibility of a cured photoresist film was assessed through static and dynamic mechanical bending (Briand,D. 2011).

2.3.2.3 Shear Testing

Shear forces are unaligned forces that are being pushed in opposite directions. Shear testing aimed to measure the shear strength properties of materials (Coughlan,F.M. 2006). Two identical object were stuck together by the material under test, and then pulled in opposite direction. The standard test method is included in American Society for Testing and Materials (ASTM) D1002-94 Adhesive Lap Joint Shear Testing.

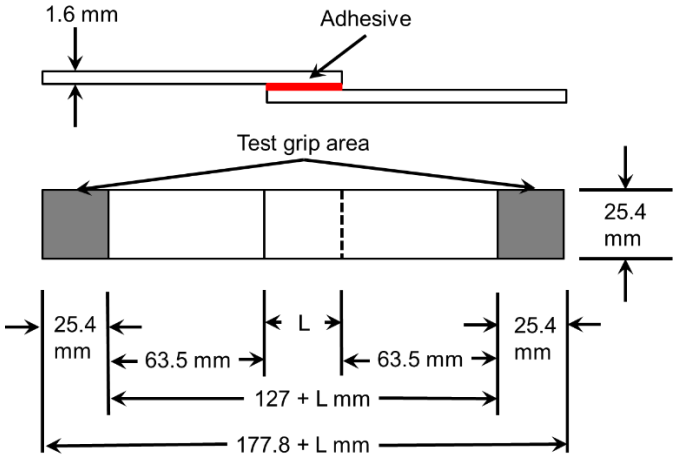

Figure 19 The sample dimension based shear standard method

The test setup for shear testing is shown in Figure 19. Some of the important recommended parameters are the overlap length (L), test grip area, and the load test parameter. The overlap length (L) is 1.62 mm for most metal. The length of grip should be 25.4 mm for the testing machine to clamp the sample securely. The shear test load is 80 kg•cm^2 - 100 kg•cm^2, equivalent of 1.2 kpsi – 1.4 kpsi of shear per area per min and should be applied until the sample fail (Chanda, Roy 2008).

2.3.2.4 Dynamic Mechanical Analyser (DMA)

Dynamic Mechanical Analyser (DMA) works by applying oscillating force to the sample and measuring its response (Jeong,W.-J. 2005). The oscillating force is called the stress and represented by the symbol σ. The response of the material to the oscillating force is called the strain γ. The force motor introduces stress to the sample by the driveshaft.

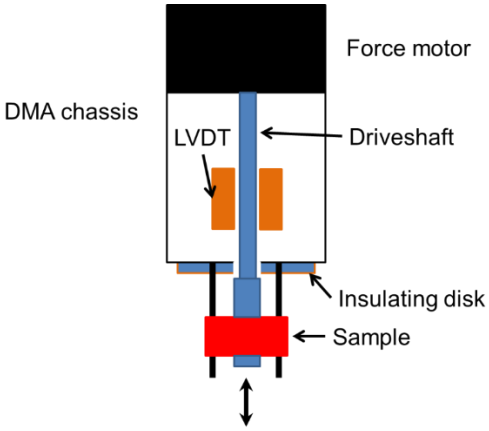

Figure 20 Basic components of a dynamic mechanical analysis (DMA)

The schematic of a dynamic mechanical analysis is shown in Figure 20. The Linear Variable Differential Transformer (LVDT) measures the displacement of the driveshaft. The measured stress and strain are plotted.

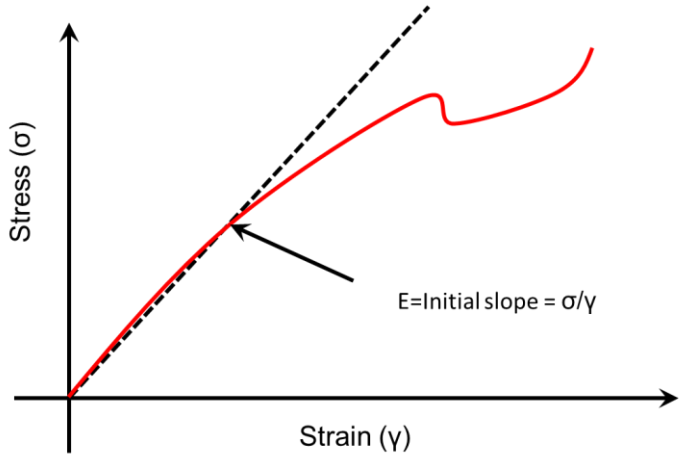

Figure 21 The ratio between stress and strain

The material's stiffness or its resistance to deformation is an important characteristic. It is often referred to as its Young's modulus (E). The modulus can be determined by the initial ratio between the stress-strain curves as shown in Figure 21. Modulus is an indicator of material performance in real world. The advantage of using DMA over other method is that a range of temperature and frequency can be swept. Aside from determination of modulus, DMA is effective in testing any change in glass transition of a polymer (Wunderle, Kallmayer et al. 2008). The polymer change from rubbery to glass happens during glass transition.

Several decade drops in modulus happens during glass transition. When a product reaches the field in with wrong glass transition, catastrophic failure will occur (Menard 2008).

2.3.2.5 Thermo mechanical analysis (TMA)

The purpose of the thermo mechanical analysis is to measure the dimensional and mechanical property of a material as a function of temperature. High magnitude of force and temperature can be applied to the device under test. The sample is placed in the furnace that is heated at certain range of temperature.

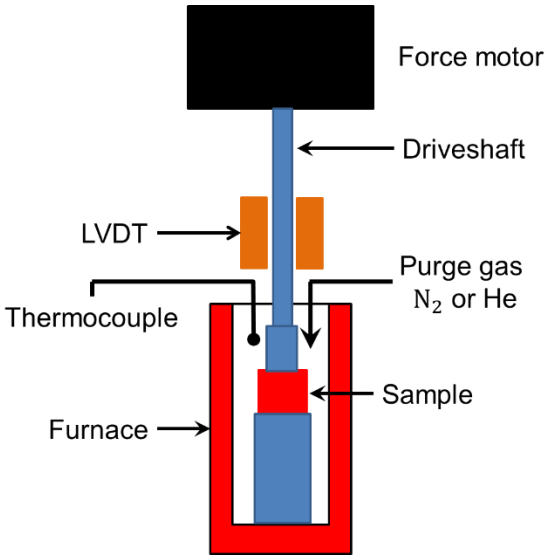

Figure 22 Basic components of TMA

The basic configuration of thermo mechanical analysis equipment is shown in Figure 22 (Menard 2008). While the sample is being heated, a load is applied to the sample and its response is measured by LVDT detector. Thermocouple placed inside the furnace monitor the temperature. TMA measurements result will provide data coefficient of thermal expansion and glass transition calculations (Harper 2006). The anisotropic conductive adhesive coefficient of thermal expansion (CTE) were measured by thermo-mechanical analysis (TMA) under dry condition and cure shrinkage was measured by mercury volume Dilatometer (Wunderle, Kallmayer et al. 2008).

2.3.2.6 Thermo gravimetric analysis (TGA)

The thermo gravimetric analysis can provide important information about the thermal stability, evaporate rate and of solvent loss. The microbalance measures the weight of the sample while the furnace is heated at a range of temperature (Sperling 2015).

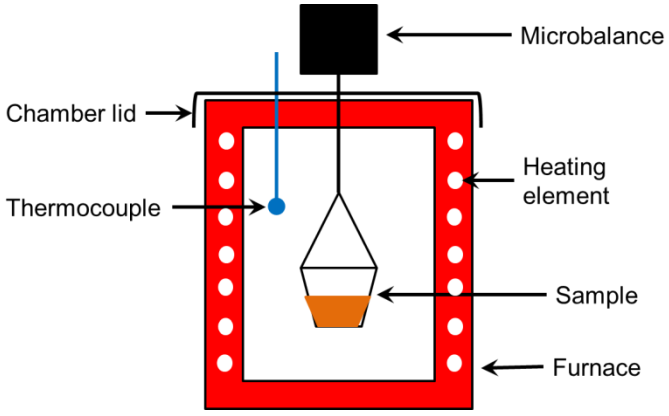

Figure 23 Basic component of a TGA

The basic components of TGA are shown in Figure 23. Particle loading of a conductive paste can be determined using TGA by the removing of organic solvent. The evaporation of the solvent used in conductive film can be measured using TGA (Kim, Chung 2002). In addition to compositional details, TGA can also determine the thermal stability of a material (McCauley, - Weiss 2013).

2.3.2.7 Differential Scanning Calorimetry (DSC)

Differential scanning calorimetry (DSC) is a process of determining the difference in heat flow rate between the reference and the sample. The instrument that performs the measurement is called the differential scanning calorimeter. The two main types of DSCs are called heat flux and power compensated. DSC is useful in determining the curing temperature of conductive ink (Jeong, Nishikawa et al. 2005).

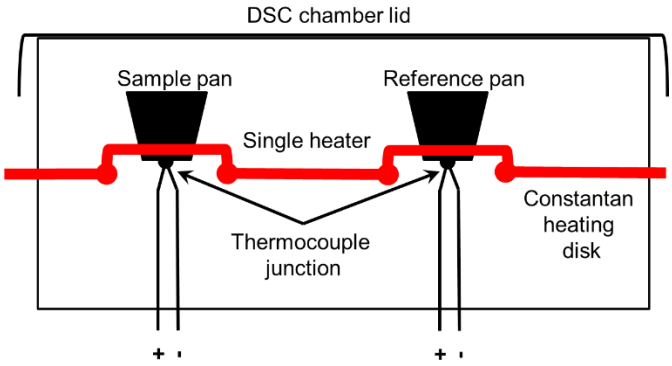

Figure 24 Components of heat flux DSC

Heat flux DSC is shown in Figure 24, the temperature difference between the sample pan and the reference pan is converted into heat flow rate. A single DSC cell contains the sample and reference pan. The two pans share a common heating element. Each pan has its own thermocouple. This setup ensures that any thermal error is removed since both pans are contained in one single cell.

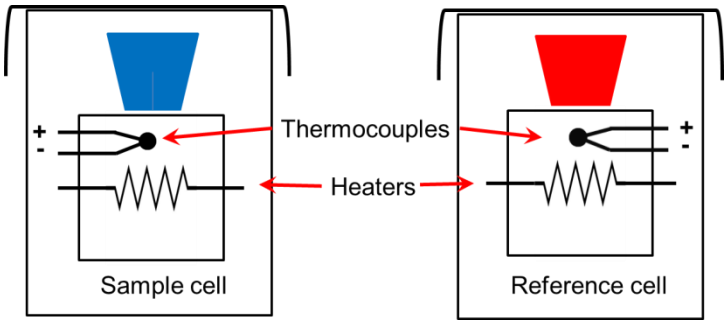

Figure 25 Components of power compensated DSC

The power compensated DSC shown in Figure 25, has the sample pan and the reference pan installed in two separate DSC cells. Each cell has its own furnace that has a heater and a thermocouple. The DSC cell has two separate control loops. If the sample undergoes endothermic or exothermic reaction, or change in heat capacity there will be a temperature difference between the two cells. Endothermic reaction occurs when energy is transferred from the surroundings into the sample, while exothermic reaction is transfer of surrounding energy to the sample (Saunders 2008). The control loop will adjust the power, therefore the power output is proportional to differential heat flow rate (Höhne, Hemminger et al. 2013)(Höhne, Hemminger et al. 2013) .

2.3.2.8 Environmental Testing - Humidity and Temperature (85 °C / 85/ RH)

Humidity aging (85 °C/85RH) and temperature cycling (-40 ° to +125 °C) was used which resulted in an increase in joint resistance. Possible causes of an increase in resistance are due to galvanic corrosion because of moisture absorption and oxidation of the material. In addition, interfacial cracking may result in increase in resistivity. The humidity testing used is 85 °C/85 RH, to test the material for oxidation and moisture absorption which will lead to decrease in adhesive strength (Coughlan, Lewis 2006).

The effect of this test to the material is cracking due to different values of coefficient of thermal expansion (CTE). This failure of mechanism is due to the stress applied to different component of the material that has different coefficient of thermal expansion when categoryed to varying temperature. The crack may appear on the printed material as a result of thermo-mechanical fatigue that could lead to premature fracture of the interface. Conductive adhesive does not perform well when categoryed to this test because of oxidation and degradation of adhesive. Steady-state extreme temperature or elevated temperature will increase the conductivity performance of adhesive because of tightening of polymer matrix and increase in filler contact (Coughlan, Lewis 2006). Samples were categoryed to elevated temperature (125 ° C) for long hours (500 hours) to measure joint resistance and degradation of the adhesive strength. This is method is stated in MIL-STD-8883E standard (Coughlan,F.M. 2006).

2.3.3 Imaging

Imaging technique ranges from conventional microscope to higher magnification instruments such as Scanning Electron Microscope (SEM) (Ikeda, Watanabe et al. 2007), that provides image with great details and also has capability to determine elemental details of printed materials. Transmission Electron Microscope (TEM) (Jo, Jung et al. 2012) has been used for oxide thickness measurement and Atomic Force Microscope (AFM) (Caglar, Kaija et al. 2008) has been used to measure pre-existing cracks in conductive film. Most of the imaging techniques mentioned require samples to be characterised in a vacuum environment. Although the imaging techniques will provide better imaging result the process is slow, and could introduce defects or contamination to the sample. Measurements under vacuum therefore need to be done at the final stage of any experiments.

2.3.3.1 Infrared(IR) Imaging

The infrared detector has benefitted from the semiconductor processing technology particularly on photolithography, vacuum deposition, and etching process (Rogalski 2011). The improvement follows the development to achieve submicron feature. The number of devices is close to the number predicted by Moore's law. The total number of component in the device is predicted to be double 19 months. This resulted in smaller size, low power consumption, and integrated signal processing (Diakides, Bronzino et al. 2012). There are two main IR detectors that are based on either photon or thermal detector.

Photon detector converts the photon energy into free carriers that are sensed by electronic measurement circuit {{498 Rogalski,A. 2011}}. Two types of photon detectors are produced for the commercial market. They are photo conductor and photovoltaic detector. Photoconductive detector uses photon energy to excite bound electrons so it can move

freely. The increase of free electrons will cause the current to increase. The photovoltaic detectors converts light into electrical energy, which does not require any external energy source to perform the measurement. Detectors are judged by their response to the light wavelength. Material that are based on HgCdTe and quantum well infrared photoconductors (QWIPs) are the two of the most photovoltaic detector used.

The performance of HgCdTe is among the highest as IR photovoltaic material because of its multispectral capability and rapid reaction. Both the efficiency of HgCdTe and operating temperature is high. The drawback of this material is the nonuniformity in LWIR and VLWIR range as well its manufacturing cost is high. The type-II superlattice system is seen as alternative to HgCdTe in LWIR range. The application of HgCdte was applied to VISTA telescope where 16 array of 2k x 2k was used to produce a 67 million pixel image. HgCdTe photodiodes and QWIPS have the capability of multicolour detection at MWIR and LWIR range. Midrange wavelength Infrared (MWIR) is from 3 µm to 8 µm, while Long-range wavelength Infrared(LWIR) is from 8 µm to 15 µm.

The quantum well infrared photoconductors (QWIPs) has multicolour capability in MWIR and LWIR range. QWIPs manufacturability because the technology if based on III–V material system that produce high yield, high operability, good uniformity and economical. However, QWIPS cannot perform in higher temperature measurement where HgCdTe photodiode has an advantage. Furthermore, QWIPs detectors have relatively low quantum efficiencies, typically less than 10%. Some of its properties are high impedance, fast response time, and low power consumption and compatible with large FPAs fabrication. The main drawbacks of LWIR QWIP FPA technology are the performance limitation for low integration time applications and low operating temperature.

The thermal detectors convert IR radiation to change its temperature dependant characteristics like thermoelectric voltage, resistance or pyro electric voltage. Thermal detectors can be classified as thermopile scheme, bolometer scheme, and pyro electric scheme (Rogalski 2010). The response values of CMOS thermopiles arrays are low (5 – 15 V/W) (Oliver, Wise 1999) and requires additional processes to isolate the detector and to create gold interconnect lines (Eminoglu, Tezcan et al. 2003).

Uncooled infrared bolometer detector became popular because they are economical, lightweight, consumes less power, wide ranged spectral response and reliable compared to the photon detectors (Eminoglu, Tezcan et al. 2003). Furthermore uncooled detectors are applicable for commercial use such as automotive, astronomy and fire prevention. The uncooled IR detectors suspended structure are micro bolometers that are micro machined out of CMOS processed wafers. There are terms used for suspended structure such as bridge, and cantilever .The infrared radiation causes the resistance of the suspended

material to change based on its temperature coefficient of resistance (TCR). The value of TCR is proportional to its sensitivity.

The material for uncooled IR detector will dictate the price of the detector. To maintain the low manufacturing cost, detector need to be compatible to CMOS processing, does not require expensive photolithography process or any additional processes. Currently, vanadium oxide (VO_x) is the most popular material and has the largest market share for IR detectors. However, 1/f noise is present because it is a non-crystalline structure. Other IR detector materials are amorphous silicon, amorphous silicon carbide, and polycrystalline silicon-germanium requires to be annealed to remove residual stress that is not compatible to CMOS processing for monolithic integration. These material also exhibit higher 1/f noise than VO*x*, due to their non-crystalline structures.

YBaCuO has high TCR value but requires expensive post CMOS surface micromachining. The worst performances came from metal films IR detector due to its low TCR values and require post CMOS deposition and lithography steps.

To eliminate 1/f noise to the IR detectors, micro machined CMOS to create n-well resistor and suspended p+-active/n-well diode was performed (Eminoglu, Tezcan et al. 2003). N-well resistor is not well suited for the application because of increased self-heating. The diode type detector is better for low-cost large format infrared detector arrays, since it has a superior response even at reduced pixel sizes and lower biasing levels. These results show that the diode type micro bolometer detector is much more suitable for uncooled infrared imagers with large format arrays due to its small pixel size, low bias requirements, and reduced self-heating. RIE-based post-CMOS processing method is used.

2.3.3.2 Transmission Electron Microscope (TEM)

Transmission electron microscope (TEM) is used to image nanomaterials because it has a resolution of 0.5 nm. The TEM was used to detect surface oxidation layers hat are 2-3 nm around nanoparticles (Jo,Y.H. 2012). TEM works by transmitting electrons produced from an electron gun to the sample, hence the name.

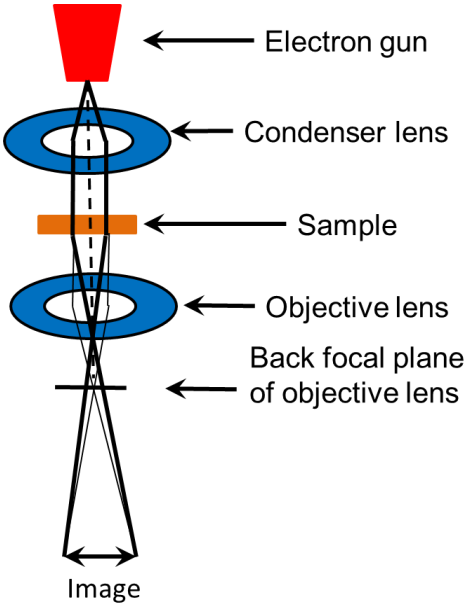

Figure 26 The basic components of TEM

The basic components of TEM as shown in Figure 26 and consists of electron gun, condenser lens, the sample, objective lens, diffraction lens, intermediate lens , projector lens and fluorescent screen. The electrons, with a very high energy of > 50 keV, produced from the electron gun travel through series of magnetic lenses. The image quality and resolution can be further improved with the addition of lenses. TEM images can be optimised by controlling the focal length of electromagnetic lenses. The basic components of a TEM are housed in a high vacuum chamber of about 10^{-3} to 10^{-4} Pa (Kulkarni 2014).

2.3.3.3 Atomic Force Microscopy (AFM)

In 1982, Gerd Binning and Heinrich of IBM Zurich demonstrated the scanning tunnelling microscope. Later on, atomic force microscope (AFM) was developed, also called scanning probe microscope. AFM's method of producing very high resolution images is different from that of other microscopes. AFM is scanning the sample line by line using a very sensitive micro fabricated probe. Each line will be combined to make up the sub nanometre resolution image.

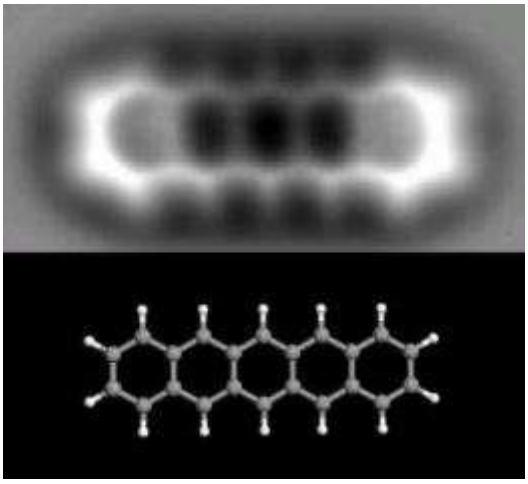

Figure 27 AFM image of pentacene

AFM has produced astonishing images similar to Figure 27 (Morita, Giessibl et al. 2015).The image taken by IBM researcher in Zurich Switzerland is a 3D image force map of 1.4 nanometres long pentacene. Pentacene is composed of 5 benzene rings. This material is used in organic semiconductor. Benzene is a ring of 6 carbon atoms, each of which has one hydrogen atom attached. The image shows the atomic structure of the molecule.

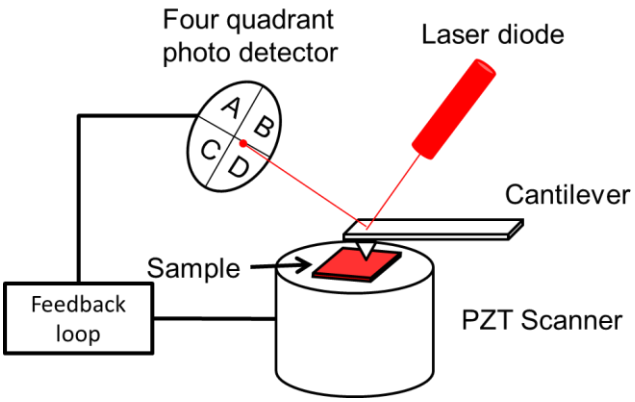

Figure 28 The main components of an AFM

The main components of an AFM are cantilever; scanner, laser diode, four quadrant detectors, and a feedback loop are shown in Figure 28. The cantilever has a cone shaped structure attached to its tip produced by a semiconductor processing technique. The surface roughness of the substrate must be less than the length of cone shaped structure at the tip of cantilever. This is to prevent damaging both the tip and the substrate. The XYZ scanner holds the sample and performs the movement for the cantilever to provide line by line measurements. The movement of the cantilever is performed by piezoelectric device. A

piezoelectric device produces mechanical movement when electrical signal is applied into it. A laser diode is focused at the back of the cantilever then the light is reflected to a four quadrant photo detector. The output of the photo detector is fed back into piezoelectric and XYZ scanner for adjustments (Kelkar, Herr et al. 2014).

An AFM has been used to prove the presence of pre-existing cracks in a copper nanoparticle printed layer. The pre-existing crack will be covered if more layers are printed on top of it. But, printing more layers beyond critical thickness will cause large crack. The use of AFM in this paper is to determine the presence of pre-existing cracks in electrodes that have been printed 5, 10 and 20 times and to identify which layer gives the best result. The three dimensional surface profile of 1um x 1um square was taken by AFM. It was been found out that the 10 times printed electrode did not result in any crack (Caglar, Kaija et al. 2008).

2.3.3.4 The Ultra High Resolution Optical Coherence Microscope

This measurement has submicron axial resolution that is needed to measure the thickness of layers of conductive film. The measurement was compared with Wyko Optical profile and Dektak Stylus profiler both manufactured by Veeco/Burch. The reference measurement justified that OCT measurement is capable of full volumetric reconstruction and high resolution needed for conductive film measurement. Optical Coherence Tomography (OCT) presented in the paper, was a novel technique in non-contact, non-destructive quality inspection tool for Conductive film. A 3D image can be rendered to get a better insight of properties and structure of the material.

Rapid development in the technology has brought Fourier Domain OCT(FD-OCT) that is capable to combine ultra-high axial measurement resolution with fast , video-rate data acquisition speed. The information obtained can be feedback to control the manufacturing process to create the best manufacturing parameters and increase device lifetime (Czajkowski, Prykäri et al. 2010).

2.3.3.5 X-Ray- computer tomography (CT) Imaging

The use of x-ray and computer tomography allows the examination of the samples beyond the surface of the material, and will therefore test what is hidden within the volume of the material. This type of technique is non-destructive testing, a similar technique to ultrasonic microscopy and thermal microscopy. The application of the measurement method is for Ball Grid Array (BGA), solder joints, and quality testing on PCB fabrication. The unit for tomography used is the voxel which is the smallest grey scale unit/pixel with third dimension or cube and less than 900nm (Oppermann, Zerna et al. 2009).

X-ray Microscopy measures the attenuation of the X-ray passing through the material. X-ray has 10 m to 10^{-12} m wavelength of electromagnetic radiation. In order to create an X-ray, an accelerated electron beam hits a target, and are all encased in a vacuum chamber. The target material, current and voltage of electron beam dictate the properties of X-ray in terms of energy and wavelength. The kinetic energy that generates x-ray produces 99% thermal energy and 1 % X-ray, and therefore tungsten material are well suited as target material (Oppermann, Zerna et al. 2009).

The absorption of x-ray depends on the material being inspected. The materials thickness, density, cube of atomic number and coefficient are the factors that cause X-rays to attenuate. X-ray can magnify up to 1000 times. The nanofocus equipment in this paper is capable of detecting structures within hundreds of nanometer. The paper produces an image that has 900nmx900nm pixel resolution (Oppermann, Zerna et al. 2009).

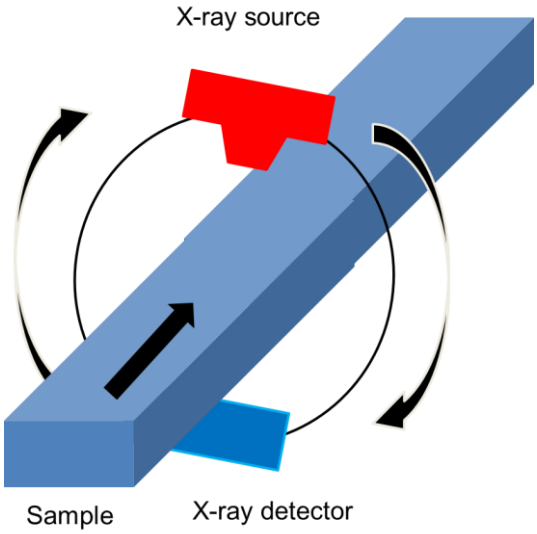

Figure 29 Computer thomography

Computer Tomography (CT) is an inspection method as shown in Figure 29 that provides information not only about shape, and size but also the structure inside the material. The material properties such as thickness and densities can be visualised in grey scale or in different colour using pseudo-colour technique. A number of 2D tomography images are taken while the material is turning 360 °C. The collected 2D pictures are put together using Radon transformation, a complex reconstruction algorithm. The final image is the volume model of the material (Oppermann, Zerna et al. 2009).

2.3.4 Literature review in measurement of conductive film summary

The important measurements in conductive film are to determine electrical, mechanical, chemical and physical properties. Electrical measurements includes eddy current (Jerance,N. 2013), impedance measurement, third harmonic or linearity measurement, four probe measurement (Selvaraj,M.K.), wheatstone bridge), and Time Domain Reflectometry (TDR) (Kang,J.S. 2010). Current-Voltage (IV) sweep (Kim,J.-W. 2008) measured the current rating. Impedance measures the combination of reactive, resistive and capacitive characteristics of conductive film. Four probe measures the sample without the error caused by test lead resistance. Wheatstone bridge measures the resistance by detecting the change in voltage change in a four arm resistor network. TDR measurement uses high frequency that result to skin effect of the tested material. Mechanical measurement includes bend testing (Briand,D. 2011), Dynamic Mechanical Analyser (DMA) (Jeong,W.-J. 2005), Thermo mechanical analysis (TMA) (Menard 2008).

Some of the novel measurement techniques have been identified such as colorimetry and Non-Contact Resistivity Corona Charger (Sugimoto,T. 2012).The colorimetry measures the degree of cure in printed ink through colour determination (Cherrington,M. 2012). There were equipment that was developed in order to measure the material properties accurately such as dynamic mechanical properties (Jeong,W.-J. 2005), to obtain stiffness and natural frequency, and coefficient of thermal expansion (CTE) (Park,J. 2009).
Imaging technique ranges from conventional microscope to higher magnification instruments such as Scanning Electron Microscope (SEM) (Ikeda, Watanabe et al. 2007), that provides image with great details and also has capability to perform elemental details of printed materials, Transmission Electron Microscope (TEM) (Jo, Jung et al. 2012) – oxide thickness measurement and Atomic Force Microscope (AFM) (Caglar, Kaija et al. 2008) – measures the pre-existing crack in conductive film.

Third Harmonic measurement has been known to the resistor manufacturing industry as quality assessment tool; however application in conductive film is unknown. This area will be interesting to venture as its application to conductive film will shorten its lifetime performance assessment.

The electrical measurement normally performed in cured conductive film. Measurement tool that provide early indication of cure is missing on the literature search. The current practice in printed electronic is to use particle loading in predicting the final cured resistance of conductive film. A measurement that can both provide the early resistivity values and degree

of cure is vital in conductive film research and manufacturing. The measurement will save time and resources in developing and manufacturing the conductive film.

Defect measurement using non-contact measurement is performed by optical, and electron microscope. Non-transparent material cannot be characterised by optical microscope and therefore not compatible with the plastics commonly used in conductive film. The defect detection technique using electron microscope can detect Nano scale defect but tremendous sample preparation is required because it requires a thin film of gold coating. The sample becomes contaminated and can only be measured once. In addition, sample is needed to be characterising in vacuum environment. The measurement technique is therefore not applicable to roll to roll printing.

3 Chapter 3 – Methodology and Background Theory

3.1 Printing process used

The popularity of conductive film is because of its ability to produce a low-cost and high through put electronics devices. Almost all printing process can be used to create electronics product. Screen printing is the only printing process that was used for throughout the investigation of lifetime performance testing of conductive film in this thesis. The literature review provided printing process that is can be used in manufacturing and research environment. The printing process for large scale manufacturing is important information because the study of novel measurement will have to be applicable to this process. However, the search for a novel measurement technique requires a process that will produce a consistent finish product. Moreover, the printing process parameters need to be easily modified. Screen printing technique is a perfect solution for this study. Inconsistencies caused by printing process are minimised and the effort will be concentrated for the main aim of the research.

The primary components of a manual screen printing process are the substrate, screen, ink and the squeegee.

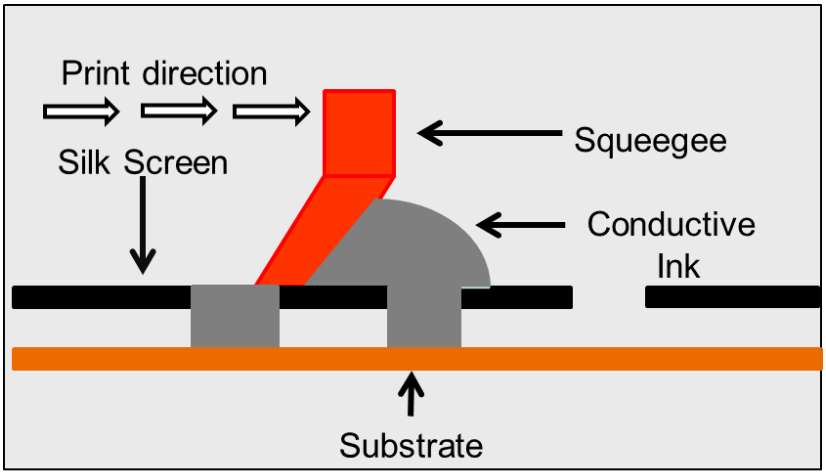

Figure 30 Silk screen printing

Figure 30 illustrates the screen printing process. Screen printing uses a set of pattern to allow or block the conductive ink from transferring into the substrate. The pattern polymesh screen is aligned over the sample. The conductive ink is placed on the screen and then spread by a squeegee. The ink goes through the opening of the screen, transferring the pattern of the polymesh screen to the substrate.

In order to increase the repeatability of the screen printing process, automated screen printer model 250 DEK was used shown in Figure 31. The automatic screen printer can store programs with different print settings designed for various conductive inks and devices. The parameters include print speed that was set to 50 $m \cdot s^{-1}$ and print pressure set at 8 lbs. The other printing parameters are print gap, flood height, and flood speed set at 2 $m \cdot s^{-1}$, 1 $m \cdot s^{-1}$ and 50 $m \cdot s^{-1}$ respectively.

The setting has been optimised to produce a quality print. Although the effect of emulsion thickness has greater on cured print thickness and eventually on cured resistivity of the conductive film that this parameters. It is important to keep these key parameters in using screen printing.

The substrate was firmly held by the vacuum plate to prevent substrate from sticking into the screen and better pattern transfer.

After the squeegee has printed the conductive ink on to the substrate, the squeegee is lifted then the metal plate is lowered to flood height of 1 mm. When the squeegee returns to its original position, at the same time the metal plate applies a thin film of ink on the screen and the process is called flooding. Flooding the screen is important because it will prevent a thin layer of ink residue to dry and block the screen aperture. Flooding also prepares the set for the next print.

Figure 31 Photo of DEK automatic screen printer

Solidworks autocad software was used to design the screen then saved as a dxf file. The maker of the screen was DEK screens. The screen was made out of mesh of polyester thread. The size of frame was 24 inch width and 24 inch length, which dictates the workable area. The stencil's important parameter is the mesh thickness that defines the conductive ink cured print thickness. The PET substrate was 120 µm ±3 um thick. The inks were supplied by Gwent Electronic Material and Electrapolymer, ED4000 and ED3000. ED4000 (see Appendix 1) is carbon filled paste while ED3000 (see Appendix 2) is silver filled paste. The development carbon conductive paste was supplied by Gwent Electronics Materials (GEM).

3.2 Curing method and equipment

Conductive ink used in conductive film consists of conductive particle or filler, and chemical additives that promote adhesion and prevent particle agglomeration. The chemical additives are useful before and at the process of printing, but after printing the chemical additives are not necessary and therefore need to be removed. The purpose of curing is to remove the organic chemicals present in the conductive ink. When the solvent is removed, it causes particle to particle contact to form.

It is the most convenient way to cure the conductive film but not the most efficient way. It heats up everything from conductive film to substrate. Efficient methods are curing process that only heats up the conductive film and not the substrate, such as microwave curing technique, flash light sintering and UV curing. The drawback of using convection oven is it causes heat stress to the substrate, and curing temperature is limited to the substrate temperature. Damaging the substrate will cause early field failures of conductive film. Furthermore, convection curing is a slow process. The slow curing of conductive film is particularly helpful in capturing the AC impedance and DC resistance during conductive ink transition from liquid to solid film. Electrapolymer inks are normally cured at 95 °C for 40 minutes. Experiments have also been performed at different temperatures, and at different particle loading. The curing temperatures used were 55 °C, 85 °C, 95 °C, and 105 °C. The particle loading used were 48 %, 52 %, 56 % and 60 %.

3.3 Dimensional analysis

The dimensional analysis of conductive film is an important measurement area because it defines the electrical properties of the printed structure. In addition to that, dimensional measurement can identify print anomalies in form of cracks, print discontinuation and islands.

3.3.1 3D optical microscope

One of the important characteristics of printing tracks is the determination of print thickness. The thickness is the difference between the base and the highest peak of the print. The peak of the print is easy to determine as it's the maximum value of the measurement. What is difficult is the determination of the base especially when the substrate is transparent. This is where a profilometer is a better measurement device than a 3D confocal microscope. The advantage of the 3D microscope is that is provides volumetric information vital for resistivity measurement. It is a non-contact and large area optical measurement technique. The disadvantage of the 3D microscope is in measuring transparent films. Conductive film are dominated by the use of flexible and transparent material. This causes problems when using 3D microscope, because it cannot measure transparent films invisible.

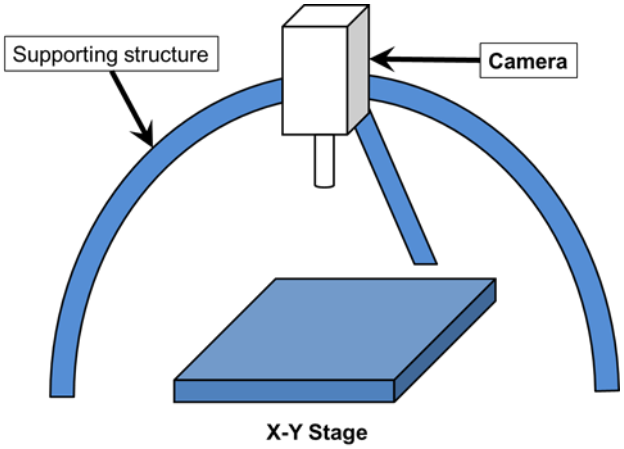

Figure 32 Alicona Infinitefocus 3D

The diagram of the Alicona Infinitefocus 3D is shown in Figure 32. This model has maximum resolution of 100 times equivalent to 10 nm. Automatic mapping of the printed structure is made possible by a motorised stage that can move in x and y direction. Once the start and end position is programmed, measurements can last for several minutes depending on the resolution and the area of measurement (Alicona 2016).

3.3.2 Step measurement – Profilometer

The thickness of the screen-printed tracks was measured using a profilometer. The profilometer uses a cantilever with stylus attached on its tip to measure the step height and profile of the printed ink. The sample has to be cured to perform this measurement. The profilometer used was a Taylor Hobson, PGI-1000 Form Talysurf.

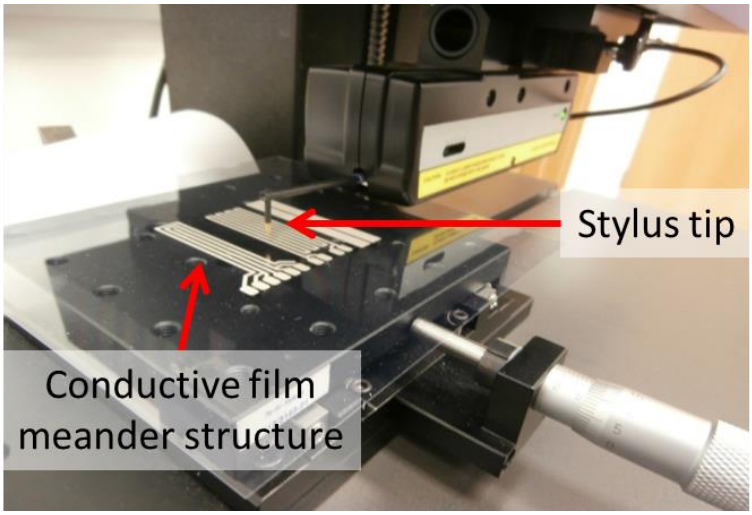

Figure 33 Taylor – Hobson Profiler

The thickness measurement setup is shown in Figure 33. The sample was placed right beneath the stylus tip and set as start of measurement. The tip movement is controlled via commands from the user through the equipment software. The cantilever is brought down until the stylus tip and the sample comes into contact. The stylus will move across the sample to measure the surface of printed structures. The measurement will stop according to the length of programmed measurement length.

The step measurement uses a stylus to create the profile of the conductive film. The advantage of this method is the ease to produce the thickness measurement, the stylus follows the contour of the surface, even with the transparent film. This method is therefore only possible for hard or cured conductive film. It cannot measure wet conductive ink as it causes damage to the test structure, and will contaminate the stylus tip of profilometer. However, this equipment can measure transparent materials such as substrates used in conductive film.

The problem that was encountered while using stylus profilometer is that the substrate tends to warp. This is could be due to the soft PET substrate that is easy to warp. The warp seen on the substrate can be due to convection heating during cure. Selective curing techniques such as pulse light, microwave or eddy current might be an option to prevent substrate from warping. There is software that has the facility to filter the data and level the steps on a horizontal plane. The profile data can be analysed by MountainsMap version 6.2.6486 software. The resistivity measurement will depend on the dimension of the printed conductive film and therefore, measurement of the deposited film is important. This commercially available product is not free, however available option of using excel program is enough to determine the film thickness in micro resolution. It is important to identify the

film thickness in flat format, than on wavy format. The error on measurement will decrease and it will produce a better film thickness determination.

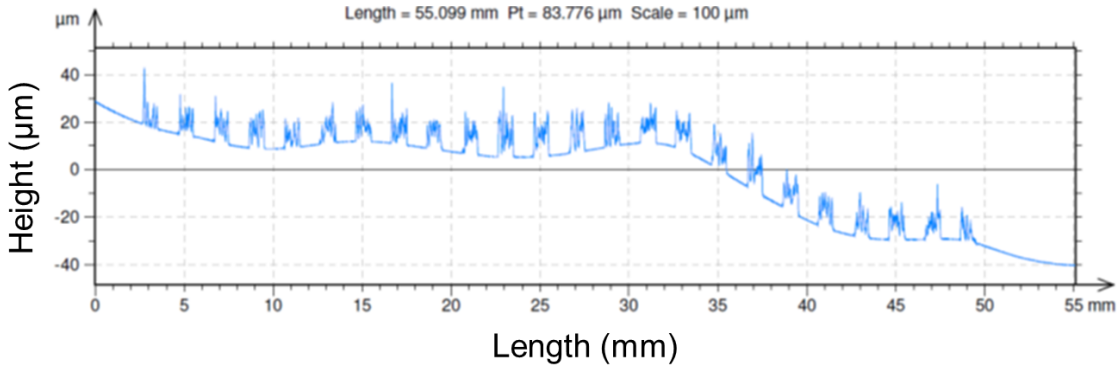

Figure 34 The raw line scan data

The graph of the raw line data with the measurement length of 55 mm is presented at Figure 34. The data from the Taylor Hobson, PGI-1000 Form Talysurf is imported to the MountainsMap for further analysis and filtering. Clearly seen in Figure 34 is the waviness of the substrate and the thickness of the print is difficult to identify at this stage.

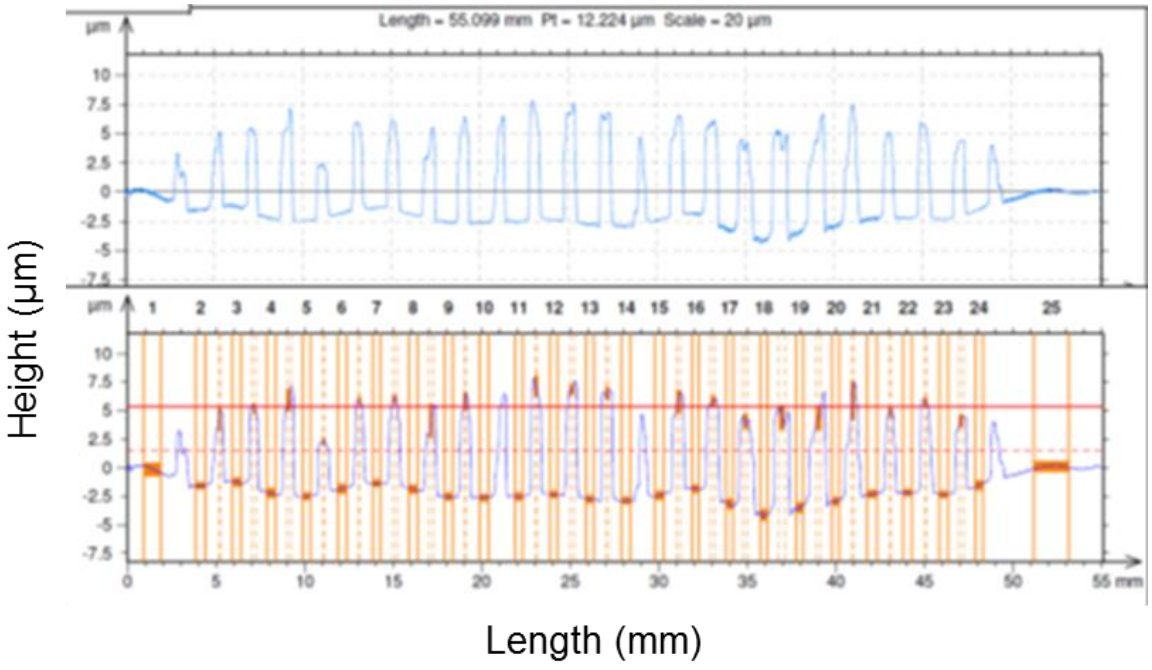

Figure 35 Form filtering of step measurement

The first step in removing the waviness of the step measurement is through form filtering. Shown in Figure 35 that the waviness of the profile has been removed, and although not perfect, the average print thickness can be identified. The average thickness of the print of 7.49 µm is reported by the program.

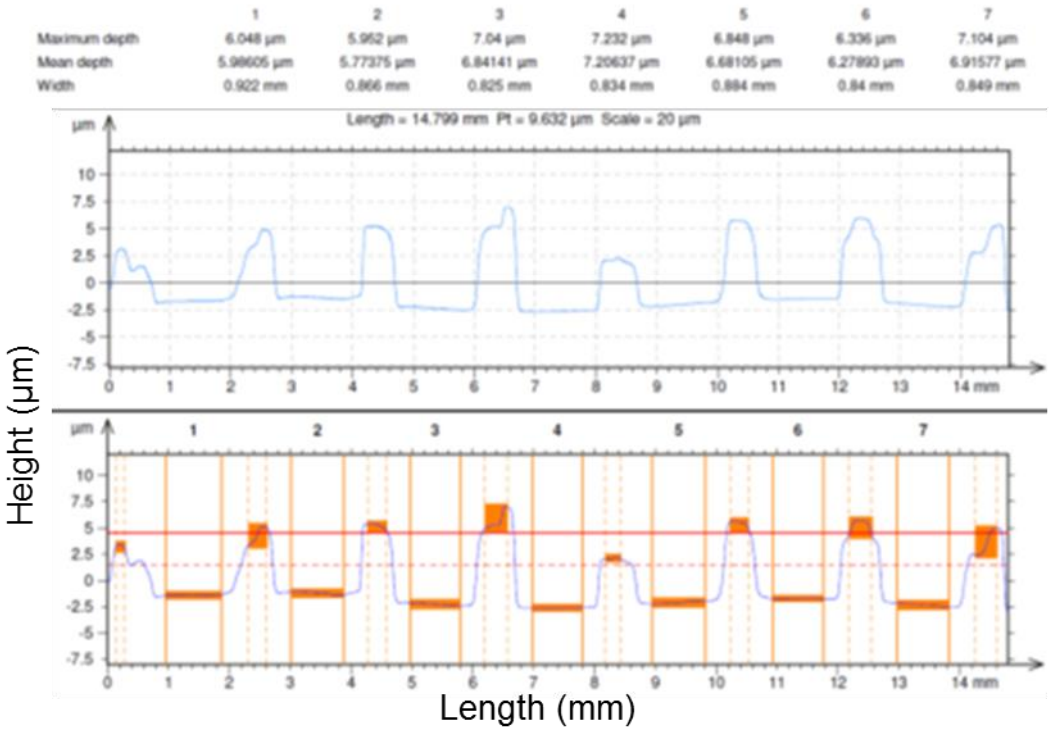

Figure 36 Magnification of the first 7 steps

The removal of the waviness of substrate has provided the data to be processed further. The next step is to magnify the first 7 steps and then remove any unwanted features. This unwanted feature is the roughness that is present on the print. The magnification of first 7 step measurement is shown in Figure 36. The measured roughness of the print was removed and individual print thickness is now identified as 6.5 µm ±0.5 µm.

3.4 Experiments

The experiments are set into three categories. First category is the lifetime performance testing, which uses environmental test and third harmonic measurement. The second category was measurement of conductive film during cure. Here the measurements were performed during cure using AC impedance and DC resistance. The third category was defect detection in conductive film using thermal imaging camera. Mechanical stress was introduced by mechanically bending the carbon and silver conductive films repeatedly at a certain radius and bend angle. The defect seen was increased power dissipation due to stressed region and increased in resistance due to material loss.

3.4.1 Lifetime performance testing

There are two main methods in predicting the lifetime performance of conductive film. The first method uses environmental testing. Samples are tested using elevated temperature and high humidity testing. This method is commonly used in material science in order to predict the lifetime performance of the material. The second approach is using third harmonic testing. This method has been utilised in resistor manufacturing as a quality assessment tool to identify product that will likely to fail in the field.

3.4.1.1 Lifetime performance - environmental testing

In this thesis, environmental testing was performed using a climactic chamber. Samples were tested using 125 °C and 85 °C / 85 RH test conditions. The test lasted for 1000 hours. The purpose of environmental testing is to determine the response of conductive film under elevated temperature and high humidity tests. The high temperature storage and high humidity tests were performed in a convection oven and a climactic chamber. The Climactic chamber used was Sanyo model HCC031. The paste used was supplied by electrapolymer and Gwent Electrical Materials (GEM). The paste from electrapolymer was silver (ED3000) and carbon (ED4000). The development ink was supplied by Gwent Electronic Materials (GEM).

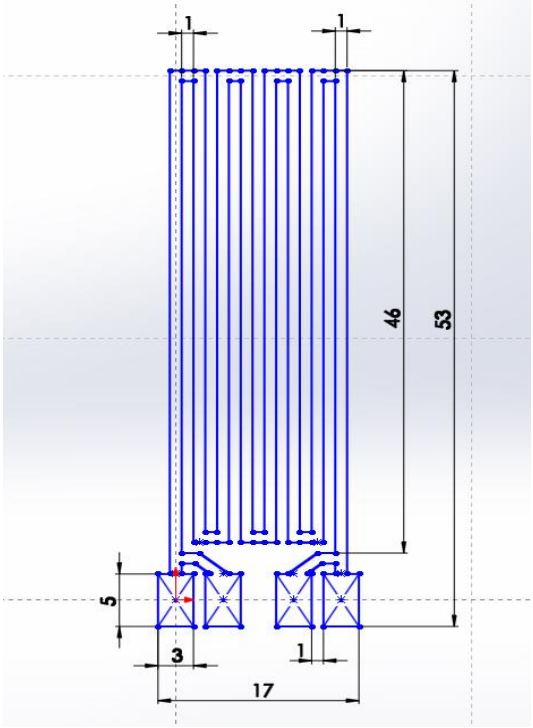

Figure 37 The 375 square mm test structure

Figure 38 Photo of test structure

The CAD drawing of the samples used in environmental testing is shown in Figure 37 and the actual photo of the printed sample is shown in Figure 38. The CAD drawing will make up the design on the screen, provided by DEK screens. The meander shaped design has an area of 375 square millimetres and each end has two pads. The dimension of the meander structure is based on the working area of the screen frame. Larger print structure requires larger frame. These pads were connected to a DC resistance meter for four wire DC resistance measurement.

3.4.1.1.1 Lifetime performance – Third Harmonic measurement

Third harmonic has been used as a realibility tester in the resistor manufacturing industry. The test is used primarily by resistor manufacturing industry to detect inhomogenous defects, improper or high resistive contacts (Salomon, Troianello 1973, Spiralski 2003). Research work has been performed into its application for capacitors (Spiralski 2003) and semiconductors (Vandamme, Vandamme 1999) to determine the components reliability and to prevent the early operational failure of the devices. In this study, the third harmonic measurement has been performed by applying a pure sinosoidal signal and the generated third harmonic signal was detected and measured. The results shows that the defective samples can produce higher a third harmonic signal. The test procedure is included in the IEC 60440 standard (Kuehl 2002) that requires the application of first harmonic frequency and the measurement of the generated third harmonic signal consequently. The definition of Third Harmonic Ratio (THR) is the ratio between the fundamental frequency and the sum of harmonic signal generated by the sample. The third harmonic is chosen because it is time consuming to measure all the harmonics, and it is enough to represent the remaining harmonics (Kuehl 2002). The formula in calculating the third harmonic ratio is given by the the following equation(The British Standards Institution 2012):

$$\text{THR}=20\log\frac{V_1}{V_3} \tag{5}$$

where, THR is the third harmonic ratio, V_1 is the input voltage at fundamental frequency and V_3 is the third harmonic signal generated by the sample tested (Kuehl 2002).

The purpose of the work in this thesis is to investigate a defect detecting technique in conductive film by the third harmonic measurements. Various types of defects were introduced on the samples and the third harmonic signal was measured using a component linearity tester (Radiometer CLT1). The relationship between the defects in the printed samples and the third harmonic signal and the third harmonic ratio was identified.

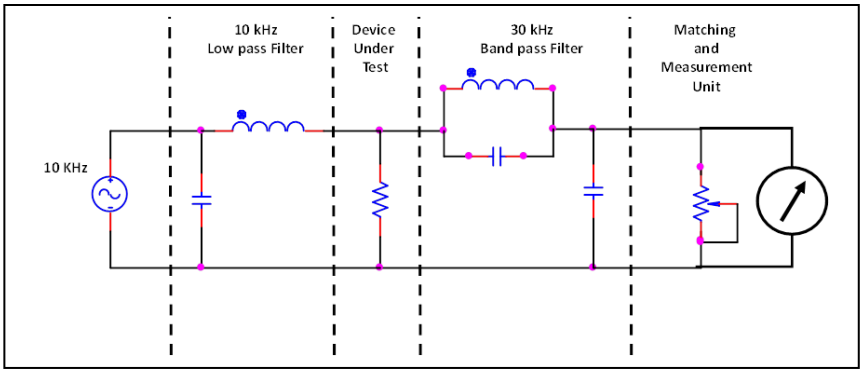

Figure 39 The main components of Third Harmonic Test equipment (Kuehl 2002)

The main components of a third harmonic tester are illustrated in Figure 39. The input voltage at 10 kHz is supplied by the machine, and passed through the 10 kHz low pass filter. The output of the filter is supplied to the device under test. In this case, the test interface and printed test structure. The third harmonic response is sent to the 30 kHz band pass filter. The matching unit is calibrated depending on the resistance of the device under test. The third harmonic measurement is displayed to the analog meter. (Salomon, Troianello 1973)

ED4000 carbon filled ink and ED3000 silver filled ink was sourced from Electrapolymer. ED3000 was used as pre-deposited electrodes while ED4000 was used to create the test structure. The conductive film was cured according to the manufacturing requirements. Various types of defects were mechanically induced on the conductive film. The pin-hole defects were introduced using a center punch; the line defects across the test structure were created by a scalpel; and two grams of ground medium density fibres were added into 15 grams of the ED4000 ink in order to obtain contaminated printed samples. All of the conductive pastes were printed using the screen printing technique. Measurements were performed on all the following different samples: fully cured samples, scratched samples, the sample contaminated with fibers, under cured sample (ambient) and 1 kΩ resistor. Radiometer CLT1 was used to measure the third harmonic frequency of the conductive film. The equipment was operated at 10 kHz frequency and the third harmonic was measured at 30 kHz. The samples were optically examined using Alicona Infinitefocus 3D surface measurement.

Figure 40 shows an example of a pin-hole defect created on the conductive film. Three indentations have been created with the following diameters: 607, 545, and 516 $\pm$ 5μm.

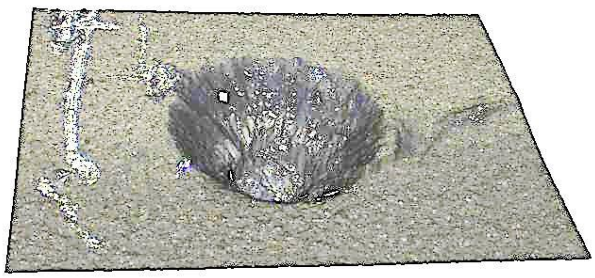

Figure 40 The photo of indentation in printed structure

A centre punch was dropped 8 cm to the substrate leaving an indentation into the sample. The sample was imaged using 3D confocal microscope. Figure 41, Figure 42 and Figure 43 show three different sizes of single line scratch defects cut over the tested structure with various width. Figure 41 is the defect of 0.40 ± 0.01 mm over 2.37 ± 0.01 mm width of the tested structure which is equivalent to 17 % of the structure. Figure 42 is the defect of 0.97 ± 0.01 mm over 2.26 ±0.01 mm width of the tested structure which is equivalent to 42% of the structure. Figure 43 is the defect of 1.45 ±0.01 mm over 2.04 ± 0.01 mm width of the tested structure which is equivalent to 71% of the structure.

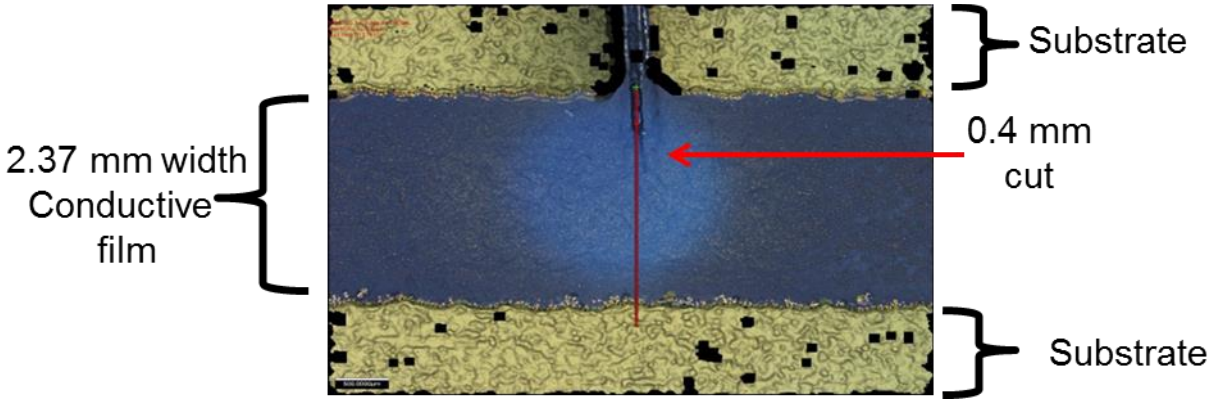

Figure 41 17% defect across the tested structure.

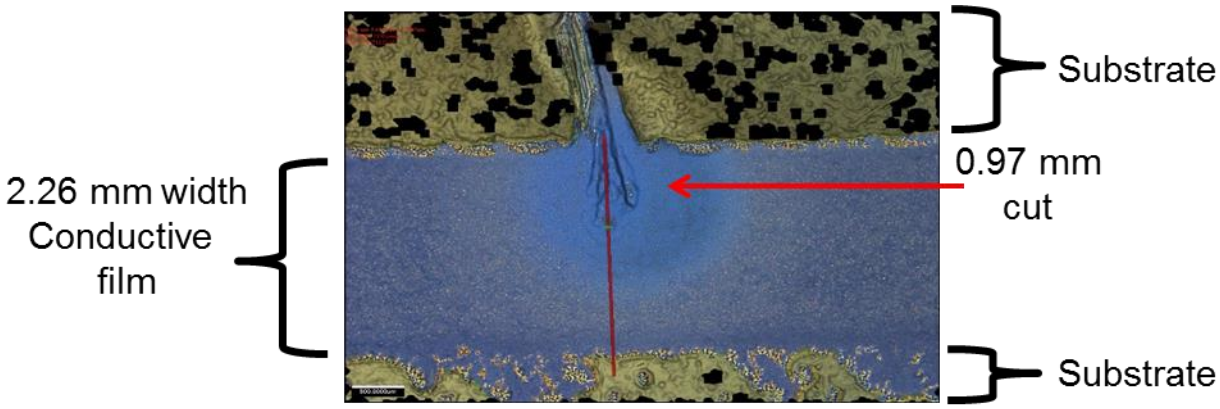

Figure 42 42% defect across the tested structure.

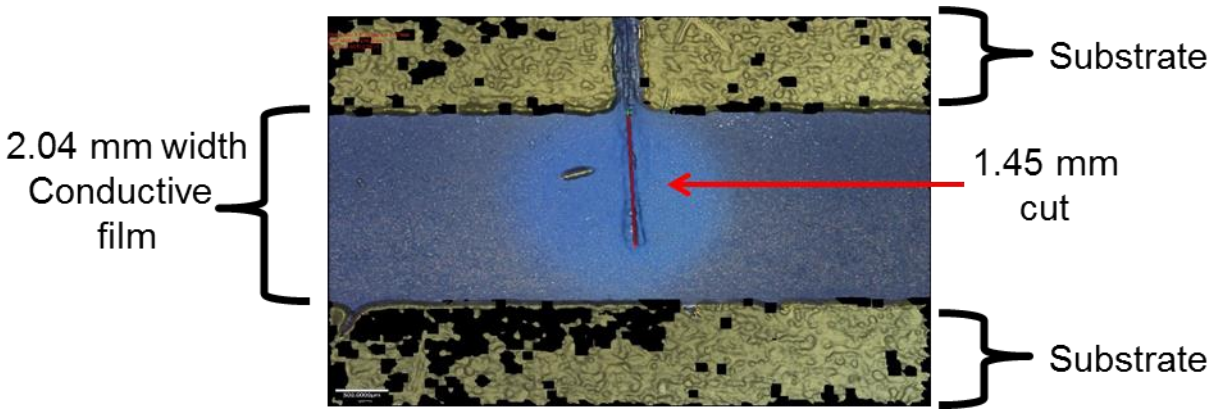

Figure 43 71% defect across the tested structure.

The scratches made by scalpel on conductive film are shown in Figure 41 to Figure 43 were performed while the ink was wet, or right after printing. The blue region of Figure 41 to Figure 43 is the printed track, the top and bottom area that is brown in colour is the substrate. The black spots are the errors created by measuring transparent film. The red line was used to identify the length of the cut and the width of printed track. It creates a structure perpendicular to the main structure, this is the residual ink. Also noticed that after scrapping the structure, the ink tends to level and fill the cut making the process self-healing. The ink is still wet and still viscous at this point. Measurement however, did not happen after the ink was cured. It requires a lot of pressure to cut through the substrate to prevent the ink from levelling. This scenario of cutting would be difficult to reproduce in manufacturing environment. Probably the most common problem that will arise in screen printing technique is a blocked screen, or rough edge cause by hardened conductive ink.

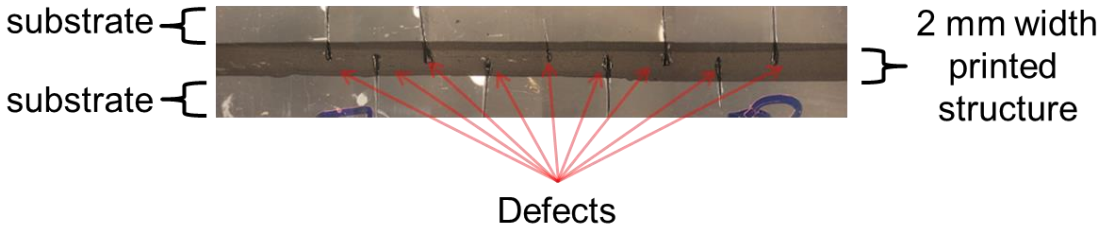

Figure 44 Alternating line defects across the tested structure.

Figure 44 shows a total of 9 line scratches made alternatively on the two sides of the tested structure. Several scratches were cut across the test structure; however, the remaining conductive path was maintained for at least 50% of the structure. Figure 44 shows a total of

9 line scratches made alternatively on the two sides of the tested structure. Several scratches were cut across the test structure, however, the remaining conductive path was maintained for at least 50% of the structure.

Alternating line defects were performed to show if the repeating structure of the defect will cause further damage than a single cut. The electrical measurement of conductive film normally pertains to the electrical resistance and conductivity of printed structure. Ohm's lawgives the following relationship:

$$R=\frac{V}{I} \tag{6}$$

Where R is the resistance in ohms, V is the voltage in volts, and I is the current in ampere. The defect is around 17 % of the total width of the conductive film. There are several methods to measure the electrical resistivity and conductivity of the conductive film. The most common method is DC resistance. AC impedance was used to measure the wet print, thus given an early indication of cure. Once printed the resistance measurement act as quality tool in identifying the quality of the print.

3.4.2 AC Impedance and DC resistance during cure

The measurement aims to measure the conductive paste transition from liquid to solid. Significant DC current will only pass through the printed conductive track once continuous particle to particle contact between measuring electrodes has been established. Ohmic heating is employed, several minutes of air drying is usually necessary to create an initial level of conductance prior to application of the curing current (Roberson, Wicker et al. 2012).

Impedance spectroscopy is a widely used measurement technique in other fields; including conductive adhesive joints (Mach, Kolár 2009), fuel cells (Yuan, Wang et al. 2007), corrosion measurement (Foyet, Wu et al. 2009) and a wide range of other applications (Familiant, Corzine et al. 2005). Impedance measurement provides information regarding the resistive and reactive component of the system. Reactive components are due to the capacitance between the (initially isolated) conductive particles and inductive properties of the printed structure. The curing process involves the evaporation of solvents and the polymerization of the resin component of the ink vehicle. As these processes occur, more particle to particle networks are formed, causing the resistance to decrease. The impedance of a freshly-printed structure therefore transitions from a largely capacitive reactance on printing to a predominantly resistive response as the ink cures. AC Impedance measurement technique was chosen over the rest of measurement technique because it has the ability to characterise materials while it is on liquid state. Portion of material present in conductive

paste is made out of liquid, solvent and adhesive, and therefore this measurement technique will be appropriate to characterise the conductive film during cure. Four-probe resistance measurement eliminates test leads resistance hence increasing the accuracy of the measurement.

3.4.2.1 DC resistance measurement

Four point probe measurement was used on both AC and DC measurement to remove the effect of lead resistance. Measurement was used using Keithley 2010 A digital multimeter. The measuring equipment was used on several occasions. The equipment is a widely used measuring tool. The drawback of using this equipment is it requires the conductive film to be cured or at least pass the percolation threshold to be able to measure within the maximum measurable state at 100 MΩ.

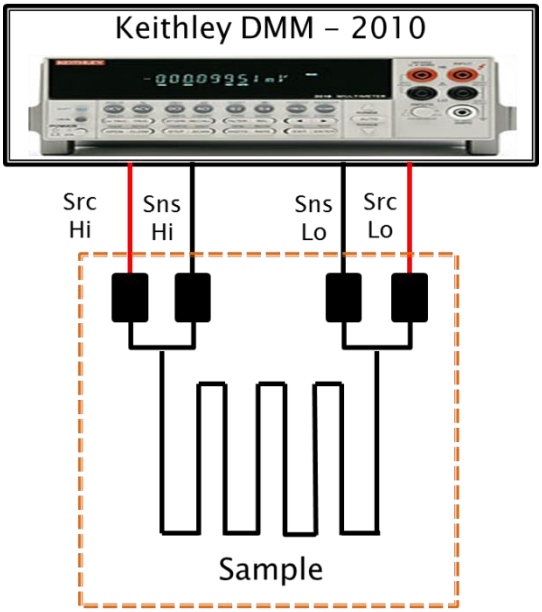

Figure 45 Four point probe measurement test setup

The DC resistance measurements were performed periodically using a Keithley 2010 A multimeter setup as shown in Figure 46. Silver and carbon prints were used in these experiments.

3.4.2.2 AC Impedance and DC Resistance

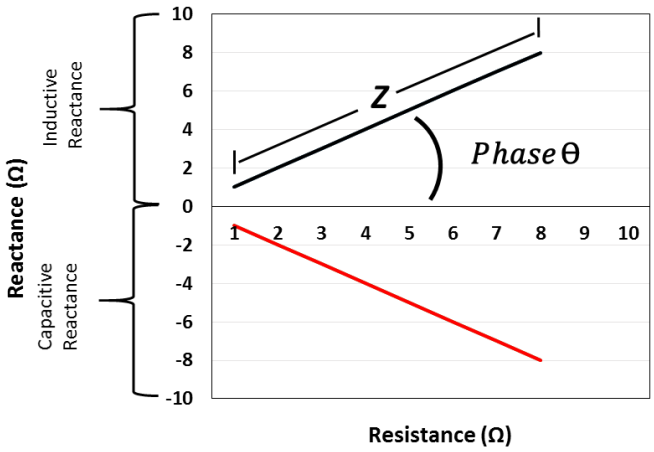

Figure 46 Illustration of reactance, resistance, impedance and phase

The Figure 47 will help to understand the relationship between the reactance (Ω), resistance (Ω), Impedance - Z (Ω) and phase (°). Normally if impedance analyser was used, the impedance and phase can be identified from resistance and reactance measurement. The following formula can help to identify the Impedance and Phase parameters.

$$Z=\sqrt[2]{R^2+X^2} \tag{7}$$

Where R is the resistance, and X is the reactance, both unit of measurement are expressed in ohms (Ω).

$$\text{Phase } (\Theta)=\text{Tan}\frac{X}{R} \tag{8}$$

Phase is expressed in degrees (°) and is calculated using the formula in equation 8. A positive figure suggests that the device under test is an inductive load, while measurement at negative figure will mean a capacitive load as shown in Figure 47. The phase measurement equivalent to zero denotes purely resistive components. The impedance analyser uses four point probe measurement. Each of the probes is connected to the sample using BNC cable. Ground was connected near to the sample to prevent noise being picked up on excess ground wire. This setup was combined with DC resistance measurement to form the measurement during cure experiment.

Since probing directly on top of wet ink was unreliable, electrodes were first deposited onto the PET substrate. The pre-deposited electrodes connect the test pins to the wet test structure shown in Figure 47. This prevents a direct contact of test pins to the sample that will cause physical defects and possibly erroneous measurement. The pre-deposited

electrode used ED3000 from Electrapolymer, a silver filled ink. Figure 47 depicts the silver ink electrode design with 5 mm diameter probe pads locations with labels that correspond to the AC impedance analyser and DC resistance meter terminals. The test electrode design also includes eight 2 mm fiducial patterns that are used to align the structure screen design to the electrodes.

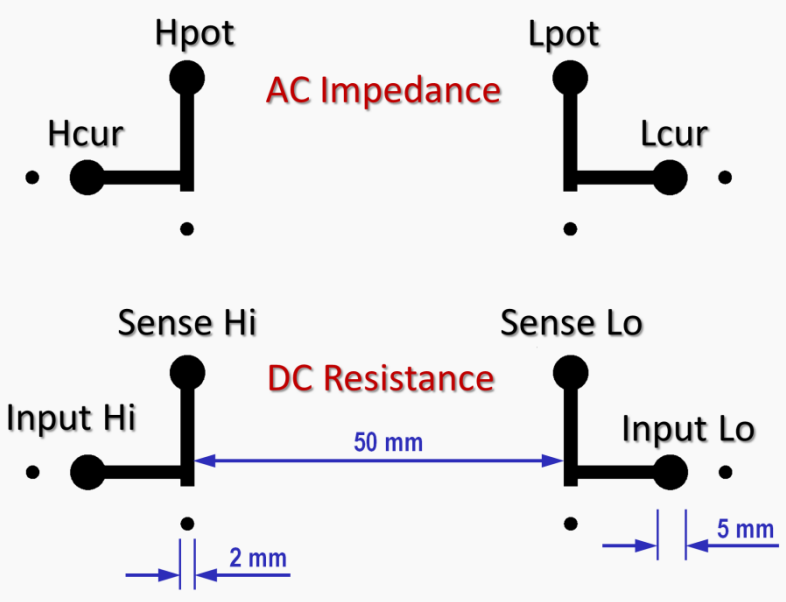

Figure 47 The pre-deposited silver electrodes design, and the location of electrical probes

The printing of the test structures, shown in Figure 48 began with the alignment of a test structure screen on top of the pre-deposited electrodes. The two sets of test structures in parallel were then printed simultaneously onto the 120 μm ± 10 μm thick PET substrates. The dimensions of the test structure are 2 mm in width and 66 mm in length as depicted in Figure 49. The test structure needed to be straight to prevent the effect of stray capacitance. The length and width of the test structure was set to make repeatable printing. Test structures that are thin and long have the tendency to break during printing and transferring to test platform. The rectangular test structure overlaps the electrodes by 8 mm to provide a good electrical and mechanical contact between the electrodes and the device under test (DUT). The separation between the sensing electrodes was 50 mm.

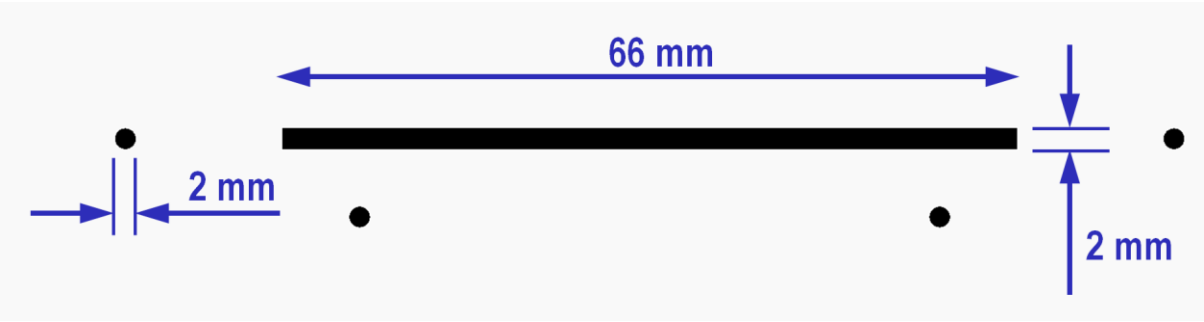

Figure 48 The test structure screen design with fiducial patterns

A screen was manufactured by DEK Screens. The polyester screen was 6 inch wide, 8 inch long, using a 27/140 mesh, 45° angle mesh orientation and 18 μm emulsion thickness. The samples were placed in the test interface and set to cure in the convection oven. All inks were cured in a convection oven at 95°C for 40 minutes.

Three carbon inks were investigated in this research; the commercial ink ED4000 from Electrapolymer (Paste E), and two inks from Gwent Electronic Materials (GEM 1 and GEM 2). Three prints of each ink were done to provide some statistical data and understanding into the repeatability of the measurement.

Both AC impedance and DC resistance measurements were performed on the test samples immediately after the conductive ink was printed onto pre-deposited electrodes. The samples were then placed into an oven to cure at 95°C for 40 minutes whilst the impedance and resistance were continually logged. The following sections detail the pre-deposited electrodes, the printing of the test inks, the test jig to hold the test structures, and the electrical equipment set-up.

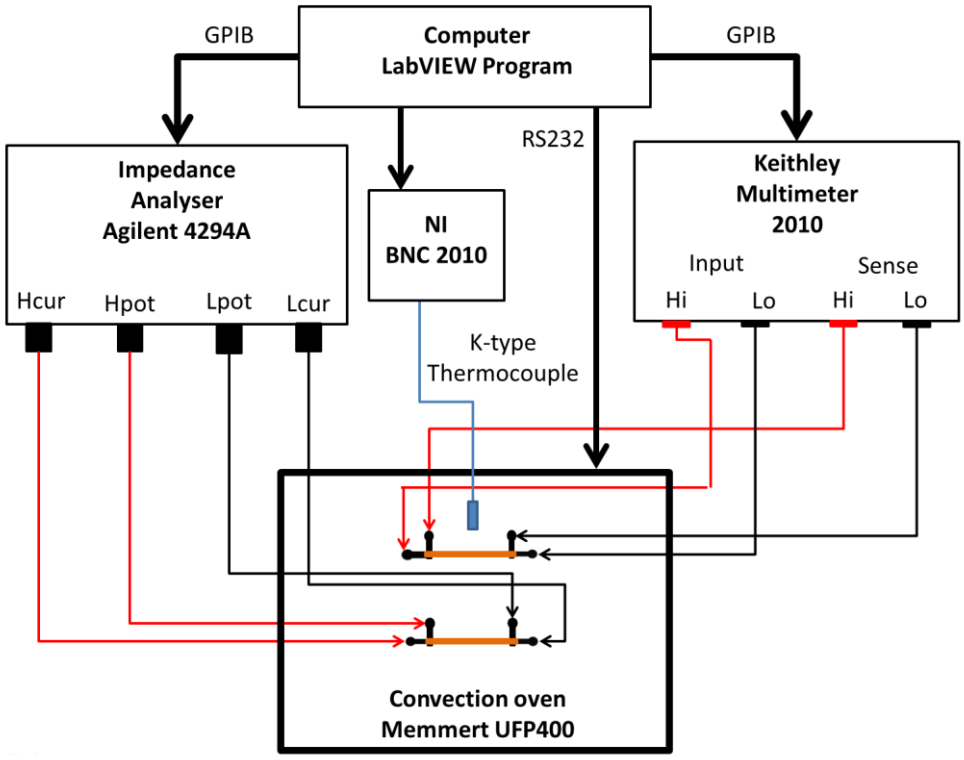

Figure 49 Block diagram of the test setup for electrical measurement

The measurement setup shown in Figure 50 provides the continuous measurement of AC Impedance, DC resistance and temperature of the DUT during cure. Impedance measurement was performed using an Agilent 4294A impedance analyser, which was set to sweep the frequency from 100 Hz to 10 MHz. The DC resistance was measured using a Keithley 2010 multimeter which has an upper range of 100 MΩ. A LabVIEW program (see Appendix 3) was written to control the convection oven, impedance analyser and multimeter. Four-probed measurement was used on both AC impedance and DC resistance measurements to eliminate the effect of probe lead resistance. The temperature was measured by a K-type thermocouple placed on the substrate 1 cm from the structure under test.

A National Instrument (NI) PCI-6251 data acquisition card to convert analogue signal to digital signal was installed in the computer. The NI BNC-2010 temperature interface was used to connect the thermocouple to the data acquisition card. Immediately after printing the test structure was placed in the jig, fastened, and electrical monitoring initiated before being placed into a Memmert UFP400 convection oven to cure the samples at 95°C for 40 minutes.

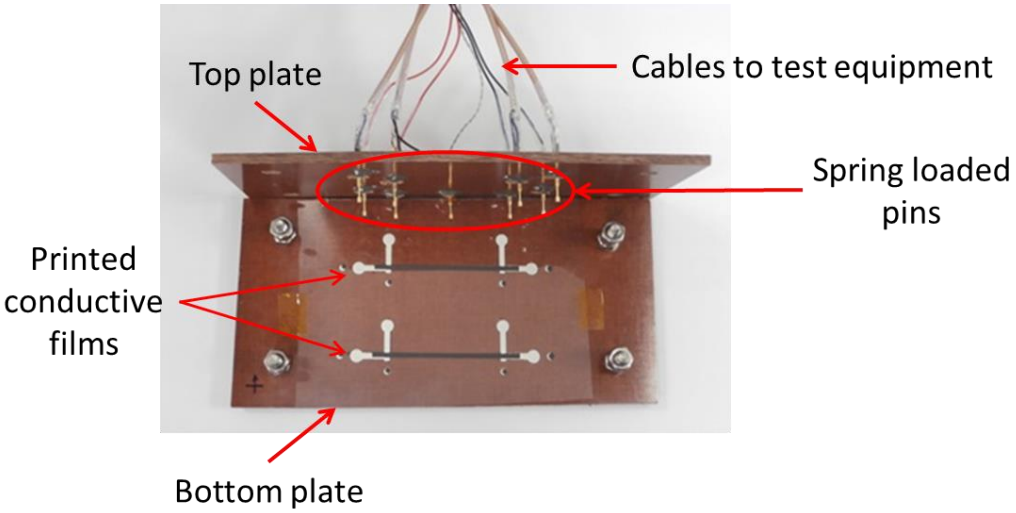

Figure 50 Photo of the test interface with device under test.

Measurement of conductive film at elevated temperature was made possible using a test interface. The test interface shown in Figure 51 was built to provide electrical connection between the sample and the test equipment. The test interface is made out of two 4 mm thick Tufnol sheets. The top plate holds the spring loaded pins that maintain electrical contact between test equipment and the test structure. The bottom plate contains the DUT. Fasteners at each corner keep both plates together and maintain the test pin to DUT pad connections. The tufnol sheet has thickness of 4 mm ± 0.1 mm. Convection oven was used and set based on the manufacturer data sheet for the conductive ink.

Some experiment requires the convection oven to be controlled, and therefore LabVIEW software was created to control the equipment via rs232 interface. The advantage of using convection curing, although a slow processing technique is that it does not require high sampling rate on the side of data acquisition. The measurement during cure can be captured easily using a low sampling rate, as we have used in the AC impedance and DC resistance during cure experiments.

3.4.3 **Infrared (IR) imaging technique defect detection**

Infrared measurement technique assesses conductive film in a non-contact and non-intrusive manner. Furthermore, it has a potential for large area measurement. The application of IR imaging technique includes astronomy, and therefore measurement of a sample with a few metre dimensions will cause no issue with this technology. These are the criteria for the measurement technique to be compatible to manufacturing of conductive film. Another reason of using IR camera is the cost effectiveness due to the development of IR detectors.

The infrared thermal measurement started with the experiment performed by William Herschel (1738 – 1822). He used a prism to separate each colour. Each colour was measured and a number was assigned. Red colour is represented by number 55, green is 24 and violet is 16. However, the unit of measurement was unknown at that time. In addition to the discovery of wavelength that represent different colour, each colour creates different temperature. The heating effect continues and peaked beyond the colour red. Also he noticed that ultraviolet has less temperature effect while infrared that is invisible to naked eye recorded the maximum temperature increase.

Temperature can be expressed in absolute and relative terms. The absolute scales has two types, they are the English system (Rankine) and Metric system (Kelvin). Relative terms has two types, the “Celsius”, or “centigrade”(metric system) and “ Fahrenheit” (English system). The expression “zero Kelvins” or “zero Rankines” mean absolute zero where at this temperature no molecular action takes place. Absolute zero is -273.15 °C or -459.67 °F. The series of equations below is the conversions of Celsius, Farenheit, Rankine and Kelvin to other unit of measurements.

$$T_{Celcius} = \frac{5}{9} T_{Fahrenheit} - 32 \tag{9}$$

Table 1 Electromagnetic Spectrum

Radiation	Wavelength (m)
Gamma	<1.0E-10
X-ray	1.0E-10
	1.0E-08
Ultraviolet	1.0E-08
	4.0E-06
Visible	4.0E-06
	7.0E-06
Infrared	7.0E-07
	1.0E-04
Microwave	1.0E-04
	1.0E-02
Radiowave	>0.01

The electromagnetic spectrum is shown in Table 1 detailing the radiation and its corresponding wavelength. Radiative heat transfer takes place in the IR portion of the spectrum, from 0.75 μm to 100 μm, although most practical measurements can be made out to about 20 um (Kaplan 2007).

There are three different mode of heat transfer. First is the conduction where the transfer of heat happens through direct contact from the heat source to the stationary media. This type of conduction normally happens on solid object, but can also occur in liquid and gases. The transfer of heat in liquid is caused by molecular collision, while in solid is through atomic vibrations. The conductive heat flow per unit area can be expressed by equation below.

$$\frac{\mathrm{Q}}{\mathrm{A}} = -\mathrm{k}\left(\frac{\mathrm{T1-T2}}{\mathrm{l}}\right) \tag{10}$$

Where Q is the heat transferred through slab perpendicular to the flow per unit time expressed in watts (W), A is the area in square meter (m^2). The symbol $\mathrm{T1}$ is the higher temperature, $\mathrm{T2}$ is the lower temperature, and k is the thermal conductivity of the slab material expressed in $\left(\frac{\mathrm{W}}{^{\circ}\mathrm{C}\bullet\mathrm{m}}\right)$ and l is the thickness of slab in meter (m) (Kaplan 2007).

The heat transfer by conduction is shown in Figure 52. The direction of heat flows from higher temperature to the lower temperature. The heat transfer on thicker slab will be slower compared to thin slab. The heat transfer is faster on materials with high thermal conductivity and slow on materials with low thermal conductivity. High thermal conductivity is normally also associated with electrical conductivity.

The second type of heat flow is convection. This type of heat transfer occurs between moving object, as well as heat transfer from solid to moving liquid and gas. There are two types of heat convection. First is force convection where external force is needed to move air or liquid. The second type is called free convection; it relies on the temperature difference to make density changes. These will in turn increase the buoyancy of air or fluid that will make it to move and rise. The two mechanisms that will provide heat transfer is fluid direct conduction while the second is the fluid motion (Kaplan 2007).

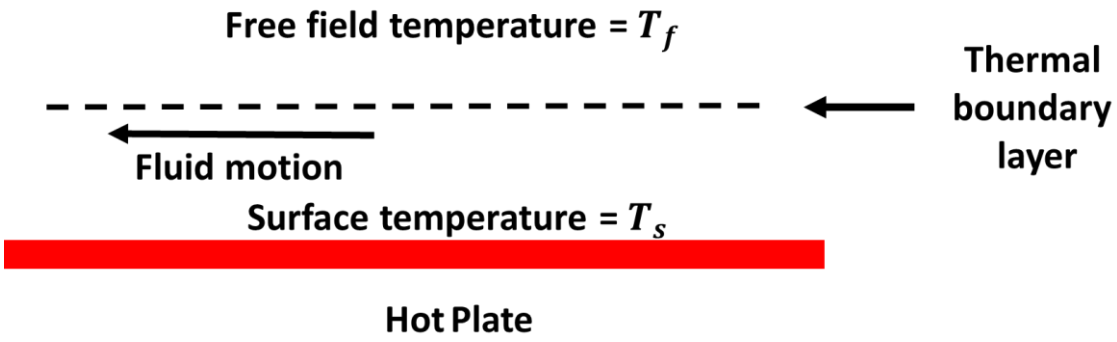

Figure 51 Illustrates convective heat transfer between a flat plate and a moving fluid

The heat transfer by convection is shown in Figure 52.The velocity of fluid is proportional to its distance to the hotplate. In other words, the velocity of fluid will decrease if it is near to the surface of the hotplate. Another factor the influences fluid velocity is the thickness of thermal boundary layer. The heat flow rate is affected by the convection layer thickness and the temperature difference between the surface temperature ($\boldsymbol{T_s}$) and the free field temperature ($\boldsymbol{T_f}$). Free field temperature is the temperature beyond the thermal boundary layer. The heat flow equation for convection heat is defined by,

$$\frac{Q}{A}=h\left(T_s-T_f\right) \tag{11}$$

Where h is the heat flow coefficient expressed in expressed in watts per meter degree Celsius $\left(\frac{W}{°C\bullet m^2}\right)$, and T_s and $T_f$are both expressed in Celcius (°C).

The last type of heat transfer is known as radiation. The different terms used for the radiation leaving a surface of the sample is called exitance and radiosity. The sample surface can act as source, reflector and channel of thermal radiation. Unlike the first two heat transfer, radiation heat transfer has the different characteristics. It can propagate in vacuum, and is affected by electromagnetic emission and absorption. It travels at speed of light and has similar behaviour to light. This type of heat transfer applies to the measurement of temperature using infrared imaging camera. The radiation is picked up by the camera detector and then converts it to electrical signal. The software maps the measured temperature to different colour (Kaplan 2007).

The advantages of using IR thermal imaging technique are non-contact, nonintrusive, remote, faster than conventional methods, and measures the temperature or radiant thermal distribution at the surface of the object of interest rather than the surrounding air. Furthermore, the sample can be in motion, it is safe especially when measuring higher

temperature, can measure very small target, fast response, and perform multiple measurement (Kaplan 2007).

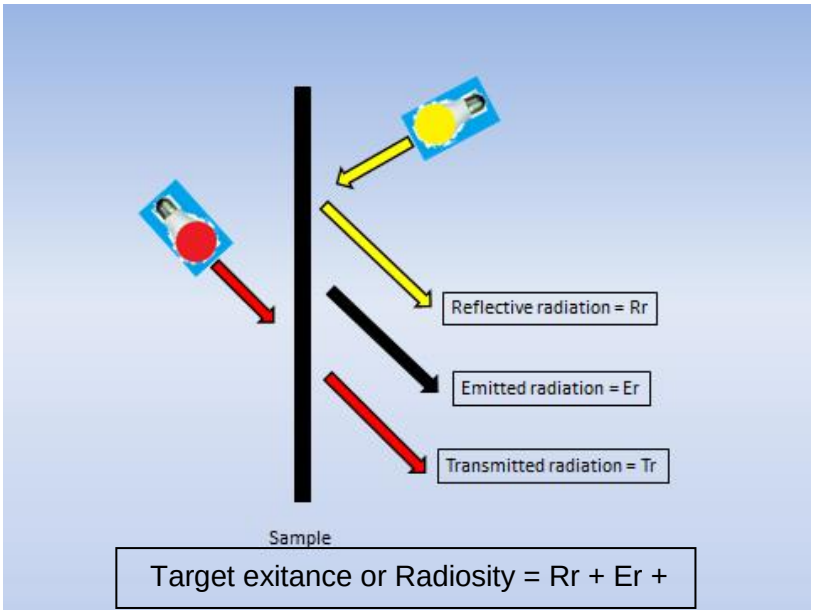

Figure 52 Radiation heat transfer

The heat radiated (W) from the surface is governed by Stephen-Boltzman law below,

$$W=\varepsilon\sigma(T_{Kelvin})^4 \quad (12)$$

The heat transfer by radiation is shown in Figure 53. Where ε is the emissivity (unity for black body target), σ is Stephen-Boltzman constant = 5.673×10^{-12} watts $cm^{-2}K^{-4}$, and T_{Kelvin} is the absolute temperature of target in Kelvin (K). Emissivity is a measure of effectiveness of a surface of material to emit thermal energy. It is expressed as the ratio between the emitted thermal radiations by the sample over the perfect emitter. The scale of emissivity is expressed between 0 and 1, where 0 is a perfect reflector while 1 is a perfect emitter which is called a blackbody. In other words, a blackbody captures all the thermal radiation but does not reflect it. Emissivity is affected by material, wavelength, camera angle, surface quality, shape and temperature. Therefore the material's emissivity is not a constant parameter unless the object is a graybody, when its emissivity is not affected by the wavelength. However, low emissivity surfaces like polished metallic surfaces can be painted or oxidised to improve their emissivity (Fehlman, William L., Hinders,Mark K., 2009).

For material testing, this can be done with a heat source to either sweep the heat or burst or flash heat then measurement of IR to measure a constant heating and cooling of the

material. Buried defect or voids inside the material can also be detected using this technique. It was applied in construction environment and on radiators where the inside tube has corroded. This causes uneven heating when the subjected to thermal imaging. IR can be teamed with mechanisms and has previously been used to generate and inject thermal energy into test samples include hot and cold air blowers, liquid immersion baths, heat lamps, capacitor-driven flash lamps, controlled refrigerants, electric current, scanned lasers, and induction heating.

Effective IR imaging technique requires excitation to the material. This excitation can be achieving either by an internal or external source. Conductors for example can pass an electrical current to create joule heating. Anomalies can either be picked up by the Infrared Imaging technique. For conductive film, this could be a challenge because it requires a homogeneous layer. Conductive film is normally is not a perfect equal layer all throughout. Therefore, identifying and discriminating good print between bad print is a big challenge.

The first step in defect detection experimentation is creating a defect on the conductive film. The defect is in the form of mechanical bending from flat to certain angle. A mechanical test system was built to bend the sample for several times while the DC resistance was being monitored. Two conductive film samples were placed side by side on mechanical bend tester. One sample will later undergo imaging under a scanning electron microscopy, while the other will be subjected to thermal imaging measurement. The SEM imaging aimed to find any physical defect inflicted by the bending of conductive film process. On the other hand1, the thermal imaging will be measuring the thermal effect, if any, on the aged samples.

3.4.3.1 Mechanical aging

Conductive film application can be used in a wider scale if it is flexible and at the same time reliable. Therefore, the measurement of the conductive film needs to assess the electrical performance while it is bend several times. This type of assessment provides electrical and mechanical strength of the conductive film. Electrical performance using DC resistance measurement was used. Scanning Electron Microscope was used to inspect the conductive film for any sign of physical defect.

The mechanical bend tester consisted of two platforms attached on both sides a stainless steel rod as shown in Figure 54. One platform was fixed to the stainless tube, while the other was fixed to the board where the rest of components were attached. The stepper motor held the stainless tube to be rotated. The stepper motor was a Mclennon 23HSX-102 and was controlled by a LabVIEW program (see Appendix 4). The stepper motor has step resolution of 1.8 ° and torque of 37 Ncm suitable to slowly rotate the DUT test platform.

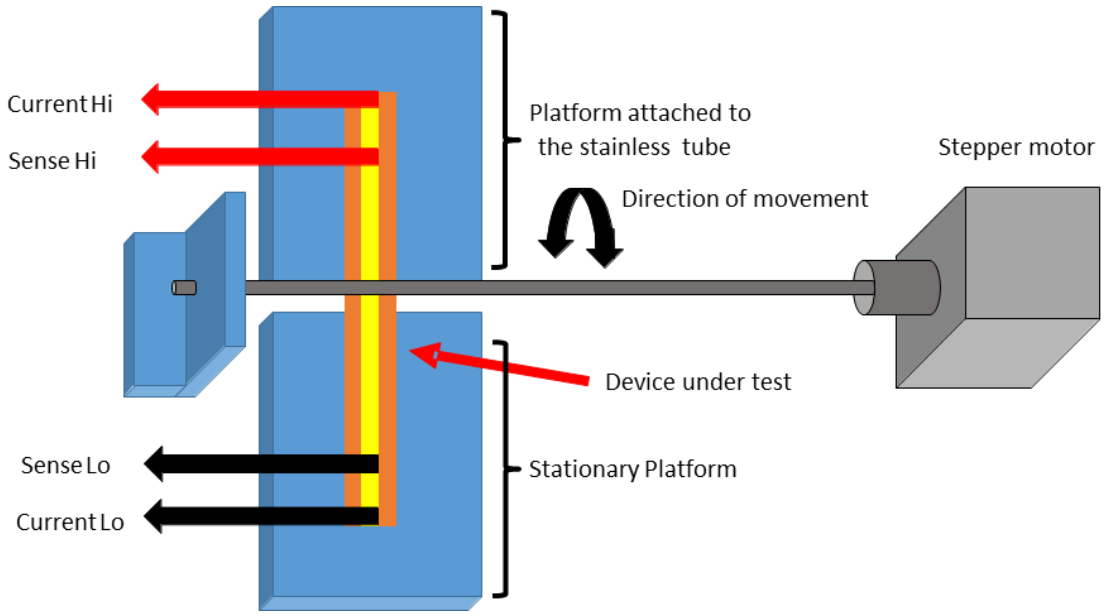

Figure 53 The conductive film mechanical test setup

The stainless tube was placed so that it will be at the centre of the bend. The other end of the tube was secured by an L-shaped bar with a hole to which the tube was inserted. The sample was attached to the platform fixed to the rod. The other end of the sample was moving freely to concentrate the effort on bending and not on stretching the conductive film. Samples were oriented so that the substrate was facing upwards. DC resistance measurements were taken when the sample was at 0 ° and at 150 ° or flat and bent respectively. Samples were screen printed to form a 2 mm wide 100 mm length structure. The pastes used were from Electrapolymer that is made from silver (ED3000) and carbon (ED4000) content.

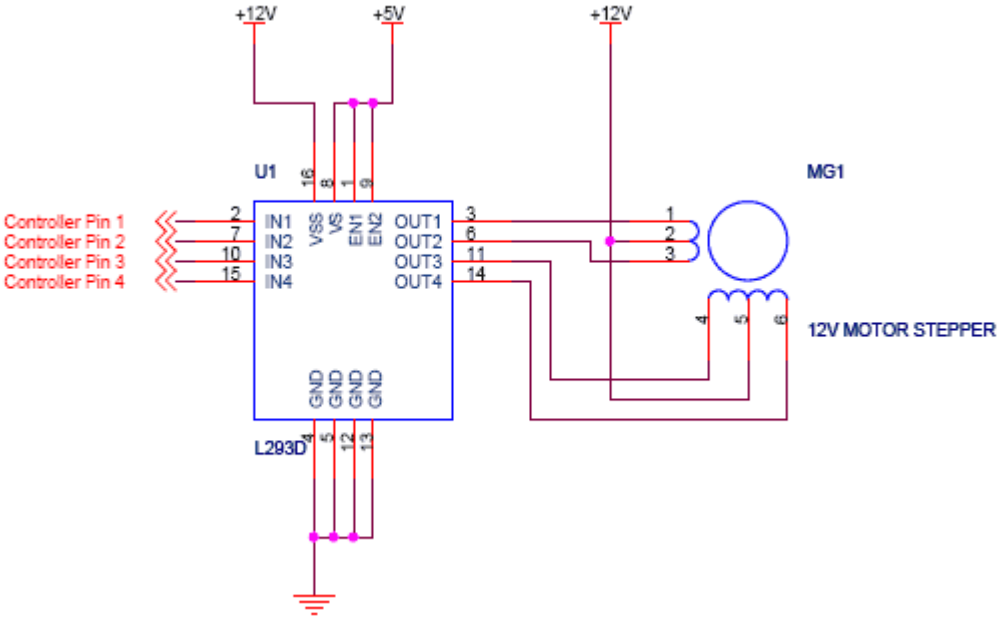

Figure 54 The schematic diagram of stepper motor and driver

The stepper motor was driven by a L293D from STMicroelectronics. Shown in Figure 55 is the schematic diagram of the driver board and the stepper motor. The controller input pins were connected to the LabVIEW interface box.

Table 2 The step instruction of the stepper motor

Step	IN1	IN2	IN3	IN4	CW / CCW
1	+5 V	0 V	+5 V	0 V	
2	0 V	0 V	+5 V	+5 V	
3	0 V	+5 V	0 V	+5 V	
4	+5 V	0 V	0 V	+5V	

The stepper motor step instruction is shown in Table 2. Each step produced a 1.8 ° motor movement. The direction of the motor was based on the step instruction sequence. Performing step sequence from 1 to 4, the motor shaft moved in a clockwise direction. While performing the step sequence from 4 to 1, the shaft moved counter clockwise.

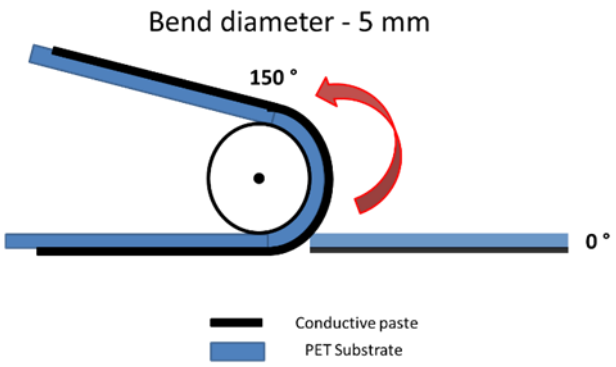

Figure 55 The conductive film is facing outward from the pivot

The sample orientation attached at the mechanical bend tester is shown in the Figure 56. The substrate was oriented at the inner radius, while the conductive film was at the outside radius. With this arrangement, the conductive film was protected from coming in contact with the stainless steel. Furthermore, the conductive film stretched further when it was placed at the outside radius. DC resistance measurements were performed when the conductive film was at flat orientation and at 150 ° ± 1.2 °. The 5 mm Stainless steel tubing was supplied by Wellington Tube Supplies. The mechanically bent conductive film was categoryed to Scanning Electron Microscope (SEM) imaging.

3.4.3.2 SEM imaging

The images of mechanically bent samples were taken by SEM. The SEM equipment used was Camscan MX2500. The drawback of using SEM is that measurement needs to be done under vacuum, thereby limiting the possible test materials that can be characterised. The conductive film was coated with a thin layer of gold, about 10 nm to prevent charging on the surface. Charging of the surface will cause the image to drift and cause error on the sample imaging. This process causes the sample to be contaminated and therefore cannot be used for further measurements. Another problem that SEM will experience is with measurement of transparent samples.

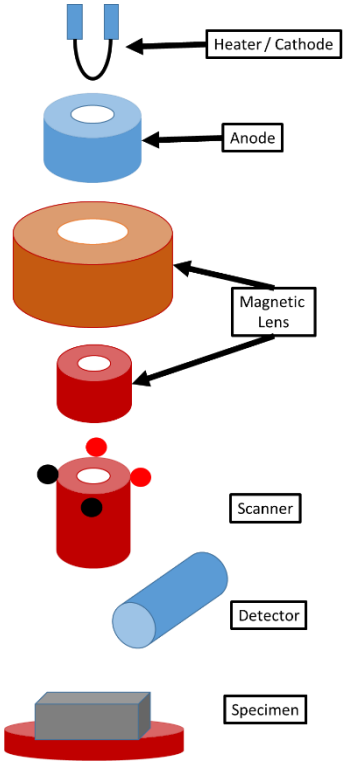

Figure 56 The main components of SEM inside the vacuum chamber

The main components of SEM equipment are shown in Figure 57. The electrons are generated by the heating filament by forcing kV of voltage. The electrons are attracted to the anode, some of the electrons pass through the anode and this will be magnified by series of magnetic lenses. When the electron beam is concentrated, the scanner will deflect the electron beam so that it will scan the surface of the sample. The loose electrons will be picked up by the scanner. The advantage of using a Scanning Microscope is down to its magnification power. The resolution of a typical electron microscope is 1 nm (Hubbard 1995). Another advantage of using SEM is the option of using elemental analysis that shows the compositional details of the material.

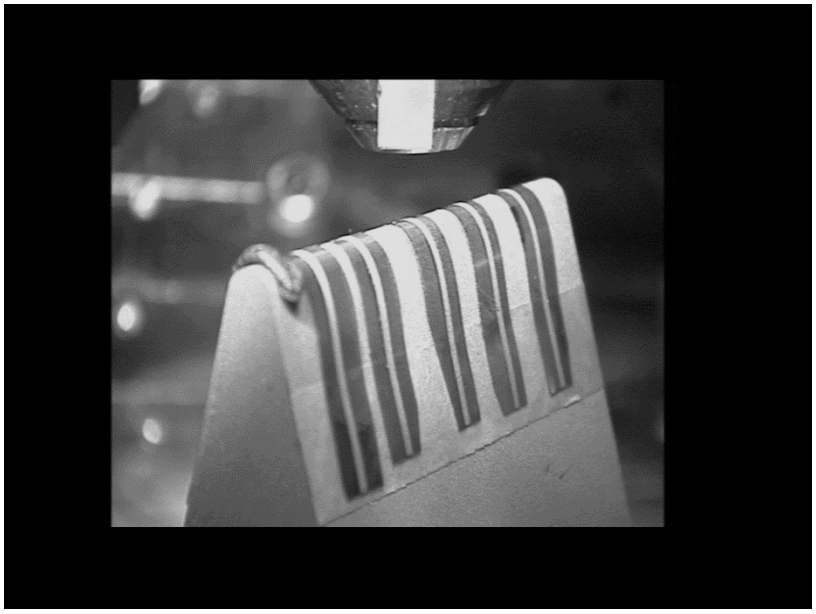

Figure 57 Photo of the sample inside the SEM vacuum chamber

The Figure 58 shows the sample attached to the sample holder. The sample holder was design to bend the sample at 150 ° which correspond to the bend angle used in the mechanical bend tester. Double sided adhesive tape was used to attach the sample to the holder. Prior to SEM imaging of the sample, the sample was coated with a thin coating of gold using plasma deposition. Sample that undergoes SEM imaging is required to have a 2 nm gold coating using plasma coater to prevent surface charging. The surface charging will cause drift of image especially at high resolution

Conductive film was bent from 0 ° to 150 ° for 100k cycles. Bending was performed at decade interval starting from 1 to 100k. Three samples at each interval were used, and different samples were used at each interval. A fresh sample was required for each interval because every time the sample is categoryed to SEM imaging it is being contaminated by the coating. Both silver and carbon prints have undergone the mechanical aging test.

3.4.3.3 Thermal imaging during voltage sweep

The final step in defect detection was the measurement of samples using infrared imaging. The mechanical bend tester produced two samples that were bent at 1 cycle to 100 k cycles at decade interval. The first sample was intended for SEM imaging, while the second is for thermal imaging. The purpose of the measurement was to determine the effect of mechanical aging on the thermal performance of conductive film. The result of the measurement was correlated to the DC resistance measurement during bending and SEM images gathered. The camera was focused on the region of interest (ROI) where the bends

occur. Measurements on the sample were only taken at flat orientation; these decisions were based on the SEM imaging results.

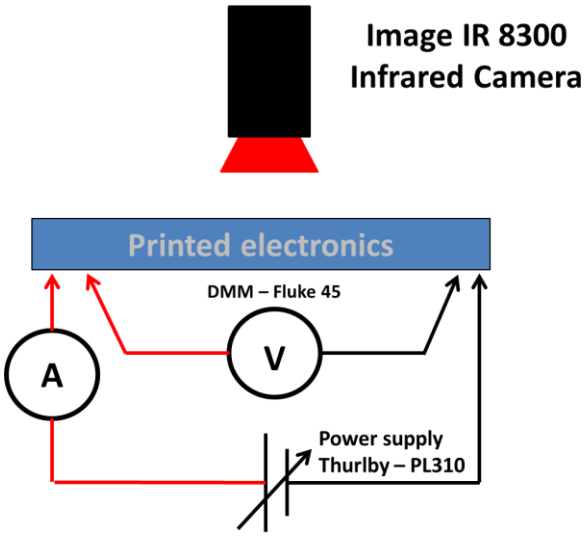

Figure 58 The thermal imaging setup to measure conductive film

The thermal imaging setup to measure conductive film is shown in Figure 59. The infra-red camera used was ImageIR 8300. The power supply was ISO tech IPS 3303s. The voltage applied to the conductive film created joule heating. The heat produced by the conductive film was measured by the IR camera that was positioned above the sample. The current of the power supply was limited to 1 A to limit the conductive film temperature to 40 °C. These prevented joule heating from damaging both the conductive film and substrate.

Table 3 The electrical test setup used in infrared imaging

Materials	Silver (Electrapolymer ED3000)	Carbon (Electrapolymer ED4000)
Voltage sweep	0.6 V to 1.6 V at 0.2 V step	5 V to 30 V at 5 V step
Measurement area	Area that was bend for 1 to 100 k times	Area that was bend for 1 to 100 k times
Test structure	2 mm wide 100 mm length No defect	2 mm wide 100 mm length No defect

The electrical test setup used in infrared imaging technique is shown in Table 3 where a voltage sweep is applied to conductive film. There is a voltage difference on the voltage sweep range between the silver and carbon paste. The temperature rises faster on silver than carbon. The thermal conductivity of the material is related to its electrical conductivity.

In this particular case it followed the relationship between the thermal conductivity and electrical conductivity. The printed structure made out of silver required a lower voltage sweep value to achieve temperature similar to that of carbon with a higher voltage sweep value.

Experiment summary

The lifetime performance measurement assessment performed on conductive film aims to determine its electrical performance when subjected to different environmental condition. The environmental tests used were elevated temperature testing and high humidity testing. The purpose of elevated testing at 125 °C is to increase oxidation rate. Commercially available silver and carbon loaded conductive pastes were used. Another carbon filled development paste from Gwent Electronic Materials was also added to the testing. These pastes are very popular in conductive film industry because of its conductivity in the case of silver paste while affordability for carbon paste. Combination testing in the form of 85 °C / 85 RH was also used to determine the effect of moisture absorption of the conductive film.

Third harmonic testing is a novel measurement to be applied for conductive film. Previously, this method is a popular quality assessment tool in resistor manufacturing industry. The purpose of this measurement technique is to remove weak product that can cause early field failure. Process improvement is another important function of this novel measurement technique for conductive film.

The AC Impedance and DC resistance measurement during cure is a novel measurement technique aims capture the development of the conductive paste from liquid to solid transition. AC Impedance was set to measure at 100 Hz to 1 MHz test frequency. Both, the AC Impedance analyser and DC resistance was configured to measure at four point probe setup to eliminate lead resistance. Pre-deposited electrode using silver paste was printed to prevent the liquid printed structure being squeezed and damaged by spring loaded pins. LabVIEW software was developed to capture the data from the equipment.

The novel measurement technique using Infrared thermal imaging was applied to conductive film for detect defection. The printed structure was stressed mechanically by bending it at 150 ° for 100 K test cycle; while its DC resistance was taken. The stressed region was

inspected using Scanning Electron Microscope during flat and at 150 ° bent orientation. Infrared thermal camera was used to measure the temperature of the conductive film's stressed region during IV sweep.

4 Chapter 4 – Results and Discussion

The results of three category areas are presented and discussed in this section. The first is results from the lifetime performance test using environmental test, and third harmonic measurement. The second is the AC impedance and DC resistance measurement during cure and the last is results from the IR imaging defect detection experiments. The conductive inks used in these experiments were commercially available paste from Electrapolymer ED3000 and ED4000. ED3000 is silver loaded paste while ED4000 is carbon based paste. In addition, carbon based development paste were used from GEM. There is limited information regarding the ink composition of the ink because of strict guidelines from the manufacturer.

4.1 Lifetime performance – environmental test result

Thermal aging will cause the expansion of polymer networks that change their original dimensions. The physical contact between conductive materials will decrease and will eventually cause a catastrophic failure. Temperature and Humidity testing at 85^{o}C/ 85 RH – The test accelerates the effect of oxidation and moisture absorption that could lead to loss of adhesion strength (Coughlan, Lewis 2006).

The increase in resistivity of silver ink on Figure 60 is due to polymer absorbing moisture that causes swelling (Coughlan, Lewis 2006). The conductive materials are being separated by these reactions. The increase in resistivity in carbon ink is similar to the reaction in the presence of high moisture and this happens when all organic chemical has been evaporated.

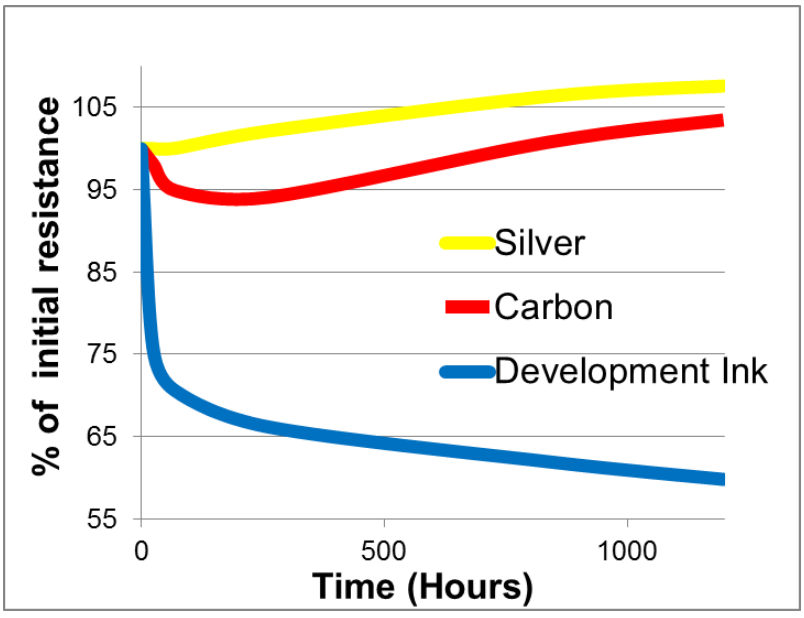

Figure 59 85 °C/ 85 RH Treated sample measurement

The combination of environmental and resistivity testing determines the performance of silver, carbon and development inks and 85 ° C/85 RH condition in Figure 60 (see Appendix 5). The reaction of silver and carbon paste to 85 ° C/85 RH treatments is that they deteriorate as the time progress. The carbon paste initially dropped in resistance of around 5% because of the further curing but rapidly increases in resistance due to the same reaction as silver paste. The increase in resistance is due to the polymer resin absorbing moisture causing it to swell (Coughlan, Lewis 2006). These will subsequently cause the particles to move apart from each other. Meanwhile, the development ink performance gets better against time. This means that the polymer resin of the development ink is better than that of the two pastes. Instead of absorbing moisture, the effect of 85 ° C/85 RH treatments causes the paste to further cure. This means that the particles became more densely packed and created more paths for conduction.

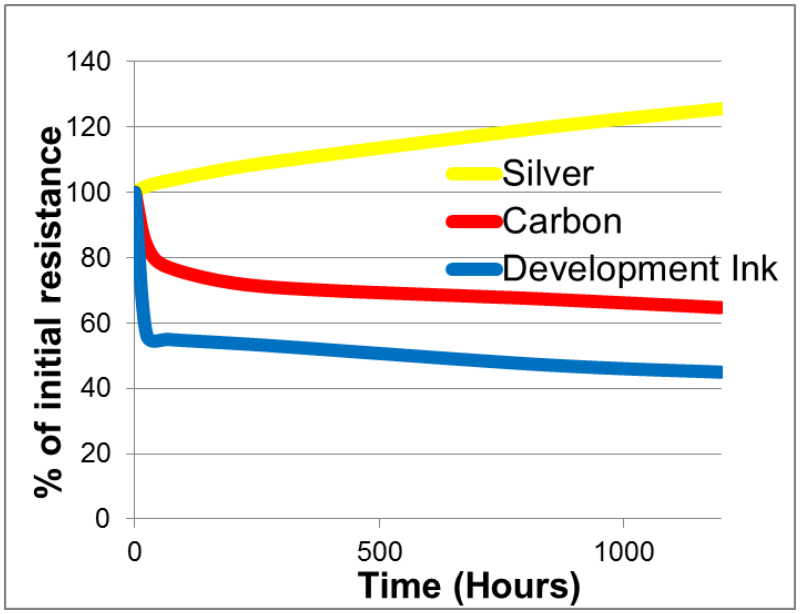

Figure 60 125 °C Treated sample measurements

The electrical performance of silver, carbon and development inks under the 125 °C condition is shown in Figure 61 (see Appendix 6). The result of the measurement shows that the silver ink increases in resistance as the testing progresses in 125 °C environment. The increase of resistance on silver is due to the fact that silver will develop an oxide layer. Although the silver oxide is still conductive, its resistance is higher than that of pure silver. Therefore, the effect of 125 °C is to increase oxidation in silver. The thickness of the oxide is unknown, but graph only indicates the presence of oxide, and that the amount is increasing. On the other hand, the carbon and development ink continues to decrease in resistance which is caused by further curing of the pastes. The polymer resin used still continues to polymerise under elevated temperature treatment. The advantage of carbon for heat

treatment is that it does not oxidise and therefore remains a good conductor under increased temperature conditions.

4.1.1 Third harmonic results

The effect of various defects on the generated third harmonic response is shown in Figure 62. Based on the result of third harmonic measurement, the alternating defect will cause the largest third harmonic response. Third harmonic will generate more error on the conductive film that has defect on the edge of the print.

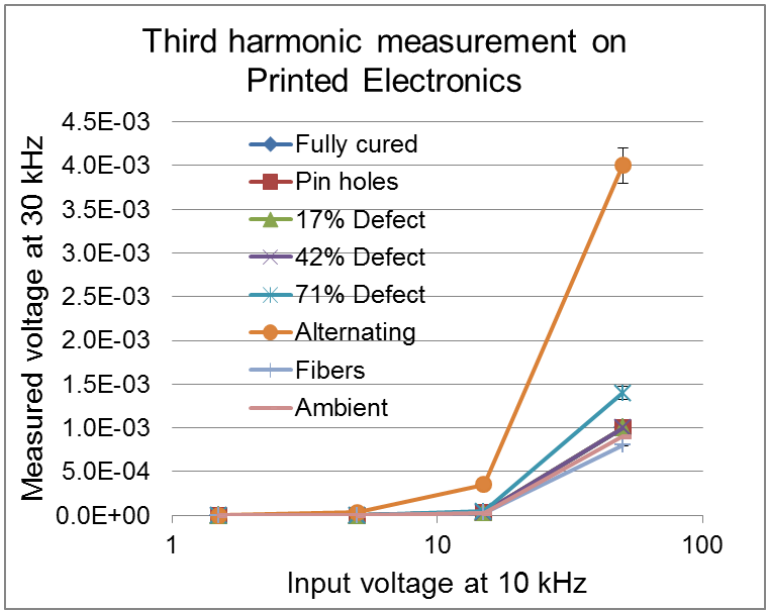

Figure 61 Third Harmonic result of conductive film with different defects

A summary of the third harmonic measurements is shown in Figure 62 (see Appendix 7). Three measurements where performed and the errors were plotted. It can be found out that the initial value of 114 dB for the fully cured conductive film decreased when more defects were introduced. The pin-holes have the least effect on the Third Harmonic Ratio (THR) value, followed by the increasing percentage of defects across the tested structure. The alternating defects with the total nine cuts across the tested structure have produced the largest third harmonic signal thus the smallest third harmonic ratio. Therefore, a number of cuts across the tested structure will generate more harmonic signal than a single cut defect. The individual pin-hole defect also generated third harmonic signal enough to differentiate it from the fully cured conductive film. The third harmonic measurement comparison between fully cure conductive film and commercially available 1 kΩ resistor which is produced through high vacuum deposition showed that the conductive film produces higher third harmonic signal as compared to high vacuum deposition process. The conductive film samples containing fibers or under cured (ambient) produced higher THR and lower third

harmonic signal than the fully cured samples. This was due to the response of the contaminants to the AC test frequency applied. Therefore, the Third harmonic Measurement is not suitable to detect this type of defects.

Table 4 Measured third harmonic result

Printed Electronics	THR (dB)	THR difference to Fully cured (dB)
Fully cured	114.0	
Pin holes	113.2	0.8
17 % Defect	112.2	1.8
42 % Defect	112.6	1.3
71 % Defect	110.5	3.5
Alternating	92.6	21.3
Fibers	114.6	-0.6
Ambient	116.3	-2.3
1 kW resistor	121.2	-7.3

The third harmonic measurement shows the higher third harmonic ratio on test structure that has defect. Using commercially available resistor as a reference for good third harmonic index, the resistor produced a much lower third harmonic ratio. The result shown in Table 4 proved that third harmonic testing is applicable to conductive film, even though the conductive film is composed of particles held by adhesive.

4.1.2 AC Impedance and DC Resistance measurement during cure result

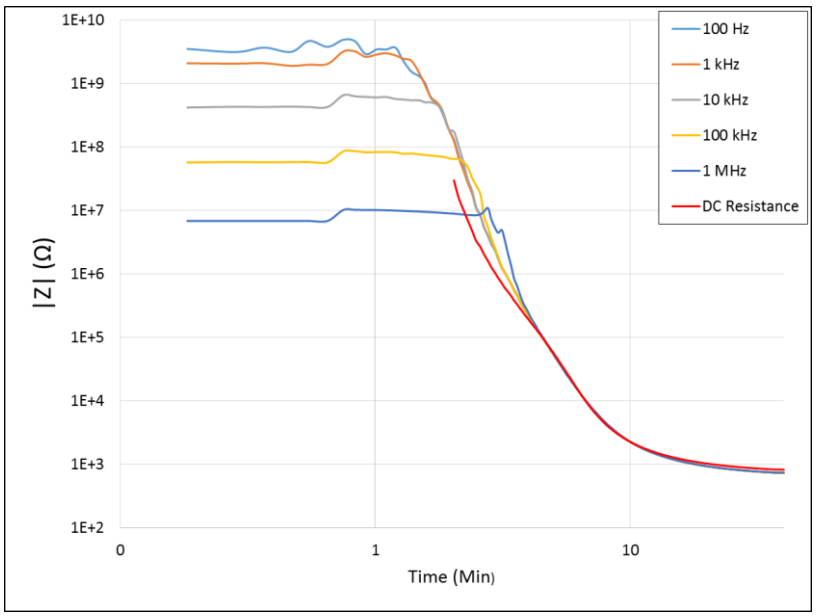

Figure 62 The AC impedance and DC resistance measurement during cure at 95°C for Paste E

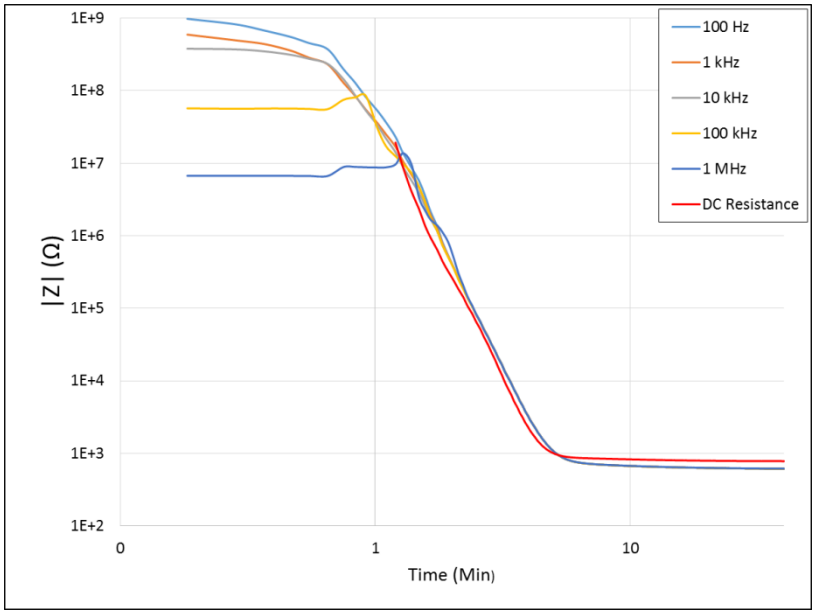

Figure 63 The AC impedance and DC resistance measurement during cure at 95°C for GEM 1

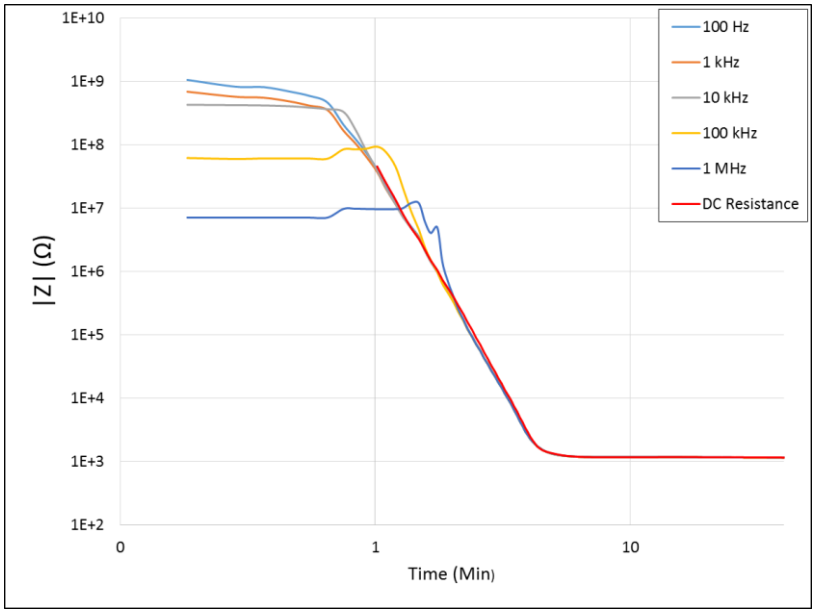

Figure 64 The AC impedance and DC resistance measurement during cure at 95°C for GEM 2

The initial measurements of the parallel test structures have produced test results for AC impedance as shown in Figure 63 (see Appendix 8), Figure 64 (see Appendix 9) and Figure 65 (see Appendix 10) or Paste E, GEM 1 and GEM 2 pastes respectively. The AC impedance analyser can measure a higher impedance range than the DC resistance meter which was limited to 100 MΩ. Interestingly the change in AC Impedance test frequency

affects the impedance of the test structure. This is better understood by considering the relationship between impedance, reactance and resistance:

$$\mathrm{Z} = \sqrt[2]{\mathrm{R}^2 + \mathrm{X}_\mathrm{c}^2} \tag{13}$$

Where $\mathbf{Z}$ is impedance expressed in Ω, $\mathbf{R}$ is the Resistance in Ω and $\mathbf{X_c}$ is the capacitive reactance expressed in Ω. The formula for reactance is shown below,

$$\mathrm{X}_\mathrm{c} = \frac{1}{2\pi \mathrm{f} \mathrm{C}} \tag{14}$$

Where X_c is capacitive reactance expressed in Ω, f is the test frequency in Hz and C is the capacitance in farad (F) of the printed structure. The initial AC impedance test frequency has an inversely proportional relationship to printed structure impedance magnitude since the impedance is dominated by the reactance. This is what we observe for the initial impedance measurements, with the impedance magnitude decreasing as measurement frequency is increased.

After sample curing had commenced, the DC resistance started to decrease in value as vehicle curing caused particle to particle contact. As the DC resistance of the test structures decreased, the AC impedance measurements converged with the DC resistance measurements. This is because the paste vehicle that hinders the electric current from passing through the test structure has cured, bringing the conductive particulate into close contact and decreasing the resistive component of the impedance. The last frequency to converge was 1 MHz since the reactance component at this frequency was lower which the equation 15 proves. Further curing of the test sample will cause a decreasing level of change in the DC resistance and AC impedance measurements. At the end of the 40 minutes cure, a low resistance structure is achieved, although its resistance, as is typical with printed pastes, will continue to decrease a little further for a few days at room temperature (Efird 1988). Whilst curing at high temperature for longer would decrease the resistivity further and faster, it will have a negative impact on the structural properties of the substrate.

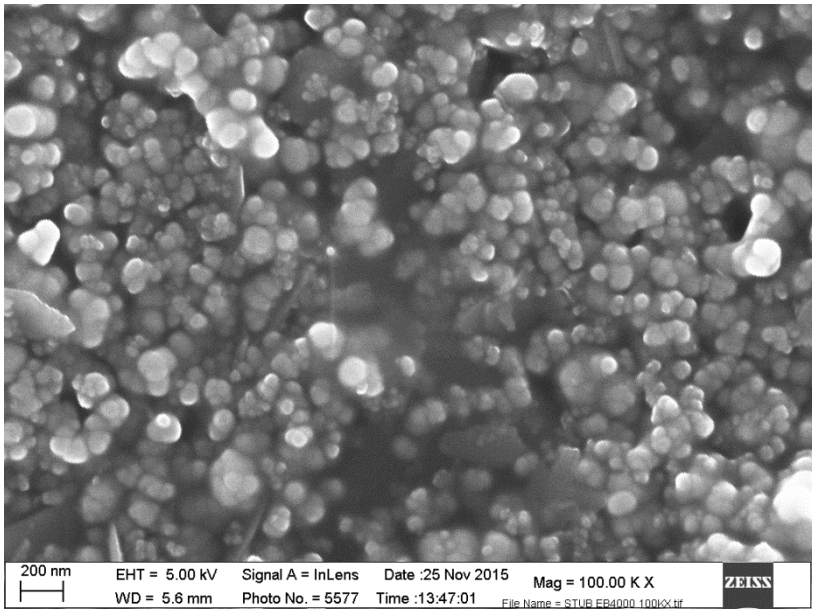

Figure 65 SEM image of Paste E

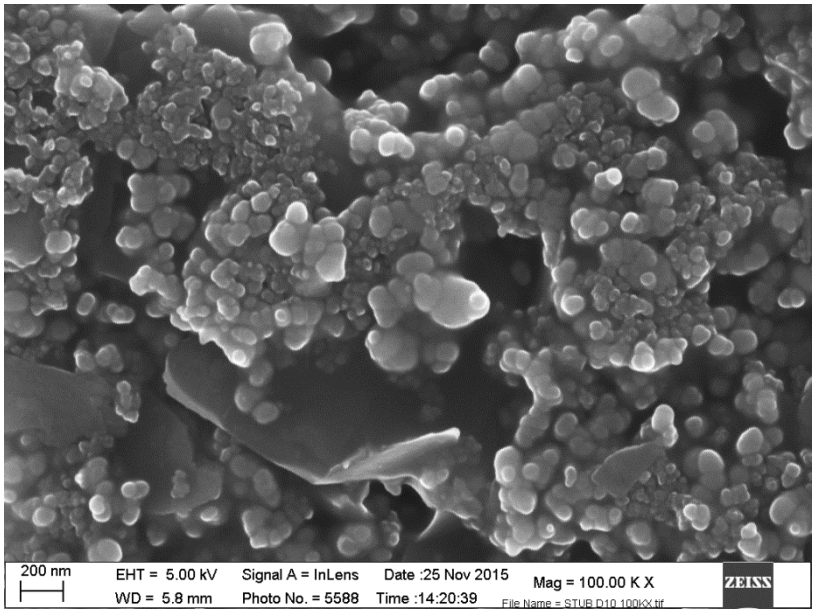

Figure 66 SEM image of GEM 1

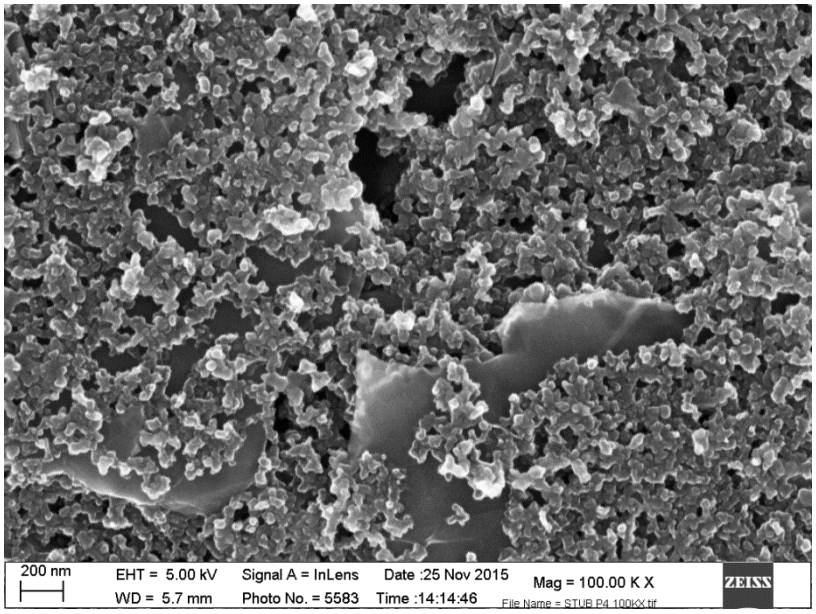

Figure 67 SEM image of GEM 2

The SEM images taken from Paste E , GEM 1 and GEM 2 pastes, shown in Figure 66 to Figure 68, indicate that the particles in the GEM 2 paste are finer and the overall structure is more dense than in Paste E and GEM 1. This could be a reason why the AC and DC Resistance after curing are the same for the GEM 2 sample, whereas for both the Paste E and GEM 1 samples the DC resistance value is higher than that of the AC impedance after 40 minutes of curing at 95 °C. At this stage of cure there are two main components that are left in the printed structure. First is the electrical component in the form of conductive particles and second, the mechanical component which is the adhesive to hold the particles together, and bind the structure to the substrate. The reason why the DC resistance is higher than the AC impedance for Paste E and GEM 1 is that Paste E and GEM 1 have more voids and spaces created between the large particles. The residual adhesive does not necessarily fill in between each of the large particles. The larger voids cause the DC resistance to increase.

Impedance measurement shows indirectly the rate of solvent loss of the pastes and it differs from paste to paste. Within 10 minutes of placing GEM paste test prints into the oven, measurement shows an impedance value that is near to 40 minutes cured resistance value. On the other hand, the Electrapolymer paste requires more than 10 minutes to reach the cured resistance value. The final resistance value of Paste E and GEM 1 pastes after 40 minutes of curing was below 1 kΩ, while GEM 2 paste is higher than these two pastes and above 1 kΩ.

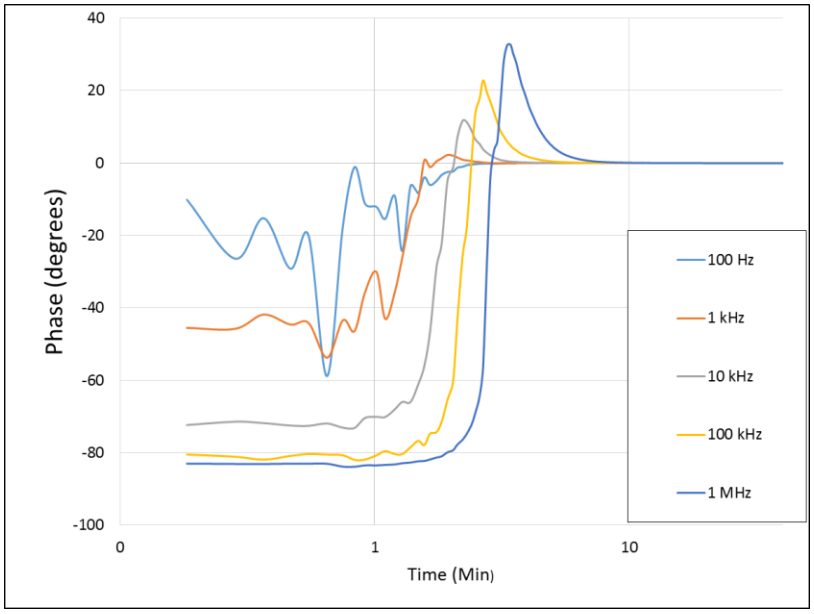

Figure 68 The phase measurement during cure at 95°C for Paste E

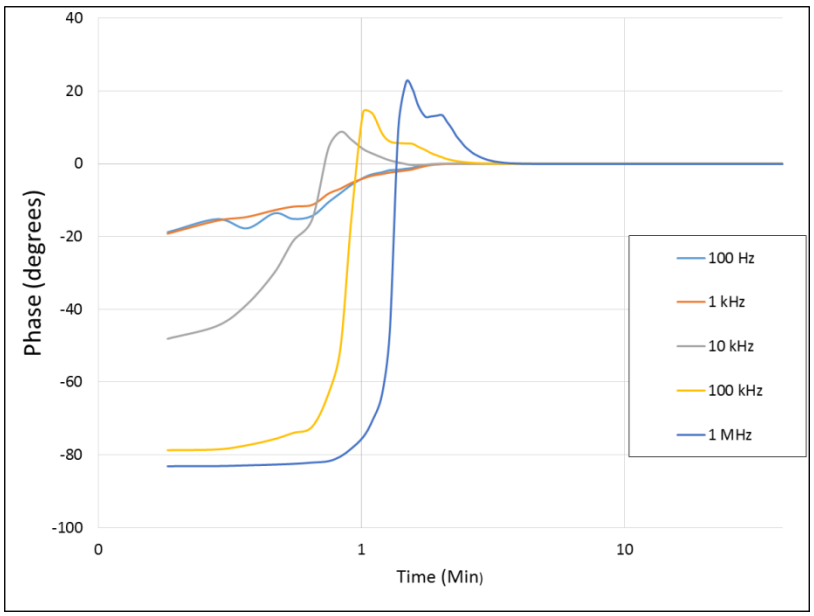

Figure 69 The phase measurement during cure at 95°C for GEM 1

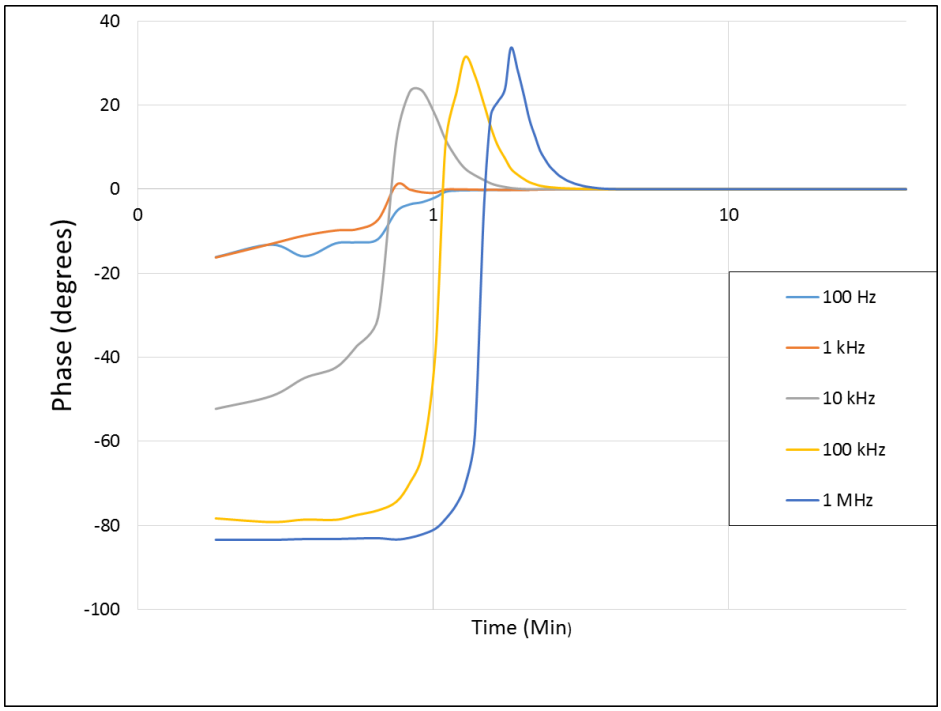

Figure 70 The phase measurement during cure at 95°C for GEM 2

The initial measurements are taken when the pastes are still at liquid state. The phase measurement as shown in Figure 69 (see Appendix 11) , Figure 70 (see Appendix 12) and Figure 71 (see Appendix 13) at this stage is between -10 ° to -90 ° to suggest that the device under test exhibits a purely capacitive component. The manufacturer datasheet for Paste E states that it contains 40 %, solvent and remainder is a combination of adhesive and conductive particle. The relationship between phase measurement and test frequency, based on equation 15, is more prominent at higher test frequency. The relationship between frequency and phase is given by equation 15.

$$\theta=\tan^{-1}\left(\frac{-Xc}{R}\right) \qquad (15)$$

Where theta is the phase in degrees, and R is the resistance in ohms (Ω). Substituting the formula of Xc gives:

$$\theta=\tan^{-1}\left(-\frac{1}{2\pi fCR}\right) \quad (16)$$

Where θ is the phase in degree (°),f is the test frequency in hertz (Hz), and C is the capacitance in farad. Based on the equation 16, the effect of increasing the test frequency is a decrease in phase.

The sample was then placed into oven for further measurement. Using a high test frequency, 1 MHz, is better because it can detect residual solvent in conductive film. As the paste cures, the phase moves from -90 ° towards 0 ° suggesting that the initial capacitive structure is turning into a resistive structure. The phase measurement of 0 ° at 1 MHz test frequency means that fully cured conductive film has been achieved, and that the test structure is a purely resistive device.

Table 5 Initial impedance and standard deviations values for Paste E, GEM 1 and GEM 2 structures between 100 Hz and 1 MHz

Frequency	Impedance (Ω) Paste E	Impedance (Ω)GEM 1	Impedance (Ω)GEM 2	Standard Deviation (%)Paste E	Standard Deviation (%)GEM 1	Standard Deviation (%)GEM 2
100 Hz	$3.52E+10^9$	$9.76E+10^8$	1.06×10^9	22.91	20.35	22.49
1 kHz	$2.08E+10^9$	$5.92E+10^8$	$6.88E+ 10^8$	40.53	19.75	15.63
10 kHz	$4.20E+10^8$	$3.79E+10^8$	$4.28E+10^8$	24.22	9.30	2.85
100 kHz	$5.72E+10^7$	$5.70E+10^7$	$6.19E+10^7$	16.83	2.36	4.06
1 MHz	$6.85E+10^6$	$6.70E+10^6$	$7.12E+10^6$	11.51	3.69	4.88

The impedance repeatability of the printing process on the uncured Paste E, GEM 1 and GEM 2 paste is shown in Table 5 for the range of frequencies investigated. The impedance measurement of the printed structure during its liquid phase produced a large variation at low test frequency, whilst frequencies in excess of 10 kHz permitted stable measurements. Based on 1 MHz AC Impedance measurement, it produces the lowest impedance measurement that is near to the cured DC resistance values and lowest standard deviation. The DC resistance measurement represents the electrical characteristic of a fully cured printed electronic structure.

Table 6 Initial phase and standard deviations values for Paste E, GEM 1 and GEM 2 structures between 100 Hz and 1 MHz

Frequency (Hz)	Paste E Phase (°)	GEM 1 Phase (°)	GEM 2 Phase (°)	Paste E Standard Deviation (%)	GEM 1 Standard Deviation (%)	GEM 2 Standard Deviation (%)
100 Hz	-48	-19	-16	28.4	10	20
1 kHz	-68	-19	-16	0.9	10	15
10 kHz	-81	-48	-52	0.44	14	8
100 kHz	-86	-79	-78	0.37	2.3	1.5
1 MHz	-86	-83	-83	0.02	0.33	0.38

The phase measurements of wet conductive test structure at (T0) together with noise information over the range of frequency are shown in Table 6. The phase measurement, similar to that of impedance measurement, of wet conductive paste produces large variation at low frequency, and less measurement variation at 1 MHz test frequency. In addition, measurement at 1 MHz produces a result that is near to -90 ° phase which is the exact representation of a purely capacitive element. This clearly defines that the test structure is wet and in liquid phase.

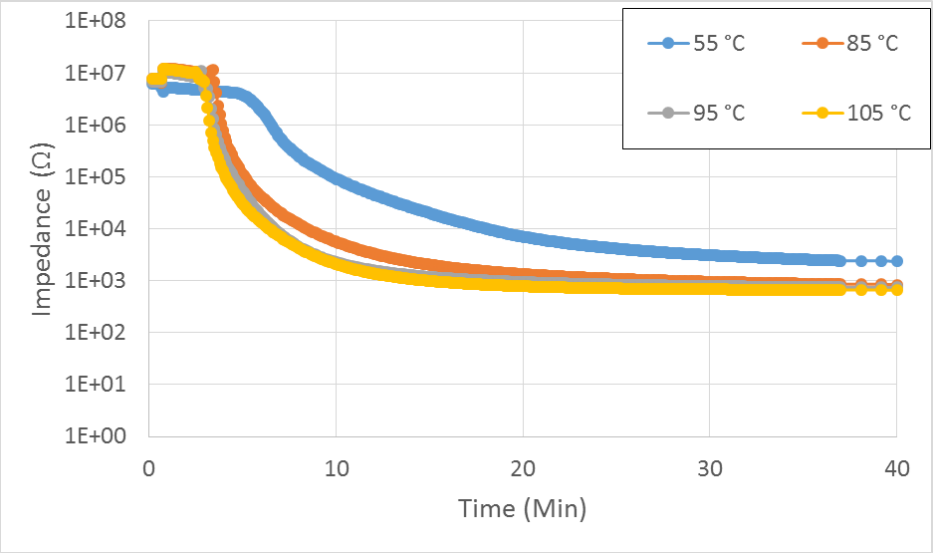

Figure 71 The AC Impedance measurement at 1 MHz for Paste E structures cured at different temperature for 40 minutes

The initial impedance measurements at 1 MHz of Paste E samples that are intended to be cured at different temperatures are the same, regardless of their curing temperature as shown in Figure 72 (see Appendix 14). The initial impedance measurement of the sample cured at 55 °C was left unchanged even after placing it into the oven. In comparison the samples placed into the oven at 85 °C, 95 °C and 105 °C temperatures the sudden increase in impedance could be due to the expansion of the solvent or the polymer binder that is present in the paste.

Increasing the curing temperature will make the conductive paste cure faster because it causes the solvent evaporation rate to increase. Subsequently this causes the rate of particle to particle contact to increase and the impedance measurement to decrease. In addition to the removal of solvent from the test structure, the higher temperature will cause further polymerisation of adhesive causing it to shrink and pull the conductive particles closer to each other (Pefferkorn 2012, Schneider, Cavalcante et al. 2010, Pires-de-Souza, Drubi Filho et al. 2009, Greer, Street 2007). The shrinking of polymer depends on the glass transition temperature of the polymer. The curing temperature must pass this temperature to be able to cause the polymer to shrink.

The effect of different curing temperature causes the delay of percolation threshold which causes the measured resistance to increase after 40 minutes of curing. The delay of the measured impedance to decrease is observed when 1 MHz test frequency was used.

Another change on the plot caused by temperature is changing the resistance of cured conductive film. This will have an effect with the ratio between T0 and T40.

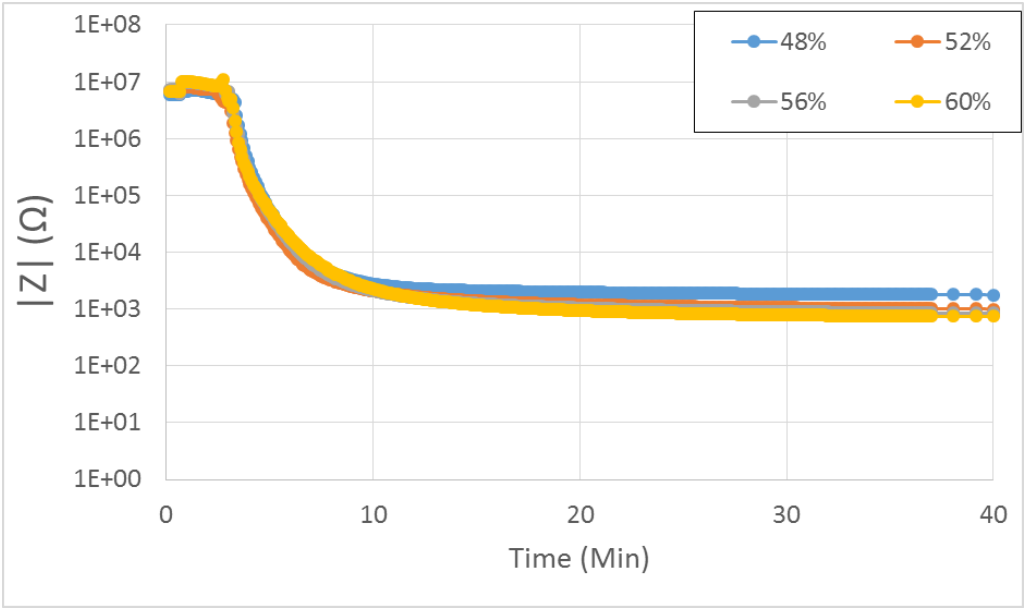

Figure 72 AC Impedance measurement at 1 MHz of Paste E at different particle loading

Particle loading was adjusted by adding solvent that the manufacturer advised use of to prevent the paste from drying. Decreasing the particle content of Paste E has caused faster curing and a higher impedance value after 40 minutes of curing at 95 °C. In Figure 73 (see Appendix 15) the pastes with fewer particles content, particularly the extreme case of 48 % content, achieved their final impedance values faster than that of the 60 % particle loaded paste. However, this does not mean that faster curing provides lower final electrical impedance. The amount and intrinsic resistivity value of the conductive particles have dictated the final cured value of the conductive film.

Table 7 shows the DC measurements performed on the three different cured print pastes. Average and standard deviation of the measurements were calculated.

Table 7 Final DC resistance for Paste E, GEM 1 and GEM 2 pastes

Paste Name	Sample 1 (Ω)	Sample 2 (Ω)	Sample 3 (Ω)	Sample 4 (Ω)	Sample 5 (Ω)	Average (Ω)	Standard deviation (%)
Paste E	716	727	718	857	810	766	8
GEM 1	770	710	902	871	657	782	12
GEM 2	1133	1262	1159	1105	1166	1165	5

The DC resistance measurement after 40 minutes (T40) at 95 °C curing is shown in Table 7. Considering all are carbon pastes, Paste E and GEM 1 values are close to each other while GEM 2 produces the highest resistance. The increase in resistance for GEM 2 test prints could be due to contamination or highly resistive material present in the test structure other than carbon particles.

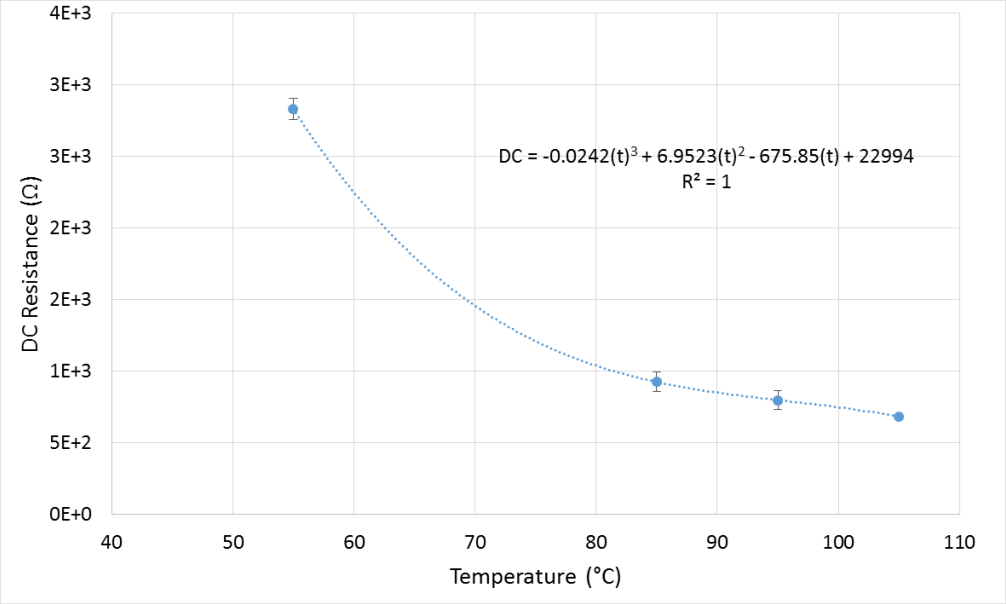

Figure 73 The DC resistance measurements of Paste E after 40 minutes at different curing temperature

Increasing the curing temperature caused the DC resistance at (T40) to decrease as shown in Figure 74 (see Appendix 16). The excel polynomial was plotted for Paste E at different level of curing is shown in the Figure 74 where t is the curing temperature in Celsius. Curing the test structure at 105 °C has produced a final DC resistance of 684 Ω, whilst 2.8 kΩ was obtained at a cure temperature of 55 °C. The increase in temperature of cure has increased

the rate of evaporation of solvent and thereby reduced the resistance measured after 40 minutes.

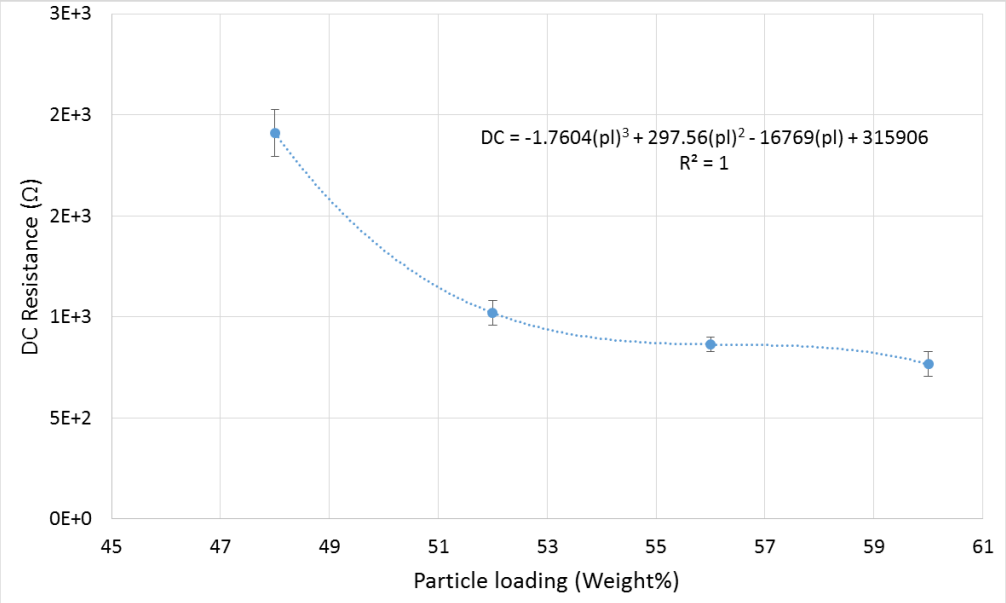

Figure 74 The DC resistance measurements after 40 minutes of Paste E at different particle loading

Lowering the particle loading causes the DC resistance measured after 40 minutes, 95 °C curing to increase as shown in Figure 75 (see Appendix 17). Also shown in the Figure 75 is the excel polynomial fit for final DC resistance where pl is particle loading. The fresh Paste E contains 60 % of carbon conductive material. Decreasing the particle content by adding more solvent results in less conductive material for a given volume of paste, and with fewer current carrying particles the resistance will increase.

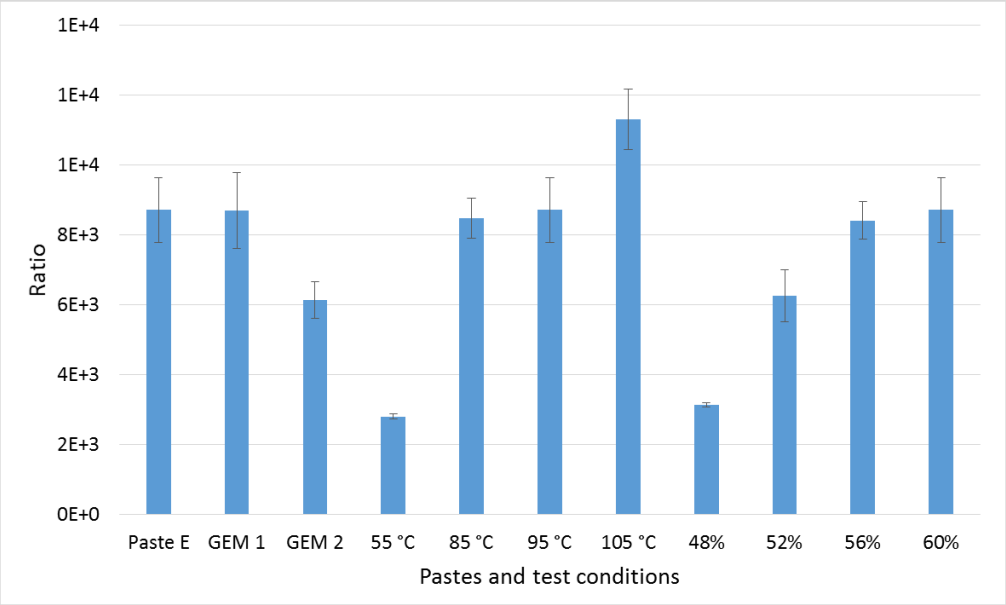

Figure 75 The AC (T0) / DC (T40) ratio of different pastes , and Paste E for various curing temperature and particle loading. The blue bars show the average values and the error bars show standard deviation for 5 measurements in each test condition

The prediction of conductive film resistivity is made possible by identifying the ratio between the initial measurement and the final cured electrical properties. In this case we compare the initial impedance at 1 MHz to the final DC resistance after cure. This ratio is shown for all 11 conditions investigated (5 samples tested for each condition) in Figure 76 (see Appendix 18). Whilst each paste has a different ratio, the repeatability of the ratio value for a given paste is good as indicated by the standard deviations of 12% or less.

There is no significant difference between Paste E and GEM 1 AC (T0)/ DC (T40) ratio, however the ratio of GEM 2 is less compared to the two other pastes. This is due to the final DC resistance of GEM 2 being the highest among the three pastes. The GEM 2 DC high resistance could be due to the manufacturer's formulation.

There is an increasing trend with the AC (T0)/ DC(T40) ratio on samples cured at increasing temperatures. Figure 76 shows that the ratio is less on samples cured at 55 °C, then increases at 85 °C and 95 °C and the highest recorded ratio is that of 105 °C. The ratio is less with low temperature curing because this will results in a higher resistance after curing at 40 minutes. As the cure temperature increases, the final cured resistance decreases.
Figure 76 shows that pastes with less particle loading produce a lower ratio between the initial and final resistance values. The paste with 48 % particle loading has produced a lower

ratio because the final resistance values are larger than that of the paste with the 60 % loading. The increase in resistance is associated with the reduced amount of conductive particles in a given volume of the paste.

The ratio as stated in Figure 76 for each corresponding paste, if divided by the initial AC Impedance at 1 MHz will produce a predicted DC resistance of the printed structures. The same applies to the paste processed in various curing temperatures or different particle loading. If the final DC resistance value departs from the expected value then an investigation of the print process and materials is warranted.

An initial level of conductance is required for ohmic curing using DC current which typically necessitates a few minutes of initial air drying. However impedance measurements reported in this experiment indicate that an AC current will flow more readily much earlier. Therefore if an AC current is used for ohmic curing, then the initial air drying can be reduced or eliminated.

4.1.3 IR imaging technique defect detection results

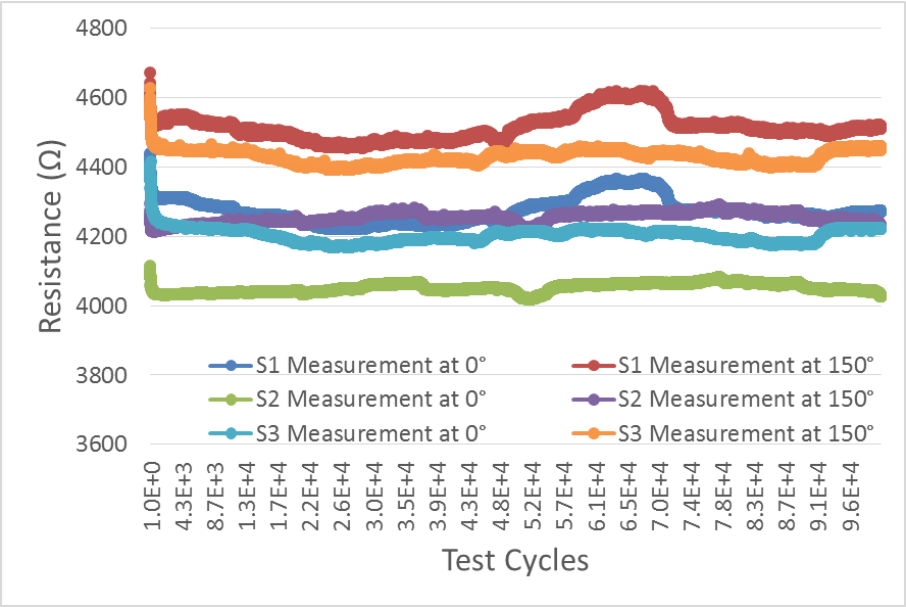

Figure 76 DC resistance of ED4000 print measured at 0 ° and 150 °

The result of DC resistance measurements during mechanical bending from 0 ° to 150 °, or flat to bent orientation respectively, is shown in the Figure 77 (see Appendix 19). The electrical performance of the carbon print at 0 ° did not deteriorate by mechanical bending. The initial measurement is higher than the succeeding measurement and these were observed on three samples. However, the DC resistance measurements at 150 ° is higher

that than the DC resistance measurement at 0 °. The strain caused to the conductive film by bending has caused the DC resistance to increase.

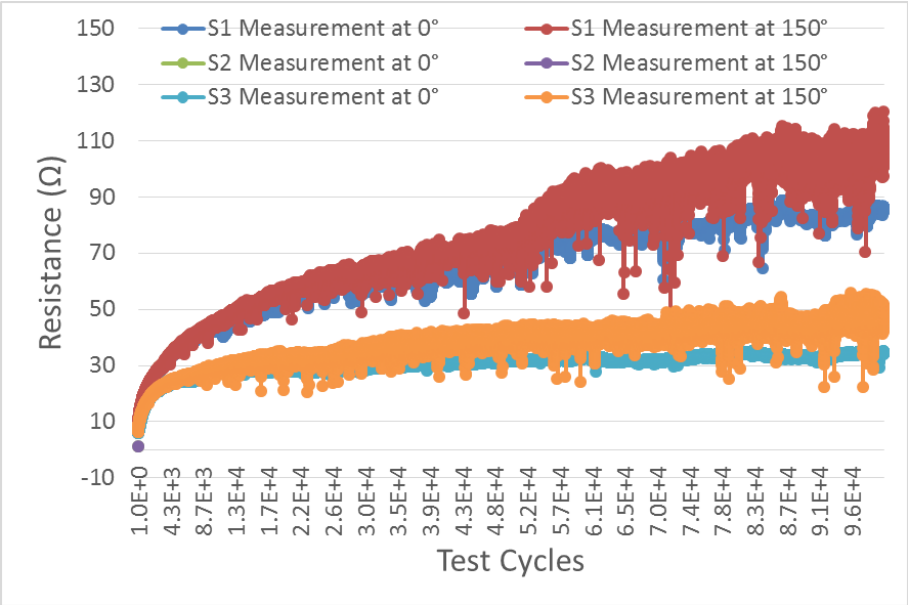

Figure 77 DC resistance of ED3000 print measured at 0 ° and 150 °

The result of silver paste DC resistance measurements during mechanical bending from 0 ° to 150 ° is shown in the Figure 78 (see Appendix 20)**.** Similar to printed carbon, the DC resistance measurement of printed silver at 150 ° is higher than that of 0 ° orientation. The DC resistance at 0 ° shows that the printed silver's electrical performance is deteriorating. This is due to the increasing DC resistance measurement as the test progress. Furthermore, the measurement at 150 ° orientation is also showing this trend. The mechanical bend testing has incurred damage to the electrical performance of the DC resistance. The effect of each bend cycle to the DC resistance of printed silver is permanent since the measurement at 0 ° continues to increase. There are a lot of measurement variations as bend test progress due silver print may have became either mechanical or chemically unstable.

4.1.4 SEM Imaging

The DC resistance of carbon prints during mechanical test remain under the initial measurement, while the silver paste DC resistance increases as test progress. Both the carbon and silver print were categoryed to a microscope imaging for physical inspection that could provide explanation on the DC resistance measurements during mechanical bending. Six printed carbon samples were mechanically bent from 1 to 100 k cycles at decade

intervals were examined. Printed carbons were categoryed to scanning electron microscope imaging at 0 ° and 150 ° orientation.

Any mechanical defect can easily be spotted at low magnification. Once a defect was identified, SEM is set to high magnification for detailed observation of the anomaly.

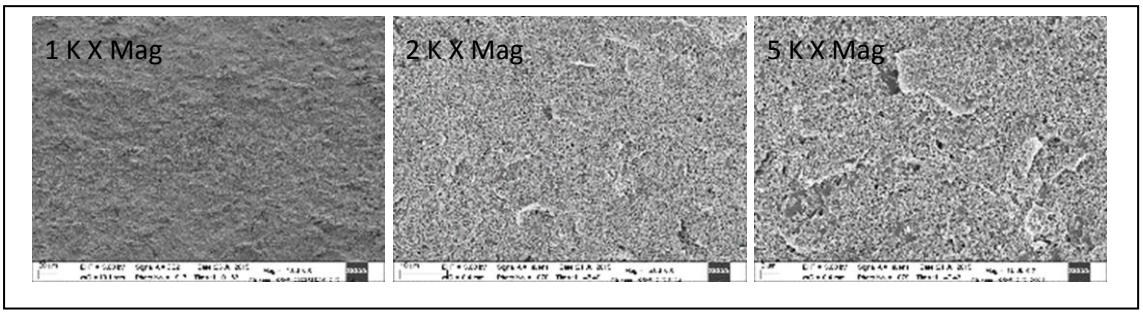

Figure 78 The SEM images of carbon print bent at 1 bend cycle

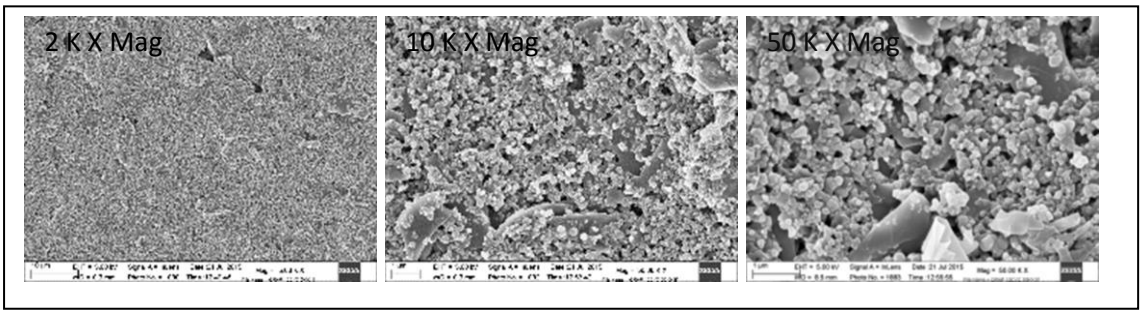

Figure 79 The SEM images of carbon print bent at 10 bend cycles

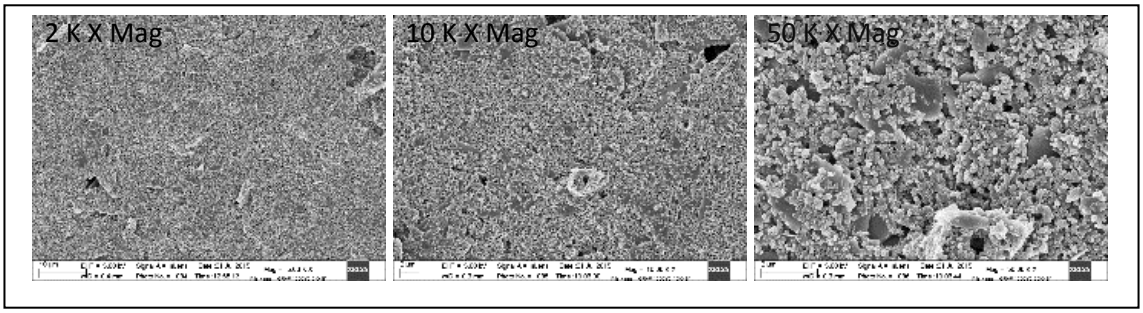

Figure 80 The SEM images of carbon print bent at 100 bend cycles

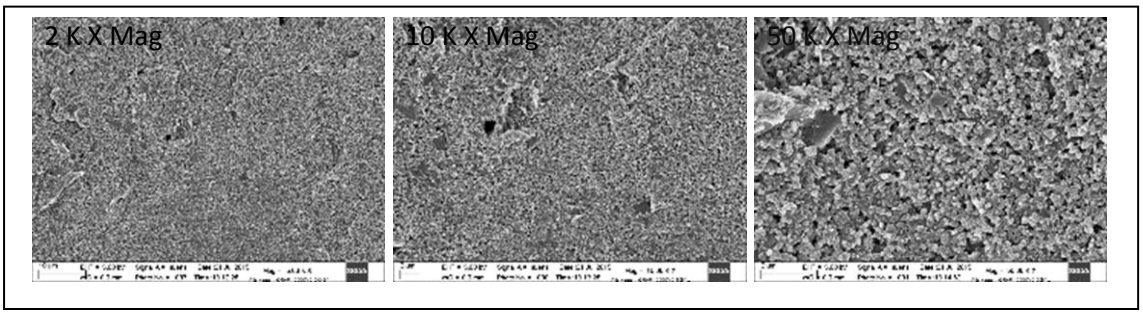

Figure 81 The SEM images of carbon print bent at 1 k bend cycles

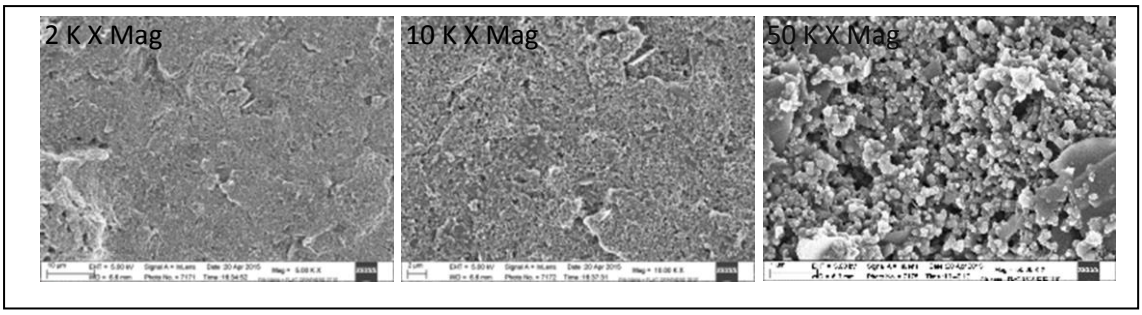

Figure 82 The SEM images of carbon print bent at 10 k bend

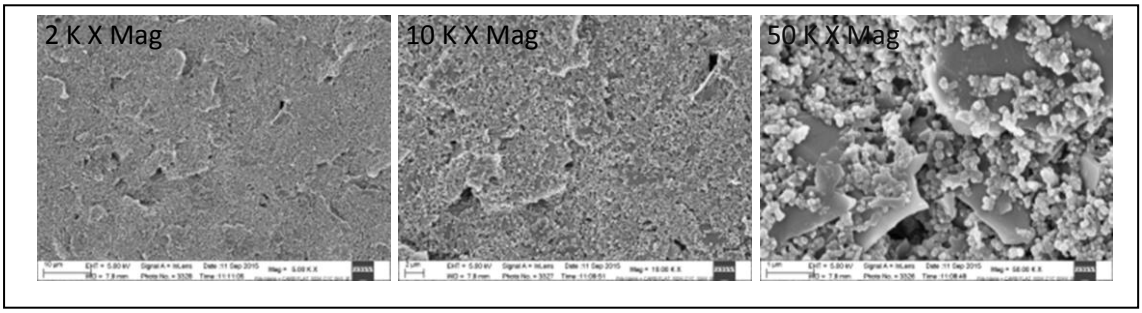

Figure 83 The SEM images of carbon print bent at 100 k bend cycles

The carbon sample bent at 1 cycle has the same appearance as carbon samples bent at 100 k cycles as shown in Figure 84 to Figure 89. The method of using SEM on carbon prints taken at flat orientation cannot reveal any defect even at high resolution. However, the SEM images on printed carbon shows the shape of the carbon used. It is composed of carbon particles and graphite flakes. The carbon particles fill in the gap between the graphite flakes making it mechanically and electrically stable. After measuring the carbon print at flat orientation, the same sample was placed into a 150 ° sample stage.

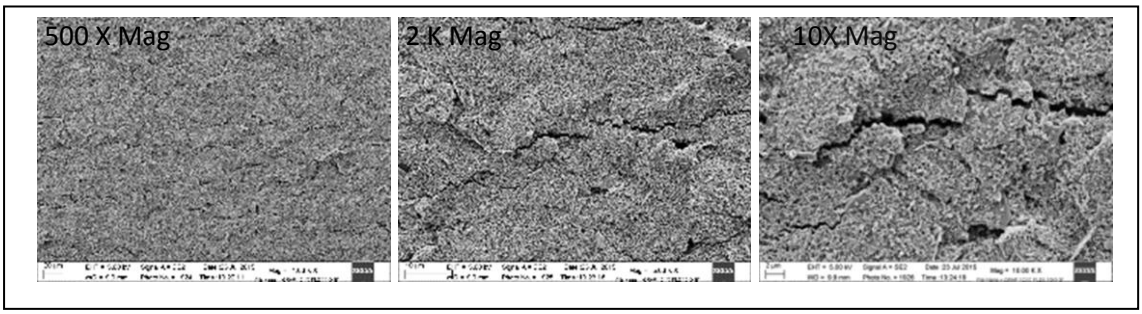

Figure 84 The SEM images of carbon print bent for 1 cycle at 150 ° orientation

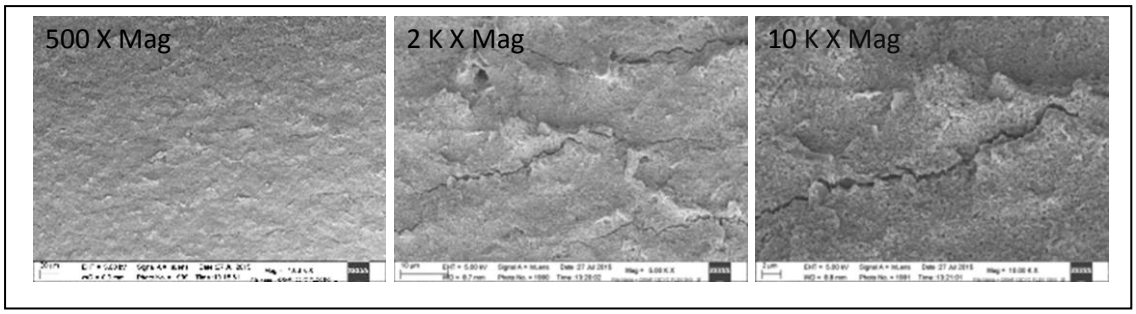

Figure 85 The SEM images of carbon print bent for 10 cycles at 150 ° orientation

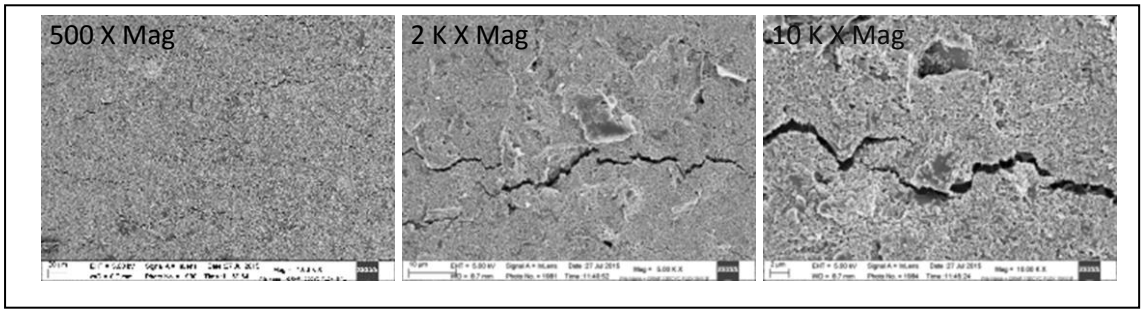

Figure 86 The SEM images of carbon print bent for 100 cycles at 150 ° orientation

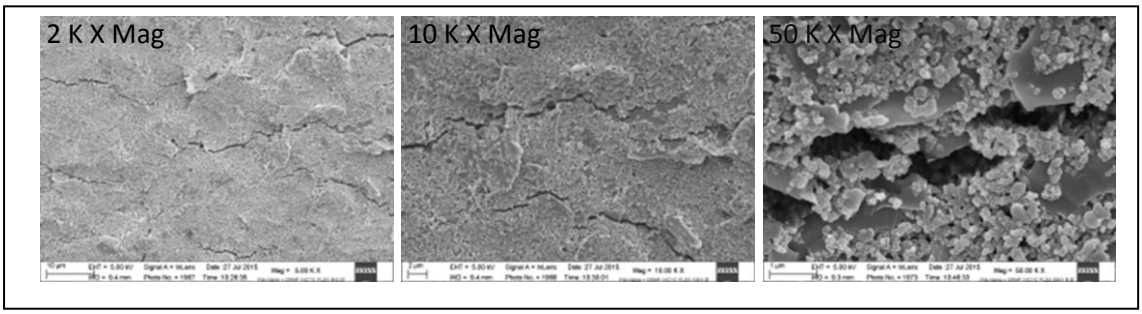

Figure 87 The SEM images of carbon print bent for 1 k cycles at 150 ° orientation

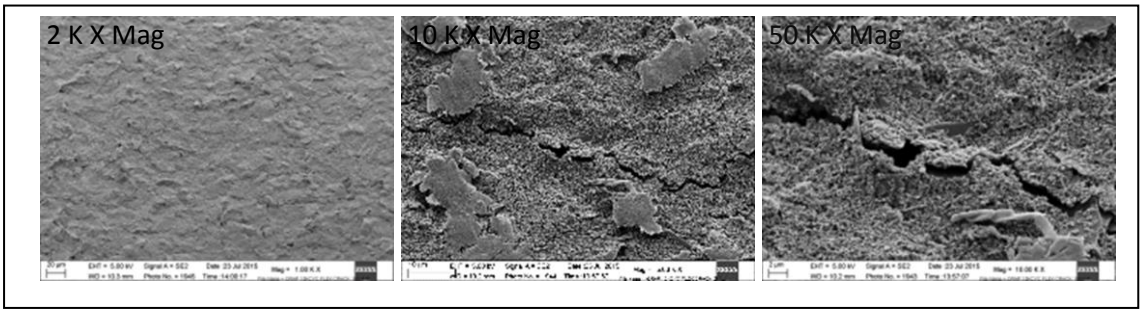

Figure 88 The SEM images of carbon print bent for 10 k cycles at 150 ° orientation

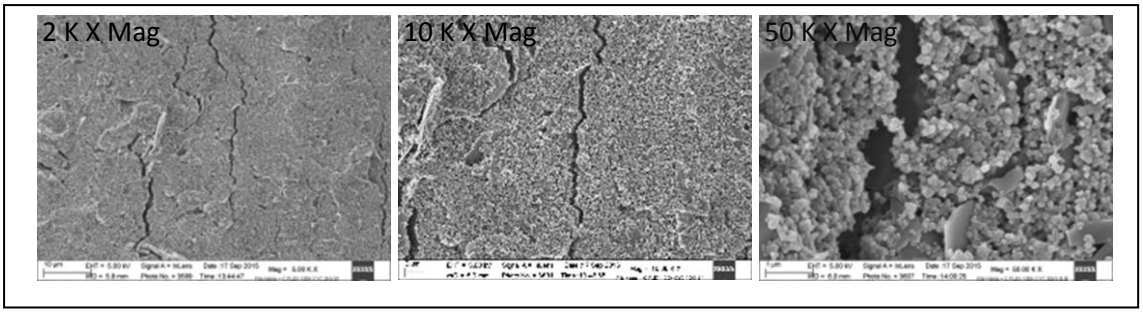

Figure 89 The SEM images of carbon print bent for 100 k cycles at 150 ° orientation

The SEM images of printed carbon at 150 ° sample holder are shown in Figure 90 to Figure 95. The crack on printed carbon appears all throughout the bend test cycles. However, the crack did not seem to propagate and there was no other sign of defect by the end of 100 k bent cycles. The physical observations from SEM images correlate to the DC resistance measurement. This is because the DC resistance of carbon print increases when it is bent. The decrease in DC resistance when it is bent is due to the reduction of particles in contact created by the crack. Furthermore, the crack appears randomly across the printed carbon and its length does not cover the entire width of the track. Hence the DC resistance measurement of printed carbon at bent orientation is not an open circuit but only shows an increase to its DC resistance. Printed silver will be next sample to be physically examined by SEM.

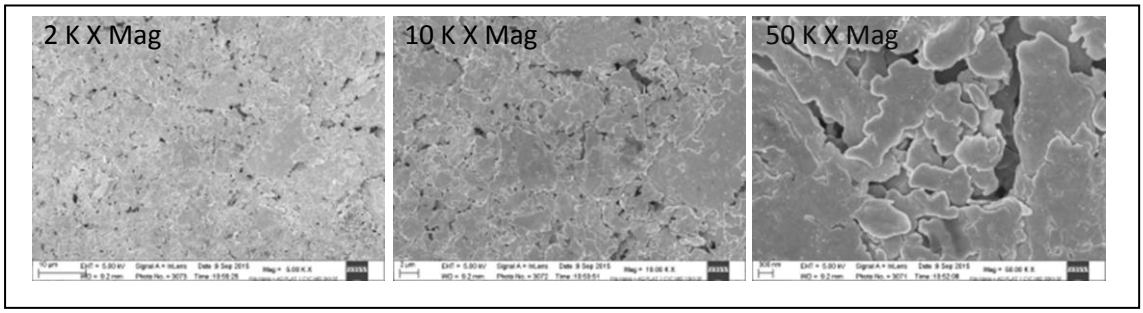

Figure 90 The SEM images of silver paste bent for 1 cycle at flat orientation

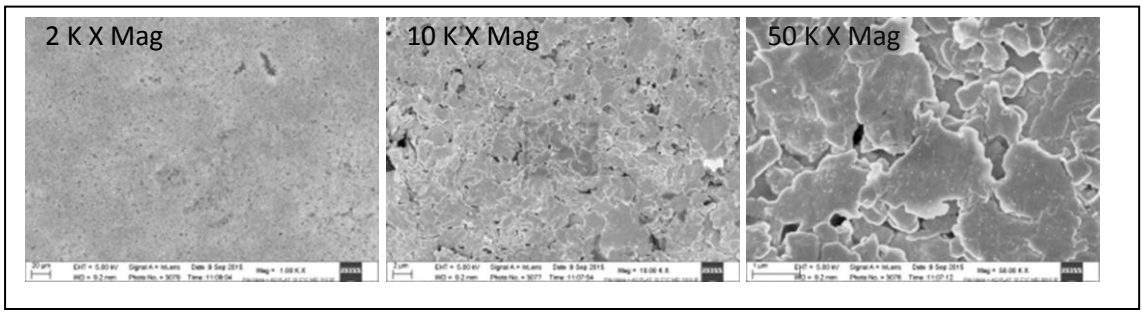

Figure 91 The SEM images of silver paste bent for 10 cycles at flat orientation

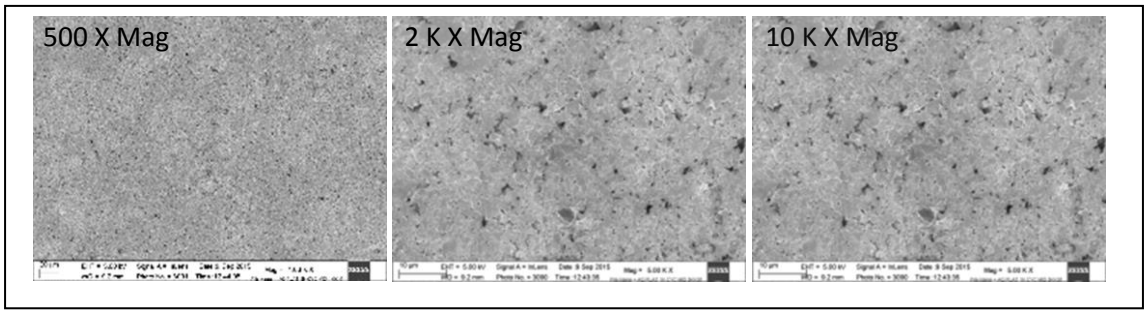

Figure 92 The SEM images of silver paste bent for 100 cycles at flat orientation

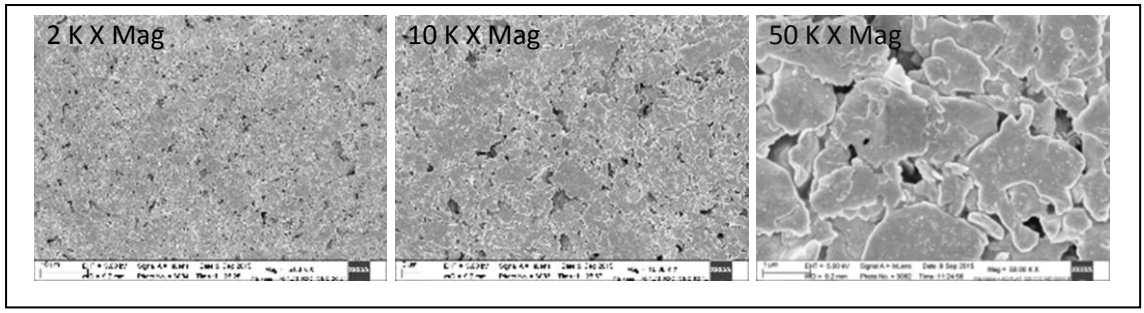

Figure 93 The SEM images of silver paste bent for 1 k cycles at flat orientation

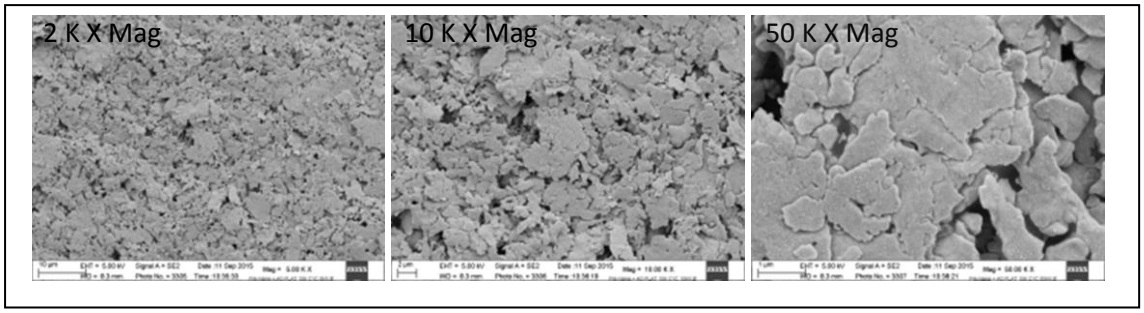

Figure 94 The SEM images of silver paste bent for 10 k cycles at flat orientation

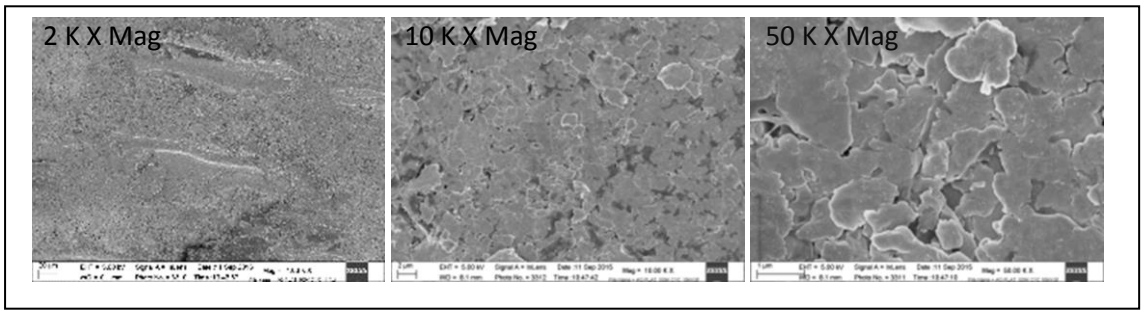

Figure 95 The SEM images of silver paste bent for 100 k cycles at flat orientation

The SEM images of printed silver at flat orientation are shown in Figure 96 to Figure 101, which reveal the silver flakes as the conductive particle shape. The silver samples were mechanical aged from 1 bend cycles to 100 k bend cycles at decade interval. There were voids seen on printed silver at low bend cycle, and scratches begin to emerge at 10 k bend cycles as shown in Figure 100.

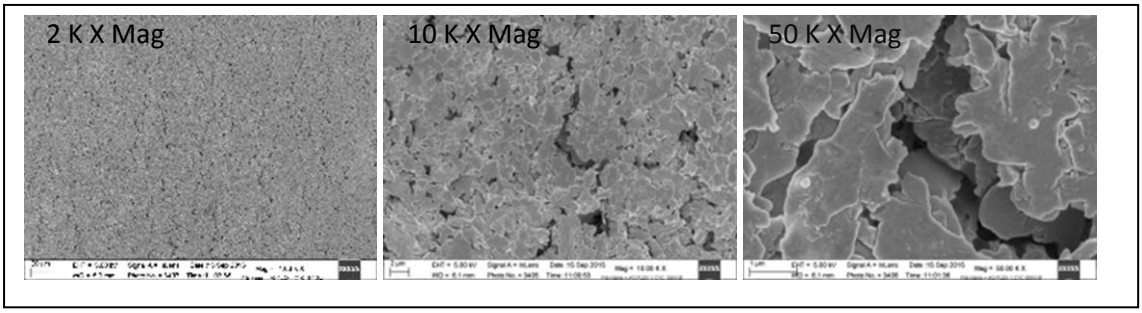

Figure 96 The SEM images of silver paste bent for 1 cycle at bent orientation

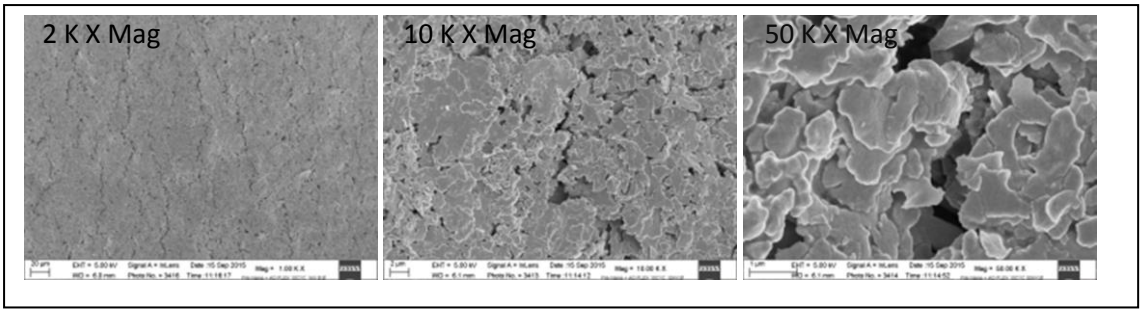

Figure 97 The SEM images of silver paste bent for 10 cycles at bent orientation

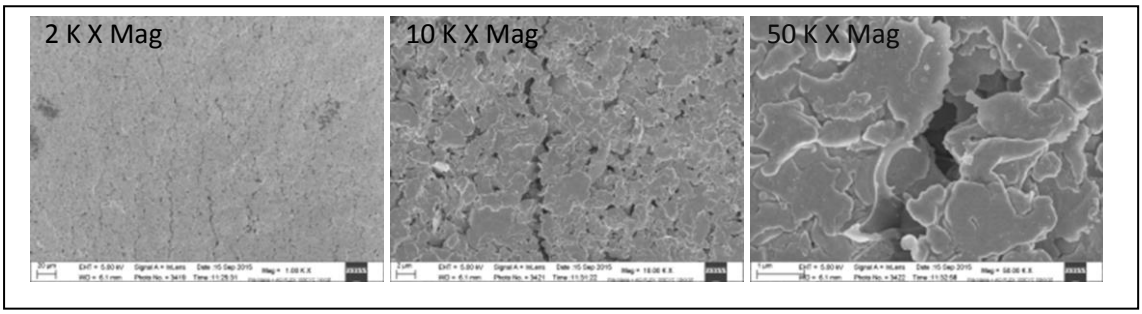

Figure 98 The SEM images of silver paste bent for 100 cycles at bent orientation

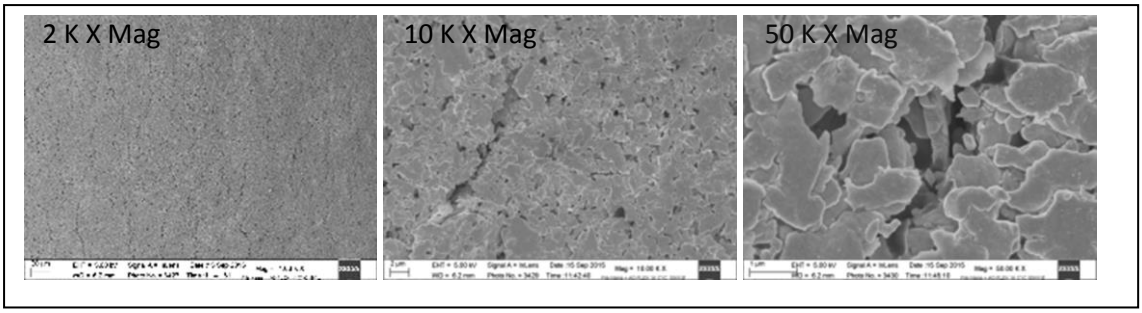

Figure 99 The SEM images of silver paste bent for 1 k cycles at bent orientation

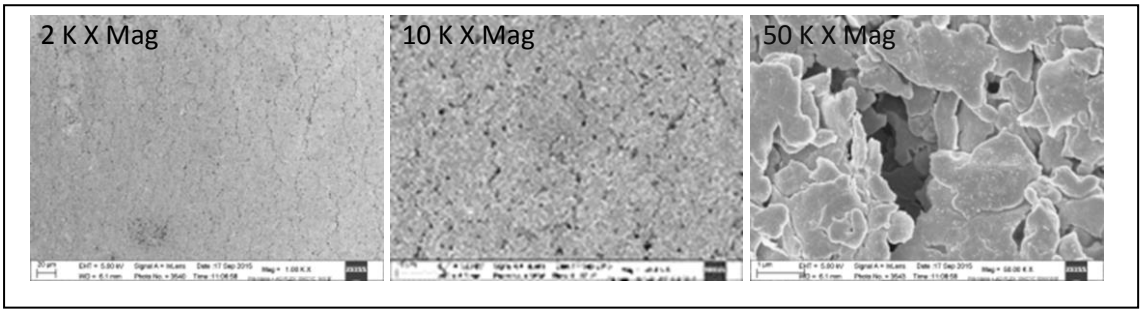

Figure 100 The SEM images of silver paste bent for 10 k cycles at bent orientation

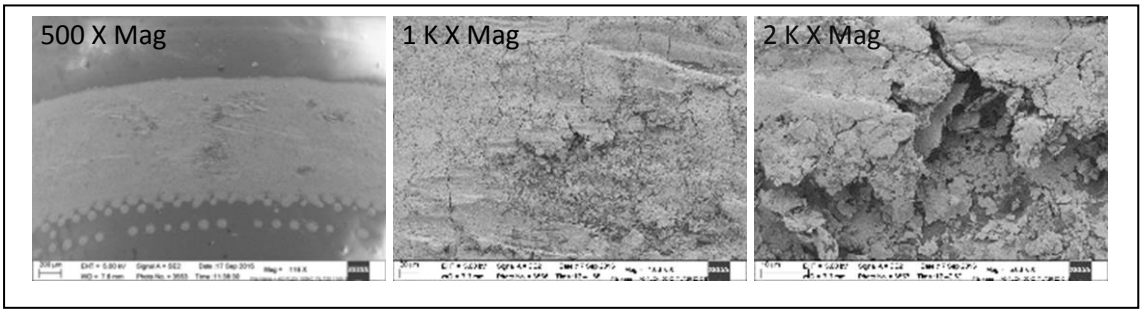

Figure 101 The SEM images of silver paste bent for 100 k cycles at bent orientation

The SEM images of printed silver at bend orientation are shown in the Figure 102 to Figure 107. The crack appears as soon as the first bend was introduced. The printed silver begins to deteriorate at 10 k to 100 k bend cycles. The magnification for Figure 106 was adjusted to show the area where the silver was damaged. The right most image of Figure 106 shows the surface appears to be scratched and there are signs of material exfoliation. The exfoliation of material caused an increase in DC resistance because of significant reduction of conductive material in test structure. Although at low bent cycles the DC resistance is increasing as shown in Figure 78, these might have been caused by oxidation of the side wall of the crack rather than material loss.

The DC resistance measurement and the SEM images of carbon and silver prints show that the carbon print performs better mechanically and electrically. There were no signs of physical defects after 100 k bent cycle on carbon prints, while the silver print images show that the surface was damaged. The effect of physical damage to the silver print causes its DC resistance to increase. Although silver has a better level of conductivity, the carbon print has good contact resistance because it does not develop an oxide layer. Furthermore, the shape of the conductive filler used in carbon paste will result in better mechanical stability than the silver print.

4.1.5 Thermal imaging during voltage sweep results

The carbon print current voltage (IV) sweep as shown in Figure 103 (see Appendix 21). The result of IV sweep on carbon print on samples that had undergone 1 bent cycle to 100 k bent cycle at decade interval shows no correlation. The measured current at a voltage setting of 30 V did not reveal any trend.

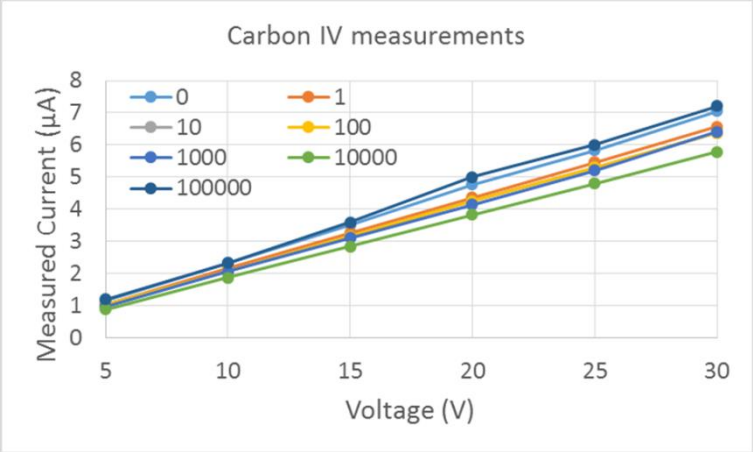

Figure 102 Carbon print IV measurement

The measurement of DC Resistance mechanical aging shown in Figure 77 correlates with IV measurement result. The measured current of 10 k bent cycles sample at 30 v was recorded as the lowest while the current for 100 k bent cycle sample was recorded as the highest, and in between were the low bent cycle samples.

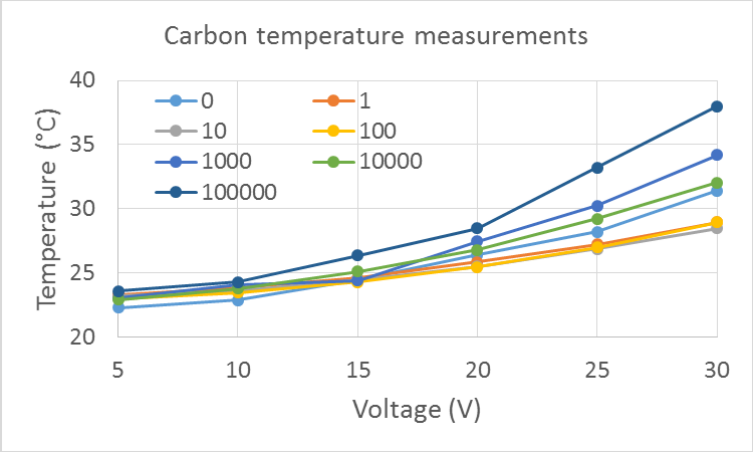

Figure 103 The carbon print measured temperature

The measured temperature on carbon samples as the voltage increases is shown in the Figure 104 (see Appendix 22). The temperature measurement of carbon print against increasing voltage shows that the 100 k bent cycle sample has degraded. There is a trend between the number of bent cycles and the measured temperature at 30 V applied voltage. So far, carbon print has eluded DC resistance measurement, and SEM imaging technique to detect its defect however the thermal imaging result clearly shows a rising measured temperature with samples exposed to increasing numbers of bend cycles.

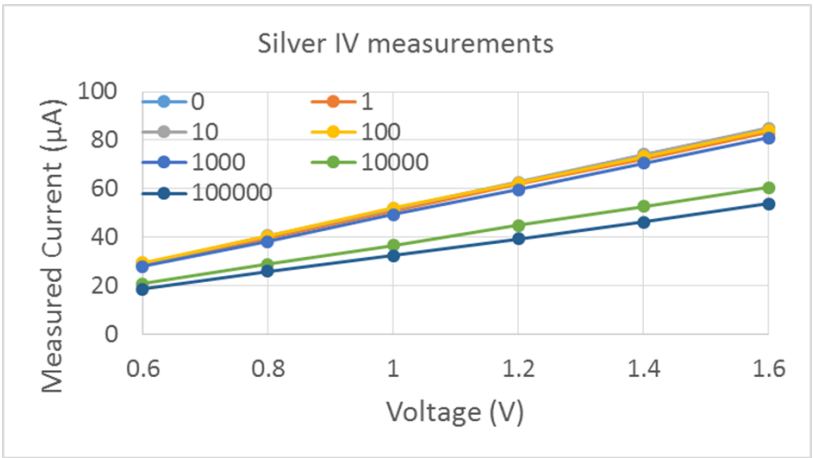

Figure 104 Silver measurements

The silver response to current-voltage test is shown in Figure 105 (see Appendix 23).The measured current decreases as the bent cycle increases, which correlates to the DC resistance measurement as shown in Figure 78. This is due to the exfoliation of silver material on the test structure. The difference in measured current increases as the applied voltage increases.

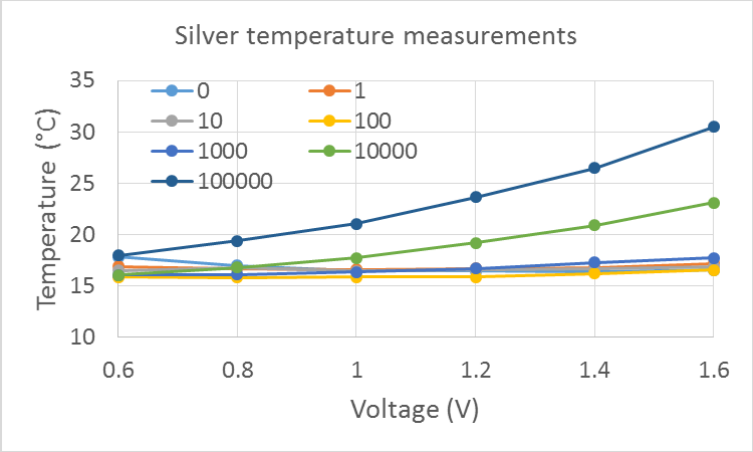

Figure 105 The silver print measured temperature

The measured temperature on silver samples in the region of interest is shown in the Figure 106 (see Appendix 24). The Figure 106 shows a dramatic increase in temperature as the number of bend cycles increase. The defect can be seen during flat orientation but is shown obviously when the sample was bent. This graph shows that the thermal imaging technique is a potentially viable measurement solution for the conductive film industry, as the solution is a form of non-contact measurement. The form of introduction of flash heating can be made in the form of convection technique by a heater, or induction heating using a coil of some sort.

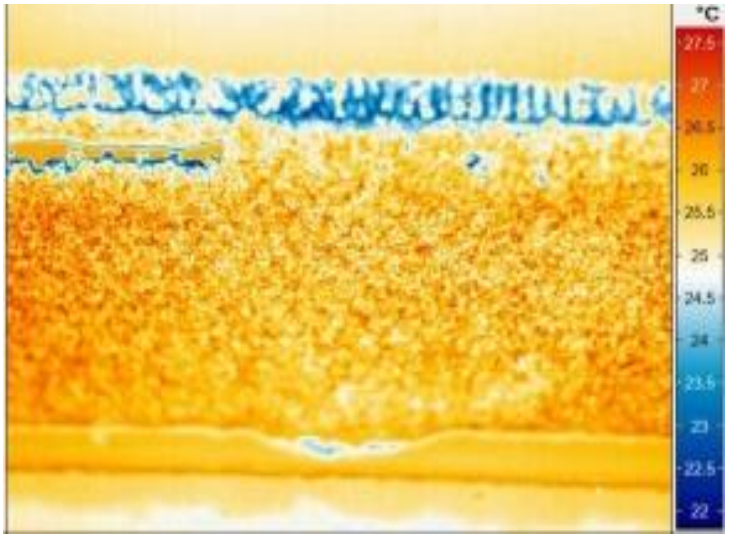

Figure 106 Thermal image of carbon paste bent for 1 cycle

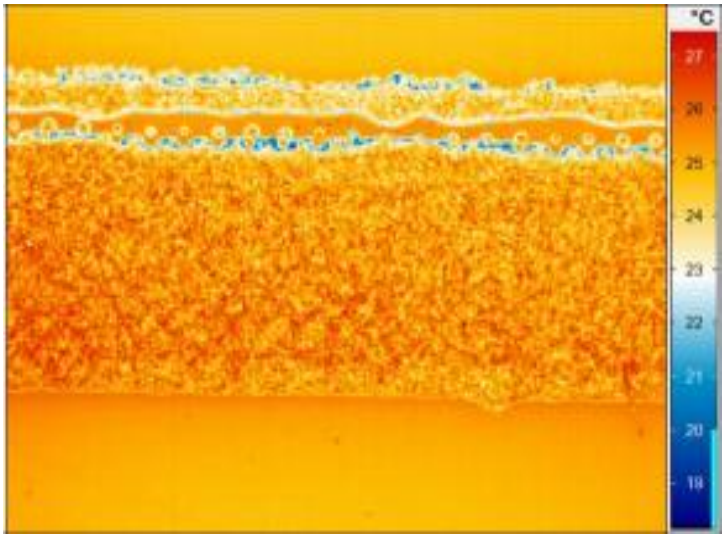

Figure 107 Thermal image of carbon paste bent for 10 cycles

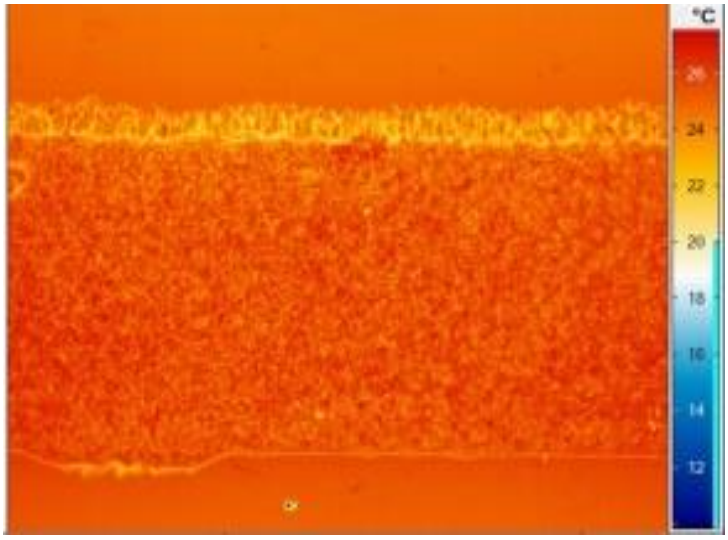

Figure 108 Thermal image of carbon paste bent for 100 cycles

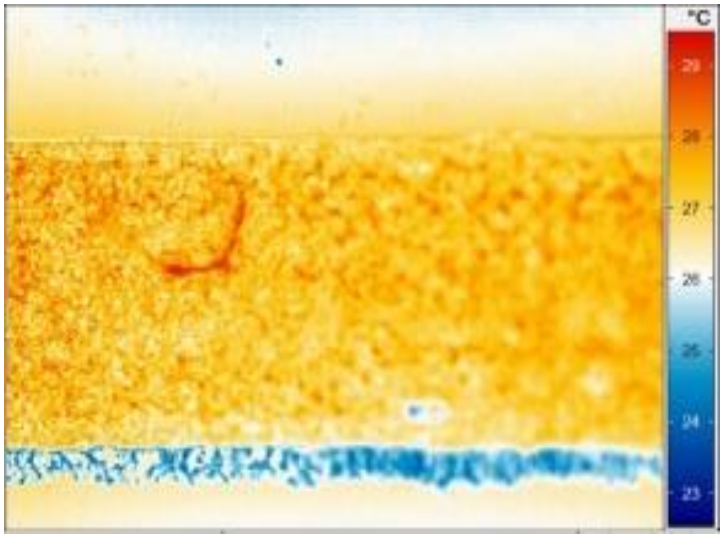

Figure 109 Thermal image of carbon paste bent for 1 k cycles

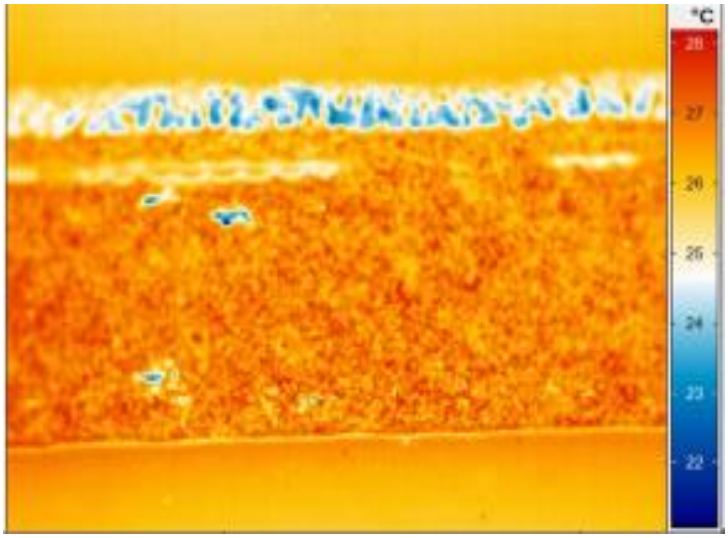

Figure 110 Thermal image of carbon paste bent for 10 k cycles

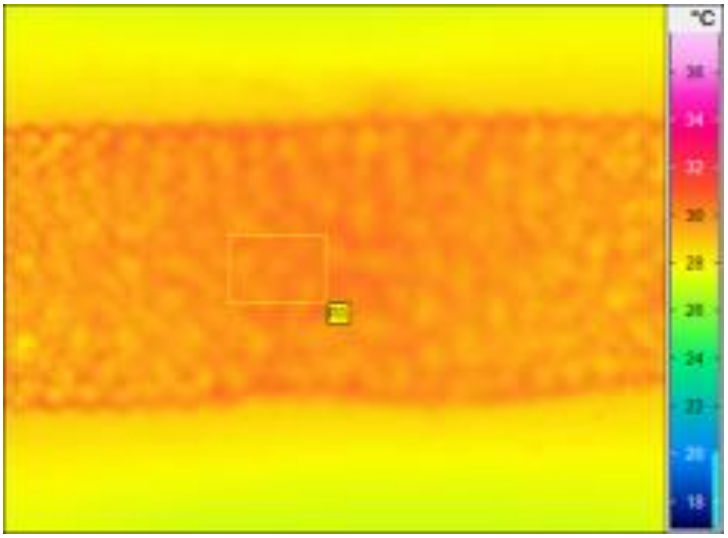

Figure 111 Thermal image of carbon paste bent for 100 k cycles

The thermal images of printed carbon are shown in Figure 107 to Figure 112 starting from 1 bent cycle to 100 k bent cycle at 10 decade interval. The response of printed carbon to the mechanical bend test has shown an improvement to its DC resistance. However, thermal measurement showed that temperature is increasing in the bent region. The electrical and thermal measurement created a conflicting result. SEM images proved the presence of a crack when printed carbon was imaged on bend. The crack disappears when the sample was laid flat on the sample stage. The buried crack although invisible and impossible to detect using SEM is still present. This increases the temperature in the bent region. This shows that although DC resistance is commonly used in quality assessment of printed carbon, thermal imaging could provide defect detection to detect embedded defects in the form of cracks. The printed carbon created a huge amount of contact between the particles. Some are low resistance and some are high. The DC resistance measures the average resistance of the interface.

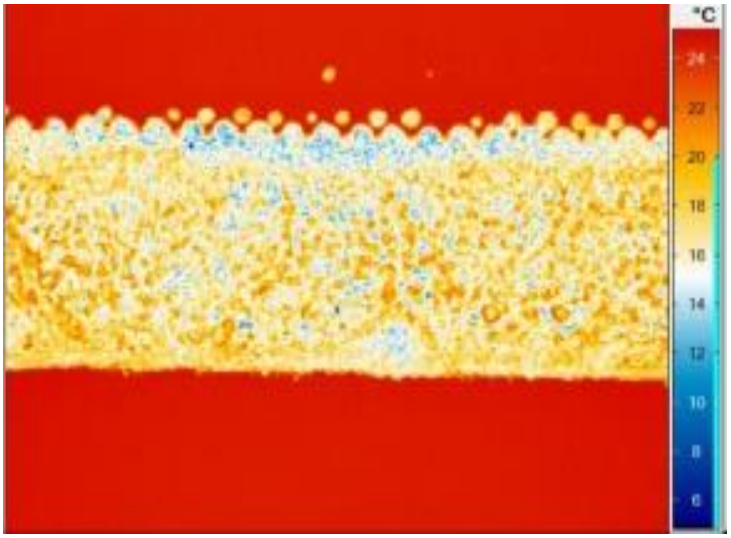

Figure 112 Thermal image of silver paste bent for 1 bent cycle

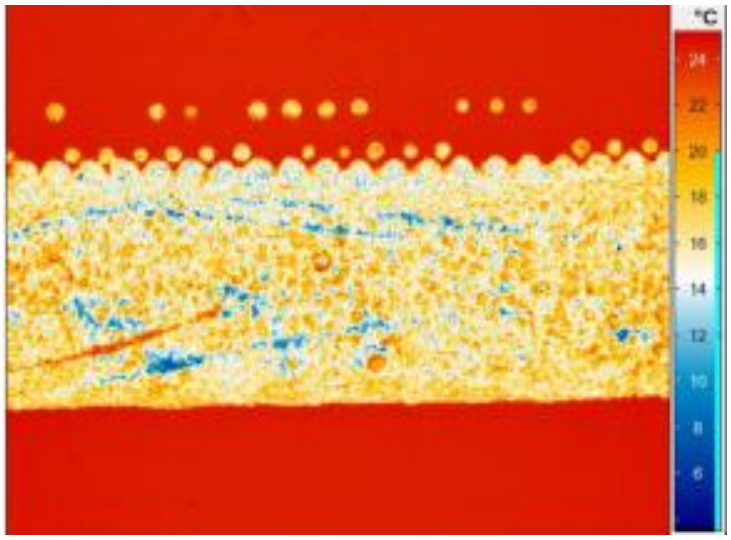

Figure 113 Thermal image of silver paste bent for 10 cycles

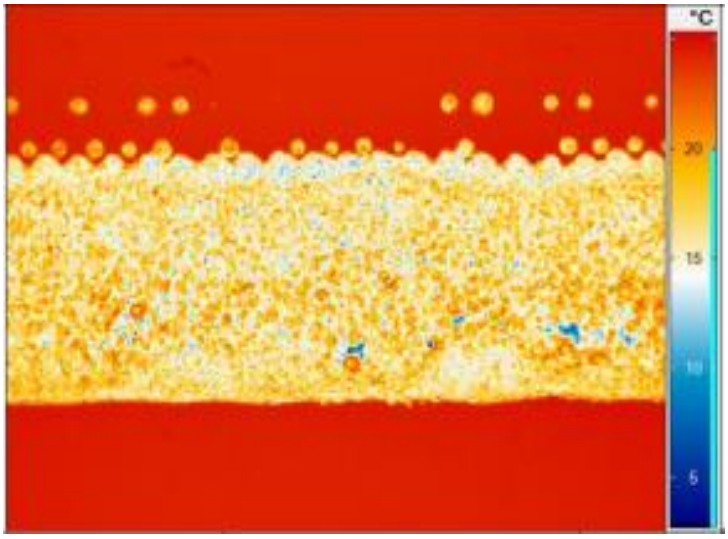

Figure 114 Thermal image of silver paste bent for 100 cycles

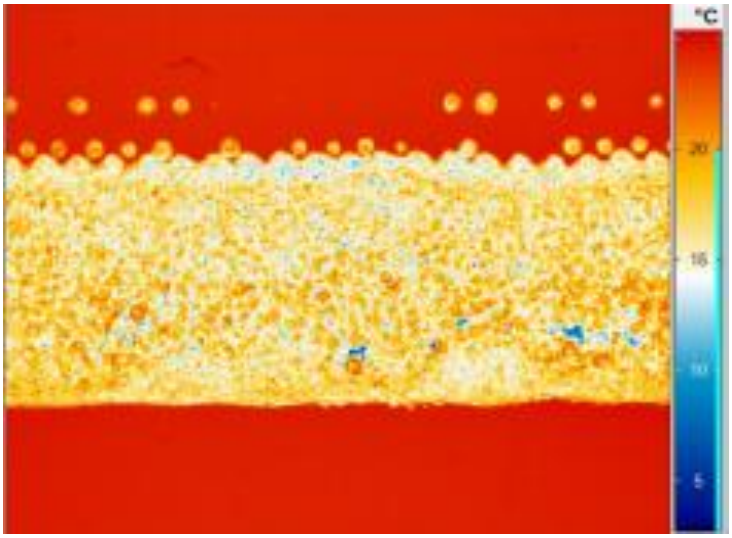

Figure 115 Thermal image of silver paste bent for 1 k cycles

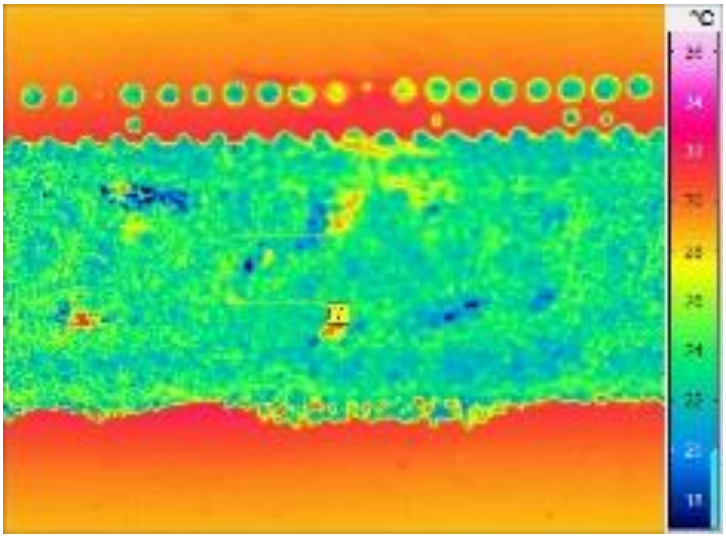

Figure 116 Thermal image of silver paste bent for 10 k cycles

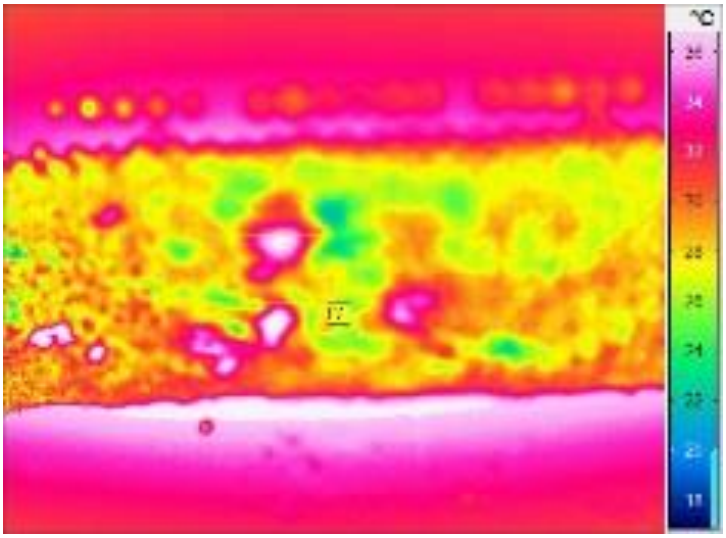

Figure 117 Thermal image of silver paste bent for 100 k cycles

The Figure 113 to Figure 118 shows the thermal imaging of the silver paste after 1 bent cycle to 100 k cycles respectively. The thermal images from Figure 113 to Figure 118 show quality failure on the silver prints. The edge definition of the bottom edge is much better than the top edge and the presence of islands of cured paste is visible that are lined on the top edge of the print. However, this defect on silver print is due to the printing process.

Packets of concentrated heat shown in Figure 118 have begun to appear at 10 k bend cycles and get worst at 100 k bend cycles. Based on SEM images of silver paste taken at 100 k bends, there were exfoliations of silver flakes on the surface of the test structure. The patches created high temperature readings concentrated in the area where the printed silver

structure was bent. The SEM image shown in Figure 107 reveals that materials removed from the surface of conductive film correlated to the heat patches of the silver bent at 100 k cycles.

The measured temperature on the patches has similar level to that observed around the edge of the conductive film. These imply that enough material was removed that the substrate is beginning to be exposed. The emissivity of the substrate is 0.1 (Optotherm 2016), slightly higher than that of silver which has emissivity of 0.02 (Hsiao 1999) to 0.04 (Pierson 1993). Therefore the substrate looks a few degrees above that of the temperature of printed structure. This is a very good example of difference in emissivity which could lead to misinterpretations of thermal measurement. However, in this particular experiment the back ground helps in identifying the area of defect because it created a contrasting effect between the printed silver and the substrate.

The carbon ink did not develop a packet of concentrated heat, and based on SEM imaging there were no defects incurred on the surface of the print due to bend test. The result of measurement in carbon is significantly higher than that of silver because of the emissivity of carbon is high . It is 0.7 to 0.9 (Pierson 1993) .

Discussion summary

The lifetime performance study of conductive paste incorporates the use of temperature, humidity and third harmonic testing. The elevated temperature test at 125 °C aimed to increase the oxidation rate on the surface of the material. Silver, carbon and development paste were used in the experiment. The result caused the silver paste to increase in resistance. This is due to the development of oxide layer that increases the contact resistance. Combination of elevated temperature and humidity test set at 85 °C/85 RH aimed to test the moisture absorption of the material. This test shows the reaction of the adhesive when exposed to high humidity environment. The development ink has decreased in resistance value compared to the commercially available silver and carbon paste. The adhesive used in the conductive paste is another important ingredient, on top of conductive filler used, to the performance of the conductive film.

The novel application of Third harmonic testing in conductive film assessment resulted in high detection rate of alternating cut on the edge of the printed structure. However, single cut across the width of the printed structure, and contamination in the film were not detected. Further investigation is needed to address detect this defects. Measurements were referenced to commercially available resistor.

The novel measurement technique using AC Impedance and DC resistance measurement during cure has produced the determination of early resistivity values and degree of cure through phase measurement. The test frequency used in AC Impedance measurement greatly affects the impedance values and the noise immunity of the test system. Test frequency of 1 MHz proved to have better test repeatability than lower test frequencies. Increasing the curing temperature causes evaporation rate to increase and lower final cured resistance value. Increased particle loading slow down the curing of the conductive film but achieve lower cured resistance value.

The novel application of Infrared measurement technique to detect signs of aging on conductive films was proven effective. Conductive films were mechanically aged by bending up to 100 k cycles. DC resistance measurements were taken while the commercially available silver and carbon printed structure where bent from flat to 150 ° orientation at centre of 5 mm diameter rod. The DC resistance has detected the sign of mechanical aging on silver prints with the increase in resistance value. The carbon print decreases in resistance value which does not reflect the mechanical stresses in which the conductive film was subjected.

The SEM images shows cracks on both carbon and silver prints only after bending and after 10 k of mechanical bending. The crack disappears when it is on flat orientation making it difficult to detect using surface inspection. Infrared camera detected the increase in radiated temperature on the stressed region. The sample was excited using an external power source that produces joule heating. The increase in temperature was recorded on both the silver and carbon prints.

5 Chapter 5 – Conclusions

Conductive film popularity has increased dramatically in the last decade. The driving force behind the technology is its cost, speed and large area manufacturing. This exciting technology still has a lot of areas to improve. Measurement on conductive film will play a very important role in shaping the technologies application based on its characteristics and its manufacturability. This thesis has shown several novel solutions to help improve measurement of conductive film electrical, mechanical, and physical properties, which are claimed as contributions to knowledge.

The environmental testing on conductive film reveals its performance in harsh conditions. The tests determine the conductive film strengths and limitations. The identification of the failure mechanism in conductive film is important so that researcher can concentrate on the weak component of the conductive paste. An improved conductive film will further it's application to areas such as aerospace, automotive and oil and gas exploration. Such areas demand a reliable product, which are able to withstand high temperature and high humidity operating conditions. Cheap and reliable electronic will bring the operating cost down and such savings will eventually be passed on to the end consumer market.

The environmental tests used were elevated temperature and a combination of high temperature and high humidity testing. Elevated temperature aimed to increase the oxidation rate while the high temperature and humidity test the moisture absorption of the material. The result of high temperature test on silver paste caused its resistance to increase. It is a common knowledge that silver develops oxide layer when exposed to atmosphere. Although the silver oxide remains conductive, its resistance is higher than that of pure silver. The effect of the high temperature test on carbon pastes, both the commercial and development paste, have caused its resistance to decrease. The adhesive has undergone further curing with the application of further heat.

The high temperature and high humidity test has caused the DC resistance of silver, and carbon pastes to increase due to moisture intake of the polymer resin. The polymer resin swells making the conductive particle to move further from each other. The development ink has different reaction to the test because its resistance decreased. The polymer resin used in development ink is different from the two commercial pastes, and its reaction to the test causes it to cure further.

Third harmonic testing identifies product that has a potential to fail at the beginning of its operation. This will prevent weak device from being installed into the finish product and end up at consumer hands. Costly repair cost and at the worst case is product being recalled that

lead to manufacturer's damaged reputation. In addition, the third harmonic test failures will prompt the conductive film production personnel to conduct investigation of the root cause of the failure.

The second category of lifetime performance measurement is the use of third harmonic testing. The third harmonic testing is effective in detecting mechanical failure in conductive film. In this test, the alternating defect created the highest third harmonic response as compared to the 75 %, 42 % and 25 % reduction in print width. Also tested with low effect on third harmonic response is the effect of pin holes, and ink contamination. High third harmonic index was recorded on sample with alternating defect and high reduction in print width. However, it cannot detect contamination such as fibres and under cured conductive film. The fully cured conductive film will generate higher third harmonic signal compared to the commercially available 1 kΩ resistor.

The initial measurement of the AC impedance of wet paste can give an early indication of the final cured resistivity for a particular paste whose cure cycle is already understood. Research performed on conductive paste can be achieved at least possible time, bringing the cost of operation down. From the manufacturer point of view, early indication of resistivity will mean less product wastage and an improved in print quality.

The measurements of the initial uncured paste film impedance and final cured resistance gives a ratio that can be used to predict future print final resistivity from an initial uncured paste film impedance measurement. For the three carbon paste systems investigated, this ratio ranged from 766 to 1165 but was consistent within each paste system and curing temperature.

AC impedance and DC resistance measurements during cure on conductive pastes with varying particle loadings show that the particle loading affects the rate of curing and the final resistance values. The percolation threshold is the beginning of a sudden reduction of AC impedance and DC resistance due to the establishment of sufficient particle to particle contact. Lowering the curing temperature delays the percolation threshold, while increasing the temperature will cause the paste to reach the percolation threshold quickly. Lower particle loading causes higher impedance and resistance values after 40 minutes of curing at 95 °C. The final resistance value for paste samples with lower particle loading is high, because there is less conductive material for a given volume of paste.

Curing temperatures for conductive film influence both the speed of curing and the final impedance values. This is due to the solvent content increasing its rate of evaporation with the increase in curing temperature. The high curing temperature causes more solvent to

evaporate, lowering the final resistance values of the printed structure. Lower curing temperature causes a delay in reaching the percolation threshold. Additionally, curing temperature affects the final resistance values obtained. Higher curing temperature evaporates more solvent forming increased particle to particle contact as compared to lower temperature post processing. The introduction of AC impedance measurement on printed conductive paste structures during cure is demonstrated as an effective tool in determining early indication of resistivity and measurement of degree of cure.

The electrical resistance on mechanically age conductive film of carbon and silver paste shows two opposite result. The carbon print decreases the DC resistance in value while the result of silver print increases in DC resistance. In case of carbon print, the material and its size place a vital role in its electrical performance while being bent. The surface resistance is low in the case of carbon because the material does not oxidise. Smaller particle have help in holding the structure together preventing further damage caused by bending. Silver particle increase in DC resistance value is due to the oxidation and mechanical stability of the particle. Removal of particle from the print causes less area to conduct.

The inspection of physical defect proves to be an impossible task even with a high magnification instrument. The Scanning Electron Microscope images were used in the determination of the crack between the carbon and silver prints. The crack appears when the sample is stressed by bending at 150 ° and disappears when it is flat. The defects on the surface of the carbon prints did not appear after 10 k bents. Similar scenario was observed in silver prints, however it is much worse because the defect that appeared on the silver prints is due to material exfoliation and can be seen with low magnification.

A novel measurement solution using Infrared Imaging technique to detect defect on mechanically aged conductive film was presented. The heat generated by mechanically bend region in carbon and silver prints was detected using thermal camera. The increase in measured temperature is proportional to the number of mechanical bents performed on both conductive films. The defect detection using IR imaging technique is possible even if the conductive film is flat in orientation and no requirement to be bent.

Since the conductive film manufacturing is moving towards large area and high speed production, the use of Infrared thermal camera is recommended be a part of this technology. This will mean minimum disruption to the manufacturing that will increase production yield and print quality. The measurement technique can also be used while the conductive film is in operation. Replacing weaken devices before it fails will prevent catastrophic failure of product.

6 Further Work

This thesis has demonstrated several novel measurement techniques that can be applied to the conductive film. The measurement techniques are Third Harmonic testing, measurement of using AC Impedance during cure and Infrared measurement technique to detect defect in cured conductive film. The value of this research will increase considerably if it is applied to actual printing process.

The use of Third harmonic measurement on conductive film was proven to be effective in detecting defect of certain defect. However, it can only responsive a defect that has alternating cuts on the edge of the conductive film. Further studies are needed to detect defect such as pin holes, a single cut of various length across the width of the structure, and contamination in conductive film. The following measurement techniques that can be a great candidate are eddy current testing, colorimetry, AC impedance and Infrared thermal imaging to measure such defects. Noticeable the mention characterisation techniques are based on non- contact measurement, which is ideal for large area and high speed production.

The AC impedance measurement during cure experiment that was included in this thesis shows the early resistivity values of conductive paste and degree of cure measurement. The early resistivity values measurement can be improved further by developing an AC Impedance test probe. The AC Impedance test probe can be dip in the pan where the paste is being developed or at ink reservoir of a printing process. Adjustment can be made in the conductive paste at an instant eliminating the need for the conductive paste to be printed, cured and be measured. This will benefit both the ink producer and conductive film producer. The measurements of cured conductive film are normally performed using DC resistance meter because this type of measurement is cost effective compared to AC Impedance. Further improvement is needed to design an AC Impedance meter that can compete with DC resistance meter in terms of cost.

Conductive film manufacturer will benefit from this research if Infrared camera is utilised in conductive film print production. The method used in this thesis requires direct contact to provide excitation to the conductive film. This direct connection can be eliminated to fully realise the application of a non-contact imaging technique. An example of excitation can be in the form of IR lamp or an inductive coil to heat the conductive film. Measurement of moving object using Infrared camera should be assessed further in terms of data acquisition sampling rate and how it will affect the result.

7 Appendix

Appendix 1. Electrapolymer ED4000 carbon loaded conductive paste datasheet

TECHNICAL DATA SHEET
ELECTRA$^{\Omega}$D'OR™
ED3000 SERIES

SILVER CONDUCTIVE PASTES FOR USE ON FLEXIBLE CIRCUIT BOARDS

PRODUCT DESCRIPTION

ED3000 Flexible silver pastes are thermoplastic conductive pastes developed specifically for use on untreated polyester, polyimide and polycarbonate films.

Typical screen-print applications are flexible circuits and membrane switches.

FEATURES & ADVANTAGES

- **High conductivity. ED3000** resistance is only 30 mΩ Ù$^{-1}$
- **High resolution.** 250μm tracks and spaces on typical thick film printers.
- **Excellent adhesion.** No peeling when tested as per cross hatch test IPC D-320.

***ELECTRA D'OR*™ ED3000 PRODUCT RANGE**

ED3000 Surface resistance: **30 mΩ** $^{-1}$ (12μm cured thickness).

PROCESSING

Printing: Screen: 200 to 325 mesh stainless steel (62T to 77T polyester)
Stencil: 12μm proud emulsion stencil.
Squeegee: 70 durometer.

Curing: Convection 30 to 40mins at 90 to 120°C.
Optimum adhesion and resistance with be attained by curing at 120°C

Viscosity: If viscosity adjustment (thinning) becomes necessary due to evaporation loss with prolonged usage, then **ethyl diglycol acetate** should be used up to a max of 5%.

Cleaning: Screens and other utensils may be cleaned using **butyrolactone**.

FINAL PROPERTIES

Test pattern:	1000 square serpentine pattern with a 12μm cured film on a 75μm mylar film substrate.
Adhesion:	X-hatch and tape - 100% adhesion
Hardness:	2H
Humidity:	200 hours at 65°C/95%RH - <5% change in resistance.
Resistivity:	After flex test (% resistance retained).
	0-180°. one fold with crease **98%**

Appendix 2. Electrapolymer ED4000 carbon loaded conductive paste datasheet

TECHNICAL DATA SHEET
ELECTRA$^{\Omega}$D'OR™
ED4000 SERIES

CARBON CONDUCTIVE PASTES
FOR FLEXIBLE CIRCUIT BOARDS

PRODUCT DESCRIPTION

ED4000 CARBON PASTES are graphite filled conductive overprint inks designed for use with ED3000 silver conductive paste. **ED4000** provides excellent protection with the lowest possible resistance. **ED4000** are thermoplastic conductive pastes developed specifically for untreated polyester, polyimide and polycarbonate films.

FEATURES & ADVANTAGES:

- **Low sheet resistance.** **ED4000** resistance is only 40 Ω□$^{-1}$
- **Low contact resistance** Less than 3Ω.
- **Excellent adhesion.** No peeling when tested as per cross hatch test IPC D-320.
- **High resolution.** 250µm tracks and spaces on typical thick film printers.

Electrador™ ED4000 PRODUCT RANGE

ED4000	Surface resistance:	**40 Ω□$^{-1}$**
	Contact resistance:	**<3Ω**

PROCESSING

PRINTING: 200 to 325 mesh stainless steel or 62T to 77T polyester mesh with a 13µm emulsion stencil. Squeegee: 70 durometer.

CURING: Convection oven 35 to 40 mins at 95°C

FINAL PROPERTIES

(12µm thick film overprinted on ED2000 with polyester substrate)

Resistance: Sheet resistance: **40 Ω□$^{-1}$** Contact resistance: <3Ω (12µm thickness)

Adhesion: X-hatch and tape - 100% adhesion

Hardness: 3H

Humidity: 200 hours at 65°C/85%RH - <5% change in resistance.

Maximum operating temperature: 70°C

VISCOSITY ADJUSTMENT:

If thinning becomes necessary due to evaporation loss with prolonged usage, then **ER17** should be used up to a maximum of 5%.

SCREEN CLEANING:

Screens may be cleaned using Electra Universal Screenwash **SW100**

Appendix 3. Labview program of AC Impedance and DC resistance during cure experiment

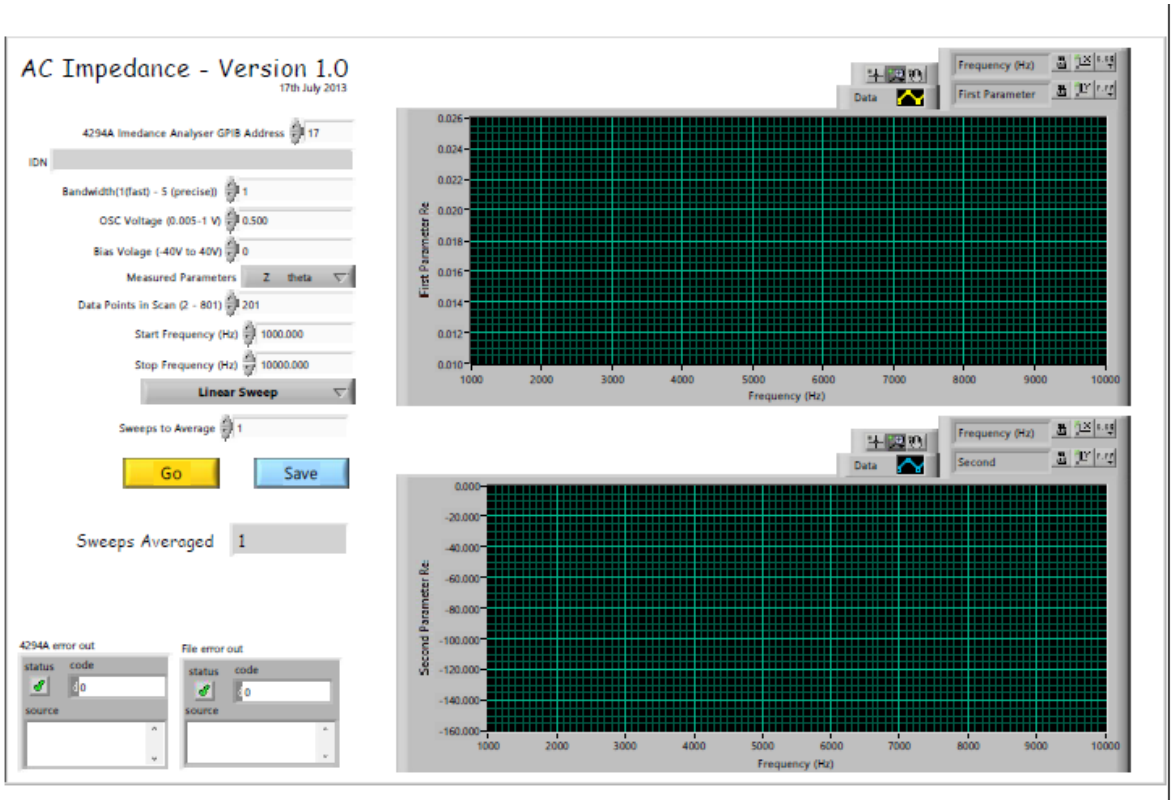

https://figshare.com/articles/AC_Impedance_and_DC_resistance_LabVIEW_program_during_cure/5212096

Appendix 4. Labview program DC resistance measurement during mechanical bending of conductive film.

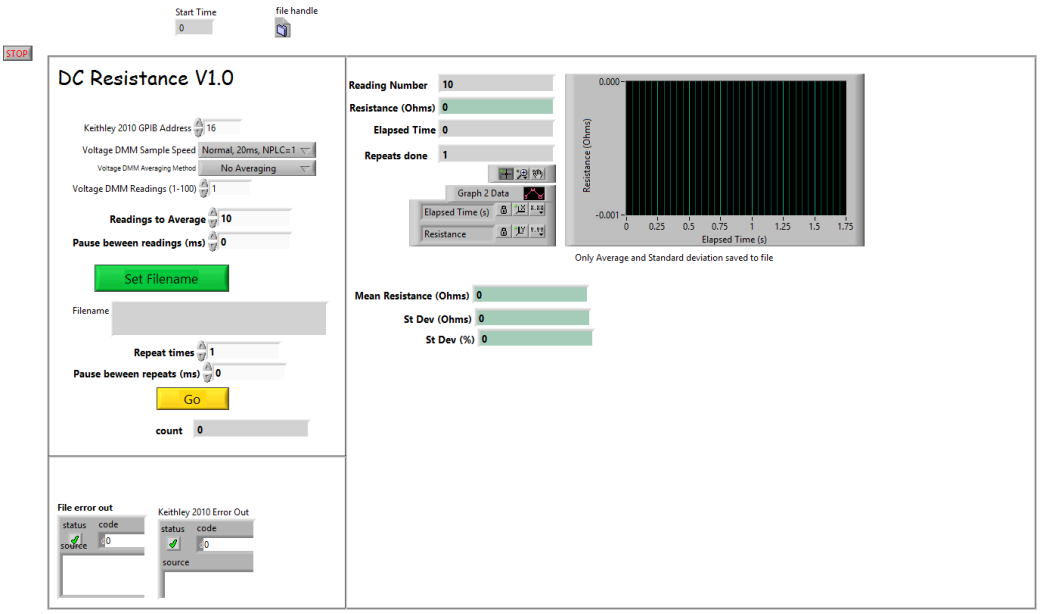

https://figshare.com/articles/DC_Resistance_measurement_during_conductive_film_mechanical_aging/5212099

Appendix 5. Resistance (% of initial resistance) 85/85 Environmental testing
Lifetime performance testing

Elapsed Time (hours)	0	24	70	262	838	1198
Development Ink	100	75.77346	70.56485	66.16337	61.93661	59.80014
Silver	100	99.99847	100.0439	102.1469	106.3546	107.6182
Carbon	100	98.16339	94.89133	94.08831	100.7905	103.4847

Appendix 6. Resistance (% of initial resistance)125 test

Elapsed Time (hours)	0	24	70	262	838	1198
Development Ink	100	56.4	55.0	53.2	47.2	45.0
Silver	100	101.9	103.6	108.8	119.8	125.6
Carbon	100	83.8	76.9	71.2	67.3	64.7

Appendix 7. Third Harmonic Testing

Conductive film	**THR (dB)**	**THR difference to fully cured (dB)**
Fully cured	114	
Pin holes	113.2	0.8
17 % Defect	112.2	1.8
42 % Defect	112.6	1.3
71 % Defect	110.5	3.5
Alternating	92.6	21.3
Fibers	114.6	-0.6
Ambient	116.3	-2.3
1 kW resistor	121.2	-7.3

Appendix 8. Impedance measurement of Paste E at 95 °C

https://figshare.com/articles/Impedance_measurement_of_conductive_film/5197264

Appendix 9. DC resistance and AC Impedance measurement of GEM 1 at 95 °C

https://figshare.com/articles/DC_resistance_and_AC_Impedance_measurement_of_GEM_1_at_95_C/5197267

Appendix 10. DC resistance and AC Impedance measurement of GEM 2 at 95 °C

https://figshare.com/articles/DC_resistance_and_AC_Impedance_measurement_of_GEM_2_at_95_C/5197282

Appendix 11. Phase measurement of Paste E at 95 °C

https://figshare.com/articles/Phase_measurement_of_Paste_E_during_cure_at_95_C/5197285

Appendix 12. Phase measurement of GEM 1 paste at 95 °C

https://figshare.com/articles/Phase_measurement_of_GEM_1_paste_at_95_C/5197291

Appendix 13. Phase measurement of GEM 2 paste at 95 °C

https://figshare.com/articles/Phase_measurement_of_GEM_2_paste_at_95_C/5197294

Appendix 14. The AC Impedance measurement at 1 MHz for Paste E structures cured at different temperature for 40 minutes

https://figshare.com/articles/The_AC_Impedance_measurement_at_1_MHz_for_Paste_E_structures_cured_at_different_temperature_for_40_minutes/5197297

Appendix 15. AC Impedance measurement at 1 MHz of Paste E at different particle loading

https://figshare.com/articles/AC_Impedance_measurement_at_1_MHz_of_Paste_E_at_different_particle_loading/5197300

Appendix 16. The DC resistance measurements of Paste E after 40 minutes at different curing temperature

Curing Temperature	Sample 1	Sample 2	Sample 3	Sample 4	Sample 5	Average	Standard deviation (%)
55 °C	2760	2870	2770	2960	2800	2830	2.7
85 °C	1130	889	861	889	861	926	7.3
95 °C	823	727	718	907	823	799	8
105 °C	701	689	672	689	672	684	1.5

Appendix 17. The DC resistance measurements after 40 minutes of Paste E at different particle loading

Curing Temperature	Sample 1	Sample 2	Sample 3	Sample 4	Sample 5	Average	Standard deviation (%)
55 °C	2760	2870	2770	2960	2800	2830	2.7
85 °C	1130	889	861	889	861	926	7.3
95 °C	823	727	718	907	823	799	8
105 °C	701	689	672	689	672	684	1.5

Appendix 18. AC (T0) / DC (T40) ratio of different pastes , and Paste E for various curing temperature and particle loading. The blue bars show the average values and the error bars show standard deviation for 5 measurements in each test condition

Ink Name	Sample 1	Sample 2	Sample 3	Sample 4	Sample 5	Average	Standard deviation (%)
Paste E	9120	9680	8320	7070	9360	8711	10.7
GEM 1	9020	9280	7060	7980	10200	8697	12.4
GEM 2	6430	5200	6280	6760	6030	6137	8.5
55 °C	6.2E+06	6.0E+06	6.0E+06	6.1E+06	6.2E+06	2800	2.6
85 °C	6550	8810	9130	8810	9130	8480	6.7
95 °C	9120	9680	8320	7070	9360	8711	10.7
105 °C	10100	10900	12300	10900	12300	11300	7.7
48%	3160	3180	3210	3040	3090	3140	2
52%	5580	5250	6990	6290	7150	6250	11.9
56%	8580	7390	8520	8970	8580	8410	6.33
60%	9120	9680	8320	7070	9360	8711	10.7

Appendix 19. Mechanical Testing DC resistance of carbon prints

https://figshare.com/articles/Mechanical_Testing_DC_resistance_of_carbon_prints/5197303

Appendix 20. DC resistance of silver prints

https://figshare.com/articles/DC_resistance_of_silver_prints/5197306

Appendix 21. Carbon IV measurement

Test Voltage	Number of bends						
	0	1	10	100	1000	10000	100000
5	1.164	1.053	1.028	1.028	0.991	0.883	1.203
10	2.328	2.168	2.086	2.086	2.067	1.883	2.323
15	3.513	3.268	3.161	3.161	3.111	2.848	3.598
20	4.764	4.365	4.248	4.248	4.148	3.829	5
25	5.838	5.465	5.296	5.296	5.21	4.803	6.012
30	7.061	6.567	6.378	6.378	6.409	5.789	7.204

Appendix 22. Carbon print temperature

Test Voltage	Number of bends						
	0	1	10	100	1000	10000	100000
5	17.84	16.88	16.52	15.84	16.08	16.07	17.96
10	17	16.67	16.72	15.83	16.1	16.79	19.38
15	16.5	16.62	16.44	15.88	16.37	17.73	21.06
20	16.45	16.67	16.53	15.84	16.7	19.19	23.64
25	16.41	16.81	16.66	16.2	17.3	20.9	26.49
30	16.53	17.2	16.88	16.56	17.73	23.12	30.46

Appendix 23. Silver IV measurement

Test Voltage	Number of bends						
	0	1	10	100	1000	10000	100000
0.6	28.99	28.579	29.037	29.548	28.038	20.738	18.568
0.8	39.92	39.43	40.62	40.41	38.1	28.946	25.865
1	51.05	50.94	51.77	51.97	49.22	36.74	32.45
1.2	62.27	62.01	62.78	62.19	59.69	44.85	39.24
1.4	74.11	72.24	74.12	73.07	70.4	52.58	46.19
1.6	84.63	83.22	85.03	83.98	80.97	60.37	53.76

Appendix 24. Silver print temperature

Test Voltage	Number of bends						
	0	1	10	100	1000	10000	100000
0.6	22.3	23.34	23.21	23.01	23.06	22.94	23.6
0.8	22.9	23.83	23.64	23.47	24.08	23.79	24.3
1	24.5	24.6	24.5	24.29	24.4	25.13	26.38
1.2	26.4	25.86	25.52	25.48	27.48	26.82	28.5
1.4	28.23	27.23	26.88	27	30.26	29.23	33.22
1.6	31.4	28.94	28.47	28.96	34.18	32.06	38

8 References

ALICONA, 2016, 2016-last update [Homepage of Alicona], [Online]. Available: http://www.alicona.com/products/infinitefocus/ [13/July, 2013].

BALLOU, G., 2015. Handbook for Sound Engineers. Taylor & Francis.

BIRD, J., 2003. Science for Engineering. Newnes.

BONEA, A., BRODEALA, A., VLADESCU, M. and SVASTA, P., 2012. Electrical conductivity of inkjet printed silver tracks, 2012, pp. 1-4.

CAGLAR, U., KAIJA, K. and MANSIKKAMÄKI, P., 2008. Analysis of mechanical performance of silver inkjet-printed structures, 2008, pp. 851-856.

CANTATORE, E., 2012. Applications of Organic and Printed Electronics: A Technology-Enabled Revolution. Springer US.

CAPASSO, A., DEL RIO CASTILLO, A.E., SUN, H., ANSALDO, A., PELLEGRINI, V. and BONACCORSO, F., 2015. Ink-jet printing of graphene for flexible electronics: An environmentally-friendly approach. Solid State Communications, **224**, pp. 53-63.

CHANDA, M. and ROY, S.K., 2008. Plastics Fundamentals, Properties, and Testing. CRC Press.

CHERRINGTON, M., CLAYPOLE, T.C., GETHIN, D.T., WORSLEY, D.A. and DEGANELLO, D., 2012. Non-contact assessment of electrical performance for rapidly sintered nanoparticle silver coatings through colorimetry. Thin Solid Films, **522**, pp. 412-414.

CHIU, Y., CHENG, C., WHANG, T. and JI, G., 2014. Effects of silicate glasses in aluminum pastes on physical and electrical characteristics of screen-printed multi-crystalline silicon solar cells. Materials Letters, **126**, pp. 143-146.

COUGHLAN, F.M. and LEWIS, H.J., 2006. A study of electrically conductive adhesives as a manufacturing solder alternative. Journal of Electronic Materials, **35**(5), pp. 912-921.

CUI, Z., ZHOU, C., QIU, S., CHEN, Z., LIN, J., ZHAO, J., MA, C. and SU, W., Printed Electronics: Materials, Technologies and Applications. Wiley.

CUMMINS, G. and DESMULLIEZ, M.P.Y., 2012. Inkjet printing of conductive materials: A review. Circuit World, **38**(4), pp. 193-213.

CZAJKOWSKI, J., PRYKÄRI, T., ALAROUSU, E., PALOSAARI, J. and MYLLYLÄ, R., 2010. Optical coherence tomography as a method of quality inspection for printed electronics products. Optical Review, **17**(3), pp. 257-262.

DANG, M.C., DUNG DANG, T.M. and FRIBOURG-BLANC, E., 2013. Inkjet printing technology and conductive inks synthesis for microfabrication techniques. Advances in Natural Sciences: Nanoscience and Nanotechnology, **4**(1),.

DEBEDA-HICKEL, H., LUCAT, C. and MENIL, F., 2005. Influence of the densification parameters on screen-printed component properties. Journal of the European Ceramic Society, **25**(12 SPEC. ISS.), pp. 2115-2119.

DIAKIDES, M., BRONZINO, J.D. and PETERSON, D.R., 2012. - Medical Infrared Imaging: Principles and Practices. - CRC Press.

DOGOME, K., ENOMAE, T. and ISOGAI, A., 2013. Method for controlling surface energies of paper substrates to create paper-based printed electronics. Chemical Engineering and Processing: Process Intensification, **68**, pp. 21-25.

DUBEY, G.C., 1974. Screens for screen printing of electronic circuits. Microelectronics Reliability, **13**(3), pp. 203-207.

EFIRD, K.D., 1988. Galvanic corrosion in oil and gas production, 1988, pp. 260-282.

EMINOGLU, S., TEZCAN, S.D., TANRIKULU, M.Y. and AKIN, T., 2003. Low-cost uncooled infrared detectors in CMOS process. Sensors and Actuators, A: Physical, **109**(1-2), pp. 102-113.

ESPALIN, D., MUSE, D.W., MACDONALD, E. and WICKER, R.B., 2014. 3D Printing multifunctionality: Structures with electronics. International Journal of Advanced Manufacturing Technology, **72**(5-8), pp. 963-978.

FALAT, T., PLATEK, B. and FELBA, J., 2012. Sintering process of silver nanoparticles in ink-jet printed conductive microstructures - Molecular dynamics approach, 2012.

FEHLMAN, WILLIAM L., HINDERS,MARK K., 2009-last update, Mobile Robot Navigation with Intelligent Infrared Image Interpretation [Homepage of Springer London], [Online].

FELBA, J., 2011. Inkjet printed electrically conductive structures for microelectronics, 2011, pp. 6-11.

FRANEY, J.P., GRAEDEL, T.E., GUALTIERI, G.J., KAMMLOTT, G.W., MALM, D.L., SHARPE, L.H. and TIERNEY, V., 1984. Conductive silver-epoxy pastes: characteristics of alternative formulations. Journal of Materials Science, **19**(10), pp. 3281-3286.

GARCÍA-GONZÁLEZ, R., FERNÁNDEZ-ABEDUL, M.T. and COSTA-GARCÍA, A., 2015. Nafion® modified-screen printed gold electrodes and their carbon nanostructuration for electrochemical sensors applications. Talanta, **107**, pp. 376-381.

GARCÍA-MARTÍN, J., GÓMEZ-GIL, J. and VÁZQUEZ-SÁNCHEZ, E., 2011. Non-destructive techniques based on eddy current testing. Sensors, **11**(3), pp. 2525-2565.

GHOSH, M.K. and MITTAL, K.L., 1996. Polyimides Fundametals and Applications. In: M.K. GHOSH and K.L. MITTAL, eds, New York: Marcel Dekker, Inc., pp. 206-207.

GILLEO, K., 1995. Assembly with conductive adhesives. Soldering and Surface Mount Technology, (19), pp. 12-17.

GREER, J.R. and STREET, R.A., 2007. Thermal cure effects on electrical performance of nanoparticle silver inks. Acta Materialia, **55**(18), pp. 6345-6349.

HARPER, C.A., 2006. Handbook of plastics technologies. 2 ed. edn. US: McGraw-Hill Professional.

HERRMANN, J., MÜLLER, K.-., REDA, T., BAXTER, G.R., RAGUSE, B., DE GROOT, G.J.J.B., CHAI, R., ROBERTS, M. and WIECZOREK, L., 2007. Nanoparticle films as sensitive strain gauges. Applied Physics Letters, **91**(18), pp. 183105.

HÖHNE, G., HEMMINGER, W.F. and FLAMMERSHEIM, H.J., 2013. Differential Scanning Calorimetry. Springer Berlin Heidelberg.

HOMOLA, T., WU, L.Y.L. and CERNÁK, M., 2014. Atmospheric plasma surface activation of poly(ethylene Terephthalate) film for roll-to-roll application of transparent conductive coating. Journal of Adhesion, **90**(4), pp. 296-309.

HONEYCHURCH, K.C., AL-BEREZANCHI, S. and HART, J.P., 2011. The voltammetric behaviour of lead at a microband screen-printed carbon electrode and its determination in acetate leachates from glazed ceramic plates. Talanta, **84**(3), pp. 717-723.

HSIAO, F.B., 1999. Microsatellites as Research Tools. Elsevier Science, .

HUBBARD, A.T., 1995. The Handbook of Surface Imaging and Visualization. Taylor & Francis.

HYUN, W.J., SECOR, E.B., HERSAM, M.C., FRISBIE, C.D. and FRANCIS, L.F., 2015. High-resolution patterning of graphene by screen printing with a silicon stencil for highly flexible printed electronics. Advanced Materials, **27**(1), pp. 109-115.

IHALAINEN, P., MAJUMDAR, H., VIITALA, T., TÖRNGREN, B., NÄRJEOJA, T., MÄÄTTÄNEN, A., SARFRAZ, J., HÄRMÄ, H., YLIPERTTULA, M., ÖSTERBACKA, R. and PELTONEN, J., 2013. Application of paper-supported printed gold electrodes for impedimetric immunosensor development. Biosensors, **3**(1), pp. 1-17.

IKEDA, O., WATANABE, Y. and ITOH, F., 2007. Corrosion measurement of a conductive paste and anisotropic conductive adhesive films, 2007, pp. 77-80.

JANECZEK, K., JAKUBOWSKA, M., MLOZNIAK, A. and KOZIOL, G., 2012. Thermal characterization of screen printed conductive pastes for RFID antennas. Materials Science and Engineering B: Solid-State Materials for Advanced Technology, **177**(15), pp. 1336-1342.

JANG, S., CHO, H., KANG, S., OH, S. and KIM, D., 2011. Inkjet-printed gold nanoparticulate patterns for surface finish in electronic package. Applied Physics A: Materials Science and Processing, **105**(3), pp. 685-690.

JEONG, W.-., NISHIKAWA, H., GOTOH, H. and TAKEMOTO, T., 2005. Effect of solvent evaporation and shrink on conductivity of conductive adhesive. Materials Transactions, **46**(3), pp. 704-708.

JERANCE, N., BEDNAR, N. and STOJANOVIC, G., 2013. An ink-jet printed eddy current position sensor. Sensors (Switzerland), **13**(4), pp. 5205-5219.

JEWELL, E.H., HAMBLYN, S.M., CLAYPOLE, T.C. and GETHIN, D.T., 2013. The impact of carbon content and mesh on the characteristics of screen printed conductive structures. Circuit World, **39**(1), pp. 13-21.

JING LI and J. K. LUMPP, 2006. Electrical and mechanical characterization of carbon nanotube filled conductive adhesive, 2006 IEEE Aerospace Conference 2006, pp. 6 pp.

JO, Y.H., JUNG, I., KIM, N.R. and LEE, H.M., 2012. Synthesis and characterization of highly conductive Sn-Ag bimetallic nanoparticles for printed electronics. Journal of Nanoparticle Research, **14**(4),.

JONES, C.S., LU, X., RENN, M., STRODER, M. and SHIH, W., 2010. Aerosol-jet-printed, high-speed, flexible thin-film transistor made using single-walled carbon nanotube solution. Microelectronic Engineering, **87**(3), pp. 434-437.

KAMYSHNY, A. and MAGDASSI, S., 2014. Conductive Nanomaterials for Printed Electronics. Small, **10**(17), pp. 3515-3535.

KANG, D.K., LEE, M.W., KIM, H.Y., JAMES, S.C. and YOON, S.S., 2011. Electrohydrodynamic pulsed-inkjet characteristics of various inks containing aluminum particles. Journal of Aerosol Science, **42**(10), pp. 621-630.

KAPLAN, H., 2007. Practical applications of infrared thermal sensing and imaging equipment. Bellingham, Wash.: SPIE, .

KATZIR, E., YOCHELIS, S., PALTIEL, Y., AZOUBEL, S., SHIMONI, A. and MAGDASSI, S., 2014. Tunable inkjet printed hybrid carbon nanotubes/nanocrystals light sensor. Sensors and Actuators B: Chemical, **196**, pp. 112-116.

KAWAHARA, Y., HODGES, S., GONG, N.-., OLBERDING, S. and STEIMLE, J., 2014. Building functional prototypes using conductive inkjet printing. IEEE Pervasive Computing, **13**(3), pp. 30-38.

KELKAR, A.D., HERR, D.J.C. and RYAN, J.G., 2014. Nanoscience and Nanoengineering: Advances and Applications. CRC Press, pp. 20.

KENG, L.B., LAI, W.L., LU, C.W.A. and SALAM, B., 2011. Processing and characterization of flexographic printed conductive grid, 2011, pp. 517-520.

KHONDOKER, M.A.H., MUN, S.C. and KIM, J., 2013. Synthesis and characterization of conductive silver ink for electrode printing on cellulose film. Applied Physics A: Materials Science and Processing, **112**(2), pp. 411-418.

KIM, K.D. and CHUNG, D.D.L., 2002. Effect of heating on the electrical resistivity of conductive adhesive and soldered joints. Journal of Electronic Materials, **31**(9), pp. 933-939.

KIM, Y., KIM, H. and YOO, H.-., 2010. Electrical characterization of screen-printed circuits on the fabric. IEEE Transactions on Advanced Packaging, **33**(1), pp. 196-205.

KO, S.H., PAN, H., GRIGOROPOULOS, C.P., LUSCOMBE, C.K., FRÉCHET, J.M.J. and POULIKAKOS, D., 2007. All-inkjet-printed flexible electronics fabrication on a polymer substrate by low-temperature high-resolution selective laser sintering of metal nanoparticles. Nanotechnology, **18**(34),.

KREBS, F.C., 2009. Fabrication and processing of polymer solar cells: A review of printing and coating techniques. Solar Energy Materials and Solar Cells, **93**(4), pp. 394-412.

KUEHL, R.W., 2002. Reliability of thin-film resistors: Impact of third harmonic screenings. Microelectronics Reliability, **42**(6), pp. 807-813.

KULKARNI, S.K., 2014. Nanotechnology: Principles and Practices. Springer International Publishing, pp. 146.

LACOSTE, R., 2009. Robert Lacoste's The Darker Side: Practical Applications for Electronic Design Concepts from Circuit Cellar. - Elsevier Science.

LEBEDEV, S.M., GEFLE, O.S., DNEPROVSKII, S.N. and AMITOV, E.T., 2015. Electrophysical properties of thermally conductive polymer materials. Russian Physics Journal, **57**(10), pp. 1423-1427.

LI, H., MOON, K.-. and WONG, C.P., 2004. A novel approach to stabilize contact resistance of electrically conductive adhesives on lead-free alloy surfaces. Journal of Electronic Materials, **33**(2), pp. 106-113.

LI, Y. and WONG, C.P., 2006a. High performance anistropic conductive adhesives for lead-free interconnects, 2006a.

LI, Y. and WONG, C.P., 2006b. Recent advances of conductive adhesives as a lead-free alternative in electronic packaging: Materials, processing, reliability and applications. Materials Science and Engineering R: Reports, **51**(1-3), pp. 1-35.

LIN, Y.C. and ZHONG, J., 2008. A review of the influencing factors on anisotropic conductive adhesives joining technology in electrical applications. Journal of Materials Science, **43**(9), pp. 3072-3093.

MÄÄTTÄNEN, A., IHALAINEN, P., BOLLSTRÖM, R., TOIVAKKA, M. and PELTONEN, J., 2010. Wetting and print quality study of an inkjet-printed poly(3-hexylthiophene) on pigment coated papers. Colloids and Surfaces A: Physicochemical and Engineering Aspects, **367**(1–3), pp. 76-84.

MCCAULEY, J.W. and - WEISS, V., 2013. Materials Characterization for Systems Performance and Reliability. Springer US.

MENARD, K.P., 2008. Dynamic Mechanical Analysis: A Practical Introduction, Second Edition. - CRC Press.

MÉNIL, F., DEBÉDA, H. and LUCAT, C., 2005. Screen-printed thick-films: From materials to functional devices. Journal of the European Ceramic Society, **25**(12 SPEC. ISS.), pp. 2105-2113.

MONTANINO, M., DE GIROLAMO DEL MAURO, A., TESORO, M., RICCIARDI, R., DIANA, R., MORVILLO, P., NOBILE, G., IMPARATO, A., SICO, G. and MINARINI, C., 2015. Gravure-printed PEDOT:PSS on flexible PEN substrate as ITO-free anode for polymer solar cells. Polymer Composites, **36**(6), pp. 1104-1109.

MORITA, S., GIESSIBL, F.J., MEYER, E. and WIESENDANGER, R., 2015. Noncontact Atomic Force Microscopy. Springer International Publishing, pp. 229.

NARAKATHU, B.B., REDDY, S.G.A., ATASHBAR, M.Z., REBROSOVA, E., REBROS, M. and JOYCE, M.K., 2011. A novel gravure printed impedance based flexible electrochemical sensor, 2011, pp. 577-580.

NJUGUNA, J., 2013. - Structural Nanocomposites: Perspectives for Future Applications. - Springer Berlin Heidelberg.

OLIVER, A.D. and WISE, K.D., 1999. 1024-Element bulk-micromachined thermopile infrared imaging array. Sensors and Actuators, A: Physical, **73**(3), pp. 222-231.

OMASTOVA, M., CHODAK, I. and PIONTECK, J., 1999. Electrical and mechanical properties of conducting polymer composites. Synthetic Metals, **102**(1-3), pp. 1251-1252.

OPPERMANN, M., ZERNA, T. and WOLTER, K.-., 2009. X-ray computed tomography on miniaturized solder joints for nano packaging, 2009, pp. 70-75.

OPTOTHERM, I., 2016, 2016-last update [06/11, 2016].

PARK, S.-. and KIM, H.-., 2014. Flash light sintering of nickel nanoparticles for printed electronics. Thin Solid Films, **550**, pp. 575-581.

PEFFERKORN, A., 2012. Shrinkage characteristics of experimental polymer containing composites under controlled light curing modes. Polymers, **4**(1), pp. 256-274.

PERELAER, J., AND SCHUBERT, U. S., 2010.
Inkjet Printing and Alternative Sintering of
Narrow Conductive Tracks on Flexible
Substrates for Plastic Electronic Applications In: C. TURCU, ed, Radio Frequency Identification Fundamentals and Applications Design Methods and Solutions. Croatia: InTech, pp. 276.

PERELAER, J., KLOKKENBURG, M., HENDRIKS, C.E. and SCHUBERT, U.S., 2009. Microwave flash sintering of inkjet-printed silver tracks on polymer substrates. Advanced Materials, **21**(47), pp. 4830-4834.

PERELAER, J., SMITH, P.J., MAGER, D., SOLTMAN, D., VOLKMAN, S.K., SUBRAMANIAN, V., KORVINK, J.G. and SCHUBERT, U.S., 2010. Printed electronics: The challenges involved in printing devices, interconnects, and contacts based on inorganic materials. Journal of Materials Chemistry, **20**(39), pp. 8446-8453.

PIERSON, H.O., 1993. 5 - Molded Graphite: Processing, Properties, and Applications. In: H.O. PIERSON, ed, Handbook of Carbon, Graphite, Diamonds and Fullerenes. Oxford: William Andrew Publishing, pp. 87-121.

PIRES-DE-SOUZA, F.C.P., DRUBI FILHO, B., CASEMIRO, L.A., GARCIA, L.F.R. and CONSANI, S., 2009. Polymerization shrinkage stress of composites photoactivated by different light sources. Brazilian dental journal, **20**(4), pp. 319-324.

PUDAS, M., HALONEN, N., GRANAT, P. and VÄHÄKANGAS, J., 2005. Gravure printing of conductive particulate polymer inks on flexible substrates. Progress in Organic Coatings, **54**(4), pp. 310-316.

QI, S., VAIDHYANATHAN, B. and HUTT, D., 2013. Conventional and microwave-assisted processing of Cu-loaded ICAs for electronic interconnect applications. Journal of Materials Science, **48**(20), pp. 7204-7214.

R. WOEHL, J. KRAUSE, F. GRANEK and D. BIRO, 2011. 19.7% Efficient All-Screen-Printed Back-Contact Back-Junction Silicon Solar Cell With Aluminum-Alloyed Emitter. IEEE Electron Device Letters, **32**(3), pp. 345-347.

ROBERSON, D.A., WICKER, R.B. and MACDONALD, E., 2012. Ohmic curing of printed silver conductive traces. Journal of Electronic Materials, **41**(9), pp. 2553-2566.

ROGALSKI, A., 2011. Recent progress in infrared detector technologies. Infrared Physics and Technology, **54**(3), pp. 136-154.

ROGALSKI, A., 2010. Infrared Detectors, Second Edition. - CRC Press.

SALAM, B., LAI, W.L., ALBERT, L.C.W. and KENG, L.B., 2011. Low temperature processing of copper conductive ink for printed electronics applications, 2011, pp. 251-255.

SALOMON, A. and TROIANELLO, T., 1973. COMPONENT LINEARITY TEST IMPROVES RELIABILITY SCREENING THROUGH MEASUREMENT OF THIRD HARMONIC INDEX. , pp. 69-76.

SAUNDERS, N., 2008. Exploring Chemical Reactions. Rosen Publishing Group.

SCHNEIDER, L.F.J., CAVALCANTE, L.M. and SILIKAS, N., 2010. Shrinkage stresses generated during resin-composite applications: A review. Journal of Dental Biomechanics, **1**(1), pp. 1-14.

SMITH, P.J., SHIN, D.-., STRINGER, J.E., DERBY, B. and REIS, N., 2006. Direct ink-jet printing and low temperature conversion of conductive silver patterns. Journal of Materials Science, **41**(13), pp. 4153-4158.

SPERLING, L.H., 2015. Introduction to Physical Polymer Science. Wiley.

SPIRALSKI, L., 2003. PRODUCTION TESTING OF HIGH RELIABILITY INTERFERENCE SUPPRESSOR CAPACITORS. IMEKO World Congress, **XVII**, pp. 1486; 1486-1488; 1488.

SUBRAMANIAN, V., CHANG, J.B., DE LA VORNBROCK, A.F., HUANG, D.C., JAGANNATHAN, L., LIAO, F., MATTIS, B., MOLESA, S., REDINGER, D.R., SOLTMAN, D., VOLKMAN, S.K. and ZHANG, Q., 2008. Printed electronics for low-cost electronic systems: technology status and application development, 2008, pp. 17-24.

SUGIMOTO, T., ABE, M. and HIGASHIYAMA, Y., 2012. Noncontact surface resistivity measurement using a cylindrical surface potential detector with a corona charger. IEEE Transactions on Industry Applications, **48**(5), pp. 1657-1661.

ŠVANCARA, I., VYTRAS, K., KALCHER, K., WALCARIUS, A. and WANG, J., 2009. Carbon paste electrodes in facts, numbers, and notes: A review on the occasion of the 50-years jubilee of carbon paste in electrochemistry and electroanalysis. Electroanalysis, **21**(1), pp. 7-28.

TEN CATE, A.T., GASPAR, C.H., VIRTANEN, H.L.K., STEVENS, R.S.A., KOLDEWEIJ, R.B.J., OLKKONEN, J.T., RENTROP, C.H.A. and SMOLANDER, M.H., 2014. Printed electronic switch on flexible substrates using printed microcapsules. Journal of Materials Science, **49**(17), pp. 5831-5837.

TENG, R.K.F., MOSTAFA, A.A. and KARIM, A., 1990. Study of Solar Cell Fabrication Using an Electrostatic Thick-Film Printing Method. IEEE Transactions on Industrial Electronics, **37**(5), pp. 419-423.

THE BRITISH STANDARDS INSTITUTION, 2012. **BS EN 60440:2012**. London, U.K.: BSI Standards Limited, pp. 9-10.

TONG, H.M., SAENGER, K.L. and SU, G.W., 1993. Thickness-direction thermal expansion of polyimide films. Polymer Engineering & Science, **33**(22), pp. 1502-1506.

UNANDER, T. and NILSSON, H.-., 2009. Characterization of printed moisture sensors in packaging surveillance applications. IEEE Sensors Journal, **9**(8), pp. 922-928.

VANDAMME, E.P. and VANDAMME, L.K.J., 1999. Current crowding and its effect on 1/f noise and third harmonic distortion - A case study for quality assessment of resistors. Microelectronics Reliability, **40**(11), pp. 1847-1853.

WEGENER, M., SPIEHL, D., SAUER, H.M., MIKSCHL, F., LIU, X., KÖLPIN, N., SCHMIDT, M., JANK, M.P.M., DÖRSAM, E. and ROOSEN, A., 2016. Flexographic printing of nanoparticulate tin-doped indium oxide inks on PET foils and glass substrates.

WOERLE, J. and ROST, H., 2011. Roll-to-roll production of transparent conductive films using metallic grids. MRS Bulletin, **36**(10), pp. 789-793.

WUNDERLE, B., KALLMAYER, C., WALTER, H., BRAUN, T., MICHEL, B. and REICHL, H., 2008. Lifetime model for flip-chip on flex using anisotropic conductive adhesive under moisture and temperature loading, 2008, pp. 799-808.

YANG, X., HE, W., WANG, S., ZHOU, G. and TANG, Y., 2013. Preparation of high-performance conductive ink with silver nanoparticles and nanoplates for fabricating conductive films. Materials and Manufacturing Processes, **28**(1), pp. 1-4.

ZACHARATOS, F., MAKRYGIANNI, M., GEREMIA, R., BIVER, E., KARNAKIS, D., LEYDER, S., PUERTO, D., DELAPORTE, P. and ZERGIOTI, I., 2016. Laser Direct Write micro-fabrication of large area electronics on flexible substrates. Applied Surface Science, **374**, pp. 117-123.